ความน่าจะเป็นในการคงอยู่ของความผันผวนของความสูงในการปลูกฟิล์มบาง โดยแบบจำลองวิยุตที่มีสมมาตรขึ้น-ลง

นางสาวรังสิมา ชาญพนา

วิทยานิพนธ์นี้เป็นส่วนหนึ่งของการศึกษาตามหลักสูตรปริญญาวิทยาศาสตรดุษฎีบัณฑิต
สาขาวิชาฟิสิกส์ ภาควิชาฟิสิกส์
คณะวิทยาศาสตร์ จุฬาลงกรณ์มหาวิทยาลัย
ปีการศึกษา 2556

PERSISTENCE PROBABILITIES OF HEIGHT FLUCTUATION IN THIN FILM GROWTH USING DISCRETE MODELS WITH UP-DOWN SYMMETRY

Miss Rangsima Chanphana

A Dissertation Submitted in Partial Fulfillment of the Requirements

for the Degree of Doctor of Philosophy Program in Physics

Department of Physics

Faculty of Science

Chulalongkorn University

Academic Year 2013

Thesis Title	PERSISTENCE PROBABILITIES OF HEIGHT FLUCTUATION IN THIN FILM GROWTH USING DISCRETE MODELS WITH UP-DOWN SYMMETRY
By	Miss Rangsima Chanphana
Field of Study	Physics
Thesis Advisor	Assistant Professor Patcha Chatraphorn, Ph.D.
Thesis Co-advisor	Professor Chandan Dasgupta, Ph.D.

Accepted by the Faculty of Science, Chulalongkorn University in Partial Fulfillment of the Requirements for the Doctoral Degree

.....Dean of the Faculty of Science

(Professor Supot Hannongbua, Dr. rer. nat.)

THESIS COMMITTEE

.....Chairman

(Associate Professor Udomsilp Pinsook, Ph.D.)

.....Thesis Advisor

(Assistant Professor Patcha Chatraphorn, Ph.D.)

.....Thesis Co-advisor

(Professor Chandan Dasgupta, Ph.D.)

.....Examiner

(Associate Professor Nakorn Phaisangittisakul, Ph.D.)

.....Examiner

(Assistant Professor Sakuntam Sanorpim, Ph.D.)

.....External Examiner

(Sornthep Vannarat, Ph.D.)

รังสิมา ชาญพนา : ความน่าจะเป็นในการคงอยู่ของความผันผวนของความสูงในการปลูกฟิล์มบางโดยแบบจำลองวิยุตที่มีสมมาตรขึ้น-ลง. (PERSISTENCE PROBABILITIES OF HEIGHT FLUCTUATION IN THIN FILM GROWTH USING DISCRETE MODELS WITH UP-DOWN SYMMETRY) อ. ที่ปรึกษาวิทยานิพนธ์หลัก : ผศ. ดร. ปัจฉา ฉัตราภรณ์, อ. ที่ปรึกษาวิทยานิพนธ์ร่วม : Prof. Chandan Dasgupta, Ph.D., 99 หน้า.

ปัญหาของการคงอยู่ของความผันผวนของความสูง ในการปลูกพื้นผิวที่ไม่อยู่ในสภาวะสมดุล และพลวัตระหว่างผิวได้ถูกศึกษาค้นคว้าอย่างกว้างขวางในหลายปีมานี้ แนวคิดของการคงอยู่นั้นน่าสนใจในทางทฤษฎี และมีการประยุกต์ใช้ได้จริงในหลาย ๆ ด้าน ความน่าจะเป็นของการคงอยู่ คือความน่าจะเป็นที่ความผันผวนของความสูงของฟิล์มที่ปลูก ไม่คืนกลับสู่ค่าเริ่มต้นตลอดช่วงเวลาที่กำหนด ในหลายแบบจำลองของการปลูกพื้นผิว ความน่าจะเป็นของการคงอยู่ลดลงตามเวลาแบบกฎการยกกำลัง ค่าความน่าจะเป็นของการคงอยู่และเลขชี้กำลังที่เกี่ยวข้องปรากฏว่ามีการเปลี่ยนแปลงเมื่อค่าเริ่มต้นของความสูงเปลี่ยนแปลง ความน่าจะเป็นของการคงอยู่ยังขึ้นอยู่กับช่วงเวลาตัวอย่าง (ช่วงเวลาระหว่างการวัดสองครั้ง ที่ใช้ในการคำนวณค่าความน่าจะเป็นของการคงอยู่) ด้วย วัตถุประสงค์หลักของการศึกษานี้คือเพื่อเข้าใจว่า ความน่าจะเป็นของการคงอยู่ ของแบบจำลองที่มีสมมาตรขึ้นลง มีการเปลี่ยนแปลงเมื่อค่าเริ่มต้นของความสูงและช่วงเวลาตัวอย่างมีการเปลี่ยนแปลงอย่างไร และเพื่อค้นหาการบรรยายการสเกลสำหรับมัน อีกหนึ่งเป้าหมายคือการศึกษาผลของรูปแบบแผ่นรองรับ เวลากลับคืนของฟิล์มบางที่จำลองด้วยแบบจำลอง Family และแบบจำลอง Das Sarma-Tamborenea ที่ปลูกบนแผ่นรองรับแบบสามเหลี่ยม และแผ่นรองรับแบบเสาและร่องได้ถูกศึกษา เวลากลับคืนคือเวลาที่อิทธิพลของรูปแบบเริ่มต้นในแผ่นรองรับหายไป และลักษณะเฉพาะของพื้นผิวที่ปลูกกลับคืนสู่ค่าที่ได้ เมื่อปลูกฟิล์มลงบนแผ่นรองรับที่เรียบ เวลากลับคืนถูกกำหนดค่า โดยการศึกษาฟังก์ชันสหสัมพันธ์ความแตกต่างความสูงของเพื่อนบ้านใกล้ที่สุด ผลเฉลยทางทฤษฎีของฟังก์ชันสหสัมพันธ์ ที่บรรยายพลวัติของพื้นผิวฟิล์มที่จำลองโดยแบบจำลอง Family ลงบนแผ่นรองรับทั้งสองแบบได้ถูกค้นหาด้วยเช่นกัน

ภาควิชา ฟิสิกส์ ลายมือชื่อนิสิต .....
สาขาวิชา ฟิสิกส์ ลายมือชื่อ อ.ที่ปรึกษาวิทยานิพนธ์หลัก .....
ปีการศึกษา 2556 ลายมือชื่อ อ.ที่ปรึกษาวิทยานิพนธ์ร่วม .....

5173844923 : MAJOR PHYSICS
KEYWORDS : PERSISTENCE PROBABILITY / DISCRETE GROWTH MODEL / DISCRETE SAMPLING TIME / PATTERNED SUBSTRATE / HEALING TIME

RANGSIMA CHANPHANA : PERSISTENCE PROBABILITIES OF HEIGHT FLUCTUATION IN THIN FILM GROWTH USING DISCRETE MODELS WITH UP-DOWN SYMMETRY. ADVISOR : ASST. PROF. PATCHA CHATRAPHORN, Ph.D., CO-ADVISOR : PROF. CHANDAN DASGUPTA, Ph.D., 99 pp.

The problem of persistence of height fluctuations in non-equilibrium surface growth and interface dynamics has been widely studied in recent years. The persistence concept is interesting theoretically and also has practical applications in many areas. The persistence probability is the probability that the height fluctuation of a growing film does not return to its initial value over a specified time interval. For several models of surface growth, the persistence probability decreases in time as a power law. The persistence probability and the corresponding exponents appear to change when the initial height changes. The persistence probability also depends on the discrete sampling time (discrete time interval between two measurements used to calculate the persistence probability). The main purpose of this study is to understand how the persistence probability of up-down symmetric models change as the initial height and the discrete sampling time are varied and determine a scaling description for it. Another goal is to study effects of patterned substrate. The healing times of thin films simulated by Family and Das Sarma-Tamborenea models grown on the smooth triangular substrate, and the rough pillar and groove substrate are studied. The healing time is the time when influences of the initial pattern in the substrate disappear and characteristics of the growing interface are healed to those obtained by a film grown on a flat substrate. The healing time is determined via the study of the nearest-neighbor height difference correlation function. The theoretical solution of the correlation function describing dynamics of film surface of the Family model grown on both patterns is also investigated.

Department : Physics Student's Signature .....
Field of Study : Physics Advisor's Signature .....
Academic Year : 2013 Co-advisor's Signature .....

Acknowledgements

This work would not have been possible without the encouragement of Asst. Prof. Dr. Patcha Chatraphorn, my helpful advisor. Her useful suggestions lead me to my purpose. Her patience and forgiveness enhance my development and cautiousness without bad atmosphere between us. Her mental support is really powerful for my step forward. My deepest gratitude goes to my co-advisor Prof. Dr. Chandan Dasgupta for his valuable guidance and comments. I am most grateful for the time he spends on my work. I would also like to thank Prof. Dr. Chandan Dasgupta and Indian Institute of Science (IISC) for giving me an opportunity to research in the Department of Physics, IISC for 3 weeks with full support. Being successful in work, friendships and good experience there are still fresh in my memory. I am very grateful to Assoc. Prof. Dr. Udomsilp Pinsook, Assoc. Prof. Dr. Nakorn Phaisangittisakul, Asst. Prof. Dr.Sakuntam Sanorpim and Dr. Sornthep Vannarat for serving as my thesis committee. I would like to thank Asst. Prof. Dr. Kajornyod Yoodee, Asst. Prof. Dr. Sojiphong Chatraphorn, Dr. Chatchai Srinitiwarawong and Asst. Prof. Dr. Surachate Limkumnerd for their suggestions and their helpful ideas for solving my problems. I would like to thank the whole Semiconductor Physics Research Laboratory (SPRL) group for their helps and interesting discussions, especially Manit Klawtanong and Wittawat Kanjanaput. I am deeply grateful for all supports from my husband, Wirin Sonsrettee. I appreciate for his love, care and sacrifice. Whatever happens and whenever the need arises, he stand by me and his help is always available. I especially thank the Department of Physics, Faculty of Science, Chulalongkorn University, my beloved place for study and work since 1998. Being student and lecturer here is the highest pride of my family and mine. Lastly, I would like to thank my parents, sister, brother, colleagues and friends for their encouragements.

The research described in this dissertation was supported financially by Chulalongkorn University Graduate Scholarship to Commemorate the 72nd Anniversary of His Majesty King Bhumibol Adulyadej, Research Center in Thin Film Physics, Thailand Center of Excellence in Physics, CHE, 328 Si Ayutthaya Rd., Bangkok 10400, Thailand, Research Funds from the Faculty of Science, Chulalongkorn University and the Special Task Force for Activating Research (STAR), Ratchadaphiseksomphot Endowment Fund, Chulalongkorn University through the Energy Materials Physics Research Group.

Contents

Page

Page

List of Tables

Table **Page**

List of Figures

Page

Page

Page

Page

Page

Chapter I

Introduction

There are many investigations of stochastic dynamics of surface growth and interface fluctuations [Barabasi and Stanley, 1995; Krug, 1997; Pimpinelli and Villain, 1998; Michely and Krug, 2004; Evans et al. 2006; Pelliccione and Lu, 2008]. Persistence is one of the quantities studied in those investigations. The persistence concept has been used to analyze dynamical fluctuations of various systems such as the simple diffusion [Majumdar et al. 1996; Majumdar, 1999], random acceleration [Majumdar, 1999], random walk [Sire et al. 2000], many body nonequilibrium systems [Bray et al. 2013] and a general smooth stationary temporal signal [Sire, 2007; Sire, 2008]. Krug and co-workers were the first to apply the persistence concept to the problem of fluctuations in non-equilibrium surface growth dynamics [Krug et al. 1997; Kallabis et al. 1999]. Since then, there have been many analytical and numerical studies of the persistence probability in surface growth phenomena [Toroczkai et al. 1999; Constantin et al. 2004; Constantin et al. 2007, Bray et al. 2013]. Persistence properties of interface fluctuations have been studied experimentally as well [Dougherty et al. 2002; Dougherty et al. 2003; Constantin et al. 2003; Conrad et al. 2007]. The persistence probability provides a quantitative characterization of the dynamics of fluctuations in these stochastic systems.

The persistence probability of step fluctuations (fluctuations that is perpendicular to the growth direction) on the vicinal surface is investigated analytically and experimentally [Constantin et al. 2007, Conrad et al. 2007]. Some experiments pointed out that step fluctuation on the vicinal surface of Si(111) [Lyubinetsky et al. 2002] and Al/Si(111) [Dougherty et al. 2004] can be explained by the Edwards-Wilkinson equation [Edwards and Wilkinson, 1982] which is the equation that describes the Family model [Family, 1986]. Another interesting problem is the persistence behavior of the height fluctuation in the growth direction of the Family model, which can be compared to results from other models and from experiments.

In this dissertation, the steady-state temporal persistence probabilities of the height fluctuation in discrete growth models are studied. The persistence probability is defined as the probability that the height fluctuation $h(t)$ of the growing film does not return to its initial value

h_0 over a specified time interval t [Krug, et al. 1997; Majumdar, 1999]. The height fluctuation $h(t)$ is the height at a site measured from the average height of the film at time t, so its value can be both positive and negative integers including zero. The initial height h_0 is the height fluctuation at the initial time t_0, which is taken to be in the steady-state regime in our study. The persistence probability is divided into positive persistence probability $P_+^S(t)$, i.e., the probability that the height fluctuation remains larger than h_0 throughout time t, and negative persistence probability $P_-^S(t)$, i.e., the probability that h remains smaller than h_0 during the interval t. Previous studies [Krug et al. 1997; Constantin et al. 2004] have shown that after averaging over all values of h_0, the positive and negative persistence probabilities are the same for models with up-down symmetry such as the Family [Family, 1986] and the larger curvature (LC) [Kim and Das Sarma, 1994; Krug, 1994] models, while they differ in models without up-down symmetry. The persistence probability usually decays with time as a power law with an exponent that depends on the model being considered. The exponents for the positive and negative persistence probabilities averaged over the initial height are the same for each growth model with up-down symmetry, whereas they have different values for models in which this symmetry is not present.

In this work, we investigate the dependence of the persistence probabilities on the choice of the initial height in the Family and LC models. Using numerical simulations, we analyze how the positive and negative persistence probabilities change when the value of the initial height is changed. For any nonzero value of the initial height h_0 (measured from the average height of the interface), the positive and negative persistence probabilities are not equal to each other. The up-down symmetry of the interface in these models implies that the positive (negative) persistence probability for a positive value of the initial height h_0 must be equal to the negative (positive) persistence probability for a negative value of the initial height with magnitude equal to h_0. Our numerical results show that the positive persistence probability for negative initial heights (and equivalently, the negative persistence probability for positive initial heights) exhibits power-law decay in time if the magnitude of the initial height is larger than the saturation width of the interface. The exponent that characterizes this power-law decay is found to be distinct from the one that describes the power-law decay of the persistence probability averaged over the initial height. This exponent decreases as the magnitude of the initial height h_0 is increased. The negative (positive) persistence probability for negative (positive) initial height does not exhibit

power-law decay in time. We present qualitative arguments that provide a rationalization of these results obtained from simulations.

We have also studied the scaling behavior of the persistence probability as a function of h_0, the system size L, and the discrete sampling time δt (the time interval between two successive measurements used to calculate the persistence probability). Persistence probabilities are known to be influenced by the discrete sampling time [Majumdar et al. 2001; Ehrhardt et al. 2002]: the probabilities increase as the discrete sampling time increases. For the (1+1)-dimensional Family model, the steady-state persistence probability, after averaging over all values of the initial height, was found to scale with t/L^z and $\delta t/L^z$ [Constantin et al. 2004] where z is the dynamical exponent that characterizes the nonequilibrium dynamics of the growth process of the model. In this work, we perform a similar scaling analysis on (1+1)-dimensional Family and (1+1)/(2+1)-dimensional LC models and show that the persistence probability for a particular value of the initial height h_0 is a function of the scaling variables h_0/L^α, t/L^z, and $\delta t/L^z$, where α is the roughness exponent that describes the dependence of the interface width in the steady-state on the system size.

Another part of this dissertation is motivated by technological application in fabrication of nanostructures and high-technology devices which has been broadly developed in recent years [Mugarza and Ortega, 2003; Hongsith et al. 2005; Conrad et al. 2007; Jnawali et al. 2009; Thongkham et al. 2010; Bhoomanee et al. 2011; Sakdanuphab et al. 2011; Wongsaprom and Maensiri, 2013]. Thin film growth on patterned crystalline surfaces has, therefore, been investigated for the application. Kinetic roughening of thin films grown on crystalline surfaces has been widely studied in experiments [Hegeman et al 1995; Redinger et al.2008; Jnawali et al. 2009; Dimastrodonato et al. 2012]. The evolution of the film interface can be directly observed in experiments using scanning tunneling microscopy (STM). Films are often grown on structures that are not perfectly flat. It is, therefore, important to understand how the growth of thin films is affected by the presence of initial rough patterns on the substrate.

In thin film growth simulations, a flat substrate is the initial pattern considered in most investigations [Krug et al. 1997, Das Sarma and Punyindu, 1999, Constantin et al. 2004]. Patterned substrates have recently received considerable interest and have been studied theoretically [Krug, 1999; Krug, 2004; Evans et al. 2006; Nguyen et al. 2009], numerically [Hontinfinde et al. 1998; Nurminen et al. 2000; Constantin et al. 2007; Kanjanaput et al. 2010;

Tang et al. 2010; Chatraphorn and Chomngam, 2012; Lin et al. 2012; Marques et al. 2012; Mondal and Sengupta, 2012; Bergamaschini et al. 2012; Asgari and Moosavi, 2012; Hedayatifar et al. 2012] and experimentally [Hegeman et al 1995; Giesen, 1997; Rousset et al. 1999; Dougherty et al. 2002; Lyubinetsky et al. 2002; Dougherty et al. 2003; Mugarza and Ortega, 2003; Dougherty et al. 2004; Conrad et al. 2007; Redinger et al.2008; Jnawali et al. 2009; Nguyen et al. 2009; Persichetti et al. 2009; Dimastrodonato et al. 2012]. Effects of a patterned substrate on a growing thin film can be explicitly observed from surface morphology and the change of some statistical properties such as the interface width and the correlation functions [Krug, 1997; Nurminen et al. 2000; Nguyen et al. 2009; Kanjanaput et al. 2010; Chatraphorn and Chomngam, 2012].

In this work, we investigate how shape and size of the initial pattern as well as substrate roughness affect films grown from the Family model. In experiments, one of the benefits in using a patterned substrate is that the deposited atoms can stick on the rough substrate more tightly than on a flat substrate because atoms can form lateral bond with the substrate at the step edge. The patterns of interest are the vicinal and triangular substrates. There are many experimental researches on film growth on vicinal surfaces with many purposes. Examples of these works are study of the step-step interaction [Giesen, 1997; Persichetti et al. 2009], surface stress [Rousset et al. 1999], electronic properties of lateral nanostructures [Mugarza and Ortega, 2003], and fluctuations of step edges [Dougherty et al. 2002; Lyubinetsky et al. 2002; Dougherty et al. 2003; Dougherty et al. 2004; Conrad et al. 2007]. As a result, a theoretical study on effects of vicinal substrate on statistical properties of a growing film may help us to better understand real film fabrication processes. The triangular or tent-shape pattern is chosen to compare the results with the vicinal substrate. Another reason is that the triangular substrate has periodic boundary condition which can be studied analytically. Simulation results can then be compared with theoretical results in this case. Statistical properties of interest in this work are the interface width, the critical exponents, the transient persistence probability and the height-height correlation functions.

Our results show that the statistical properties of the growing film are different from those obtained from growth on a flat surface when a film is grown on a patterned surface. A question naturally arises in this context: how long does the initial pattern influence the morphology of the growing film? To answer this question, the "healing time" t_h, which is the

time when the initial pattern on the substrate no longer has any effect on the growing film [Hedayatifar et al. 2012], is investigated. The dependence of t_h on various factors, such as the characteristics of the original pattern on the substrate and the lateral size of the interface, are studied using simulations. Two different growth models – the Family [Family, 1986] and the Das Sarma-Tamborenea (DT) [Das Sarma and Tamborenea, 1991] models – are considered here. Two patterned substrates investigated in this dissertation are a relatively smooth tent-shaped triangular substrate and an atomically rough substrate with single-site pillars or grooves. We find that the healing time of the Family and DT models on a $L \times L$ triangular substrate is proportional to L^z, where z is the dynamical exponent of the models. For the Family model, we also theoretically analyze the time evolution of the nearest-neighbor height difference correlation function in this system. A continuum description based on the linear Edwards-Wilkinson equation is used in this analytical work. The correlation functions obtained from the continuum theory and simulations are found to be consistent with each other for the relatively smooth triangular substrate. For substrates with periodic and random distributions of pillars or grooves of varying size, the healing time is found to increases linearly with the height (depth) of pillars (grooves). We show explicitly that the simulation data for the Family model grown on a substrate with pillars or grooves do not agree with results from the calculation based on the continuum Edwards-Wilkinson equation. This result implies that a continuum description does not work when the initial pattern is atomically rough. The observed dependence of the healing time on the substrate size and the initial height (depth) of pillars (grooves) can be understood from the details of the diffusion rule of the atomistic model. The calculated healing time for both Family and DT models is found to depend on how the pillars and grooves are distributed over the substrate.

The overview of the dissertation is as follow: In this chapter, we described literature review of persistence probability and patterned substrate growth. In chapter 2, we present quantities of interest and details of discrete growth models used in our study. The scaling concepts as well as the three critical exponents are introduced. The persistence probability and its exponent are described. The definition of the discrete sampling time, the (generalized) height-height correlation function and the nearest-neighbor height difference correlation function is also included in this chapter. The discrete limited mobility growth models considered in this study are also defined. The models consist of up-down symmetric models, which are the Family [Family, 1986] and the larger curvature (LC) [Kim and Das Sarma, 1994; Krug, 1994] models, and up-

down asymmetric model which is the Das Sarma-Tamborenea (DT) [Das Sarma and Tamborenea, 1991] model. The continuum equations that describe the models in asymptotic limit and the universality class, including values of critical exponents of considered models are also presented.

Simulation work on effects of discrete sampling time and system size on the persistence probabilities is discussed in chapter 3. In this chapter, we consider the case of average value of h_0. We extend the dimension of the substrate in the Family model to verify that the scaling relation found in Constantin et al. [Constantin et al. 2004] is still valid in (2+1)-dimensions. In addition, we obtain the same scaling relation for another up-down symmetric model i.e. the LC model, as well as the up-down asymmetric DT model (with finite size limited values of the dynamical exponent). All models have been studied in both one and two dimensional substrates.

In chapter 4, effects of the initial height on the persistence probability, specifically for models with up-down symmetry, are investigated. A particular value of h_0 is considered in this chapter and the clear power-law decay of $P_+^S\left(-|h_0|,t\right)$ (and equivalently, of $P_-^S\left(+|h_0|,t\right)$) is obtained when $|h_0| \gtrsim W_s$ where W_s is the saturation width. The new parameter κ is presented and the scaling variable h_0 / L^{α} is found to be presented in the scaling relation.

We study effects of patterned substrates on the Family model in chapter 5. In this work, characteristics of some statistical properties of a film grown on triangular and vicinal substrates are studied. Substrate size and tilt angle are varied. It is found that the interface width and the correlation function increase as the roughness of the pattern is increased. The new scaling exponents are calculated and anomalous scaling is obtained. The transient persistence probability does not show a power-law relation when the initial surface is sufficiently rough. The initial rough surface also causes multifractal behavior in the model.

The healing time of thin films simulated by the Family and the DT models on patterned substrate are investigated in chapter 6. We find that the healing time for the triangular pattern scales with L^z and can be explained from a continuum description. For the pillar/groove pattern, the healing time is found to depend linearly on the height (depth) of the pillars (grooves) and to be insensitive to the substrate size L. We show that these features are consequences of the details of the atomistic diffusion rules of models. Therefore, these features cannot be explained from a continuum description. Moreover, the calculated healing time for both Family and DT models is found to depend on how the pillars and grooves are distributed over the substrate.

Finally, we conclude all of our results in chapter 7.

Chapter II

Quantities of Interest and Models

In this chapter, we describe the definition of quantities of interest used in our study. The discrete growth models, the continuum equations as well as the universality class are also discussed.

2.1 Quantities of Interest

2.1.1 Interface Width and Scaling Concepts

During the growth process, random deposition process causes fluctuations in the surface height. The kinetic roughness during the growth process can be characterized by the interface width, W, [Barabasi and Stanley, 1995] which is the root-mean-squared height fluctuation of the growing film:

$$W(L,t) = \left\langle \left(h(\vec{r},t) \right)^2 \right\rangle^{1/2} \tag{2.1}$$

where h is the height fluctuation, $\vec{r}$ is the position or site on the surface and t is the growth time measured in units of monolayers (MLs). One monolayer is the time when n atoms are deposited on a substrate with n sites. The brackets represent an average over all sites and different realizations of the stochastic growth process. There are three critical exponents (α, β, z) that classify the universality class of a model. The universality class describes the asymptotic properties of the model. Two models that have the same sets of critical exponents belong to the same universality class and have the same growth properties in the asymptotic limit. The critical exponents can be extracted from the interface width. The increase of the interface width with time in the transient state ($t << L^z$ where z is the dynamical exponent) due to the noise fluctuation is described by $W \sim t^{\beta}$ where β is the growth exponent. As time increases, atomic diffusion on the surface creates correlation among lateral sites and the correlation length increases with time. The growing film reaches its steady-state when the correlation length equals the substrate size. In the steady-state ($t >> L^z$), the interface width becomes constant which is called W_s. The value of the saturation width depends on the size of the system. Another exponent describing the dependence of the saturated interface width with the substrate size is

called the roughness exponent α where $W_s \sim L^{\alpha}$. The time that the system reaches the steady-state is called the saturation time t_s which scales with the substrate size, $t_s \sim L^z$, where z is the dynamical exponent. The roughness of the film surface stops increasing when t reaches t_s. From different behaviors of the interface width between two region, W scales with t and L, and can be written in the form

$$W \sim L^{\alpha} f\left(\frac{t}{L^z}\right), \tag{2.2}$$

where f is the scaling function whose form depends on scaling regimes i.e.

$$f(x) = \begin{cases} x^{\beta} & \text{for } x << 1 \\ \text{constant} & \text{for } x >> 1. \end{cases} \tag{2.3}$$

From simulation, the critical exponents can be obtained from $W_s \sim L^{\alpha}$, $W \sim t^{\beta}$ and $t_s \sim L^z$, or the collapse of the scaling curves W / L^{α} and W / t^{β} as a function of t / L^z.

2.1.2 Persistence Probabilities of Models with and without Up-Down Symmetry

Starting from an initial time t_0, the persistence probability of site r at time interval t, $p(r, t_0, t_0 + t)$ is the probability that the height fluctuation at that site, $h(r,t)$, does not return to its initial value $h(r,t_0)$ over a specified time interval t. In another word, the persistence probability is the probability that the sign of $h(r,t)$ does not change throughout the time interval.

$$p(r, t_0, t_0 + t) = \text{Prob}\left[h(r, t_0 + t') \neq h(r, t_0) \ \forall t' : 0 < t' \leq t\right]. \tag{2.4}$$

The persistence probability $P(t)$ is the average of $p(r, t_0, t_0 + t)$ over all sites on the substrate:

$$P(t) = \left\langle p(r, t_0, t_0 + t) \right\rangle. \tag{2.5}$$

$P(t)$ is found to decrease as a power law with time [Krug, et al. 1997; Majumdar, 1999]:

$$P(t) \propto t^{-\theta} \tag{2.6}$$

where θ is the persistence exponent whose value is model-dependent.

There are two types of persistence probability. The first is the transient persistence probability $P^T(t)$, which is the persistence probability in the early stage of the growth process starting at $t_0 = 0$. The second is the persistence probability in the long-time steady-state of the

growth process starting at $t_0 >> t_s$. It is called the steady-state persistence probability $P^S(t)$. Each type consists of the positive persistence probability $P_+(t)$ which is the probability that h remains larger than h_0, and the negative persistence probability $P_-(t)$ which is the probability that h remains smaller than h_0 over time t. The transient persistence probability decays with time as a power law [Krug, et al. 1997], $P_\pm^T(t) \propto t^{-\theta_\pm^T}$, where θ^T is the transient persistence exponent. The steady-state persistence probability also scales with the same function but with the steady-state persistence exponent θ^S as $P_\pm^S(t) \propto t^{-\theta_\pm^S}$.

It was pointed out by Krug, et al. [Krug, et al. 1997] that the steady-state exponent, θ^S, is related to the growth exponent, β, as $\beta = 1-\theta_+^S = 1-\theta_-^S$ for linear models such as the Family and the LC models. For nonlinear models such as the Das Sarma-Tamborenea model (DT model), the relation was found to be $\beta = \max[1-\theta_+^S, 1-\theta_-^S]$ [Constantin et al. 2004].

2.1.3 Discrete Sampling Time

The discrete sampling time δt is the time interval between two successive measurements used to calculate a quantity. Some physical quantities such as the persistence probability vary with the value of the discrete sampling time. In computer modeling of thin film growth, all time-dependent quantities are computed at every time steps separated by a discrete interval and the smallest possible value of δt is 1 deposited layer. In experiments of thin film fabrication, the time used to measure the persistence probability is also a discrete quantity. Studying effects of the discrete sampling time helps compare the results between experiments and numerical simulations.

2.1.4 Height-Height Correlation Function

The correlation between two sites on the film surface can be characterized by the height-height correlation function, $G(\Delta r, t)$, defined as [Krug, 1994]

$$G(\Delta r, t) = \left\langle \left(h(\vec{r} + \Delta\vec{r}, t) - h(\vec{r}, t) \right)^2 \right\rangle^{1/2} \tag{2.7}$$

where $\Delta r = \left|\Delta\vec{r}\right|$ is the distance between the two sites. In systems with normal scaling, $G(\Delta r, t) \sim \Delta r^\alpha$ for small Δr when α is the roughness exponent – the same exponent as obtained from W_s scaling, while $G(\Delta r, t)$ saturates to a constant for large Δr. In some cases, the roughness exponents obtained from G and W_s are different. Those are the cases with *anomalous scaling*. The exponent from G is called the local roughness exponent while the one from W_s is the global roughness exponent.

Some complicated systems also exhibit *multifractality*. To investigate this, generalized correlation function, $G_q(\Delta r,t)$, defined as [Krug, 1994]

$$G_q\left(\Delta r,t\right)=\left\langle\left|h(\vec{r}+\Delta\vec{r},t)-h(\vec{r},t)\right|^q\right\rangle^{1/q} \tag{2.8}$$

where q is the moment of the correlator, is usually calculated. When Δr is small, $G_q \sim \Delta r^{\alpha_q}$. A system is said to be self-affine when α_q does not depend on q. On the other hand, a system is multifractal when α_q is $q-$dependent demonstrating that different moments of correlations scale with different exponents. It has been shown [Punyindu, 2000] that films grown with the Family model on flat substrates have normal scaling while those grown from the DT model have both anomalous scaling and multifractality in both one and two dimensional substrates.

2.1.5 Healing Time and the Nearest Neighbor Height Difference Correlation Function

Studying effects of the initial pattern on a growing thin film, the main goal is to search for "the healing time t_h", the time when statistical properties of the growing films are no longer effected by the patterned substrate [Hedayatifar et al. 2012]. Several quantities can be used to identify the healing time. One such quantity is the nearest neighbor height difference correlation function, σ, defined as

$$\sigma\left(t\right)\equiv\left\langle\left|H\left(\vec{r}',t\right)-H\left(\vec{r},t\right)\right|^2\right\rangle^{1/2}, \tag{2.9}$$

where $H(\vec{r},t)$ is the height of site $\vec{r}$ at time t, $\vec{r}'$ is the position of a nearest neighbor of site $\vec{r}$. t_h is defined as the time at which σ of a film grown on a patterned substrate becomes equal to that of a film grown on a flat substrate.

2.2 Discrete Limited Mobility Growth Models

Numerous discrete growth models have been used in studies of thin film growth process via computer simulations. In this work, we study three discrete models. These are the Family model [Family, 1986], the larger curvature (LC) model [Kim and Das Sarma, 1994; Krug, 1994] and the

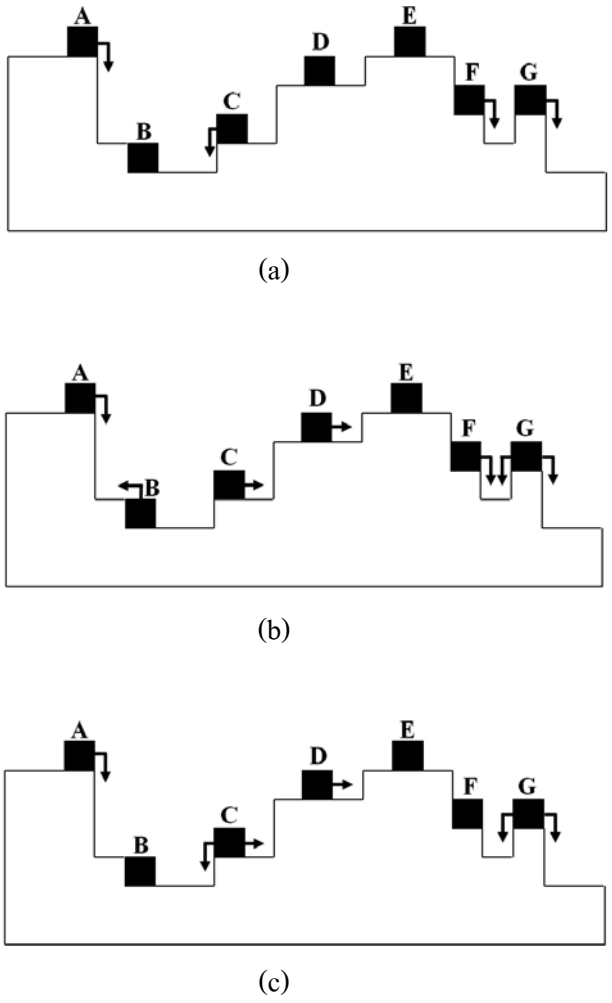

Figure 2.1Diagrams showing diffusion rules of (a) the Family model, (b) the LC model and (c) the DT model.

Das Sarma-Tamborenea (DT) model [Das Sarma and Tamborenea, 1991]. In all models, the deposited atoms are allowed to diffuse to one of their nearest neighbors depending on the diffusion rule of the model after a random deposition (see Figure 2.1).

2.2.1 Family Model

The diffusion rule of the Family model [Family, 1986] states that after deposition, the deposited atom searches for a site with the minimum height from its nearest neighboring sites. From Figure 2.1(a), if an atom is deposited at position A, C, F or G, it will move in the direction of the arrow in order to minimize its height. However, if an atom is deposited at position B, D or E, it will stick at the deposition site. In the case that there are more than one sites that have minimum height, the deposited atom chooses one of them by random. The diffusion rules lead to very smooth films [Family, 1986]. A typical morphology grown from the Family model is shown in Figure 2.2. It is explicitly seen from the morphology that the Family model has up-down symmetry i.e. the morphology is statistically unchanged when the film is turned upside-down.

2.2.2 Larger Curvature Model

For the larger curvature (LC) model [Kim and Das Sarma, 1994; Krug, 1994], the deposited atom searches for the site that the local curvature has the largest value as shown in Figure 2.1(b). For one dimensional substrate, the local curvature of the site i is $H(i+1)+H(i-1)-2H(i)$ and the local curvature of the site (i, j) for two dimensional substrate is $H(i+1, j)+H(i-1, j)+H(i, j+1)+H(i, j-1)-4H(i, j)$. If there are more than one neighbors whose value of the local curvature is largest (atom G in Figure 2.1(b)), one of them is chosen with equal probability. A typical morphology grown from the LC model shown in Figure 2.3 presents the mound formation of the model. Similar to the Family model, the up-down symmetry can be seen from the morphology of the LC model.

2.2.3 Das Sarma-Tamborenea Model

For the Das Sarma-Tamborenea (DT) model [Das Sarma and Tamborenea, 1991], the deposited atom diffuses to one of the nearest neighboring sites in order to increase its bond and stops moving when the number of bond is greater than one (see Figure 2.1(c)). For example, atoms A and D have only one bond and each has only one neighbor with a larger number of bonds so they move in the direction of the arrows. Atoms C and G choose one of the neighbors by random because both left and right neighbors offer more bonds. Atoms B and F do not move because they

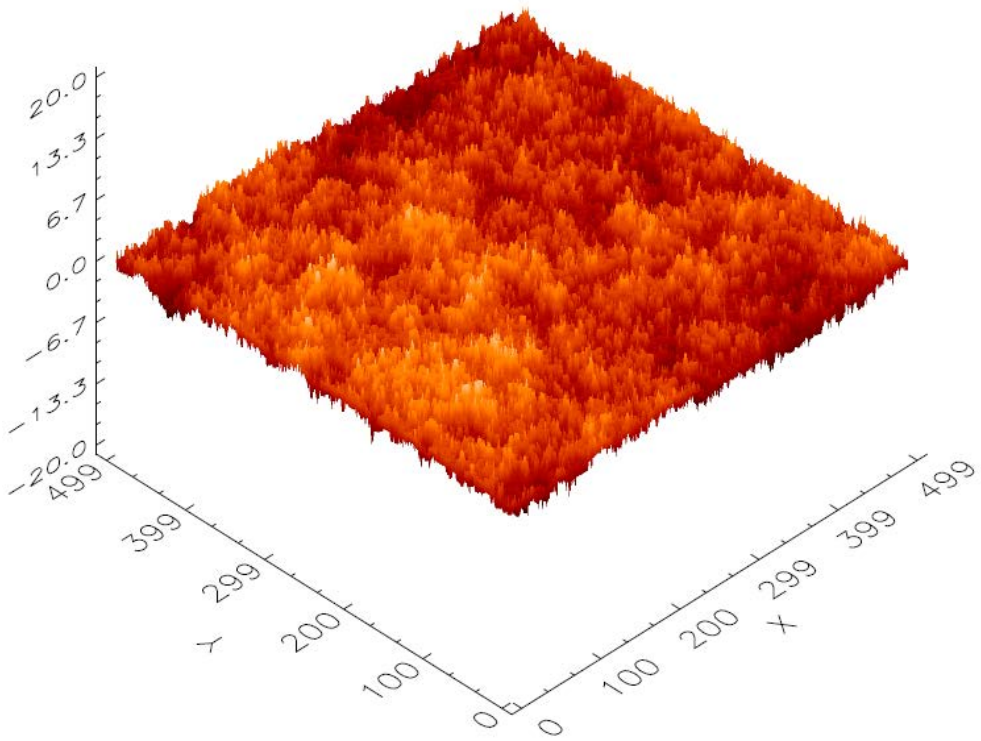

Figure 2.2 A morphology of the (2+1)-dimensional Family model at $t = 10^5$ MLs of the system size $L \times L = 500 \times 500$ sites.

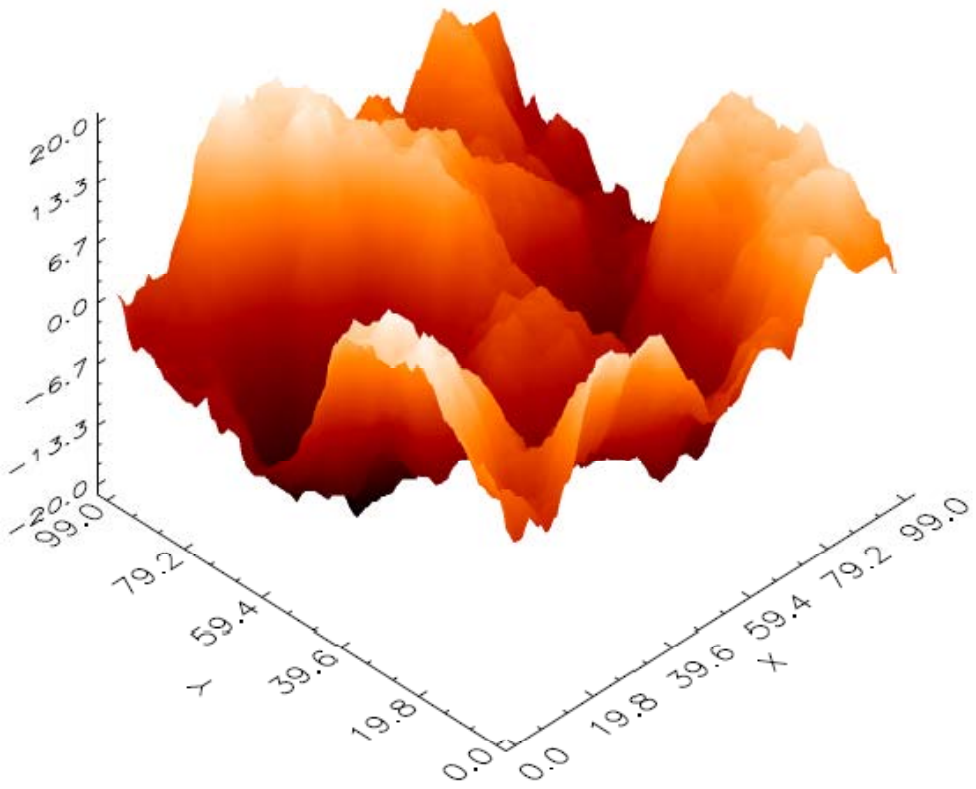

Figure 2.3 A morphology of the (2+1)-dimensional LC model at $t = 10^6$ MLs of the system size $L \times L = 100 \times 100$ sites.

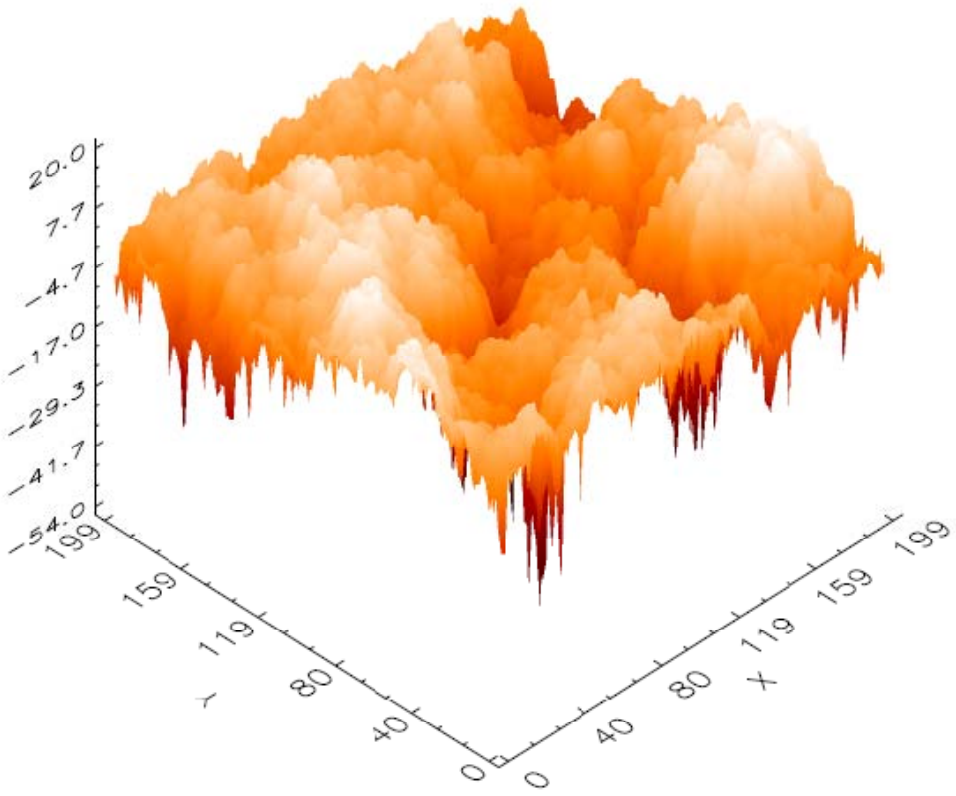

Figure 2.4 A morphology of the DT model at $t = 5 \times 10^5$ MLs of the system size $L \times L = 200 \times 200$ sites.

already have 2 bonds at the deposition site. Finally, atom E does not move because it cannot increase bond after moving. As can be seen in Figure 2.4, the morphology of the DT model shows round top surface and deep grooves which is obviously different when the film is turned upside-down. As a result, the DT model does not have up-down symmetry.

2.3 Continuum Growth Equation

All models studied here are conserved growth model which means that the number of atoms is constant i.e. all deposited atoms are incorporated on the substrate to create the whole film. The continuum growth equation described the particle conservation law can be written as

$$\frac{\partial h(\vec{r},t)}{\partial t} = -\vec{\nabla}\cdot\vec{J} + \eta(\vec{r},t) \tag{2.10}$$

where $\vec{J}$ is the particle current and η represents uncorrelated non-conserved noise. The current $\vec{J}$ is assumed to be a gradient of K [Kim and Das Sarma, 1994] as

$$\vec{J} = -\vec{\nabla}K. \tag{2.11}$$

The form of the function K depends on models and the symmetry of the field. For surface growth phenomena, K can be written in the form of h, $\nabla^2 h$, $(\nabla h)^{2n}$ where $n = 1, 2, 3....$

The Family and the LC models are described by linear growth equations. The linearity indicates that the models have up-down symmetry which means the morphology looks the same when it undergoes a transformation of $h \to -h$ (see Figures 2.2 - 2.3). For the Family model, the continuum growth equation that describes long-time properties of the model is the Edwards-Wilkinson (EW) equation [Edwards and Wilkinson, 1982] with $K = v_2 h$:

$$\frac{\partial h(\vec{r},t)}{\partial t} = v_2\nabla^2 h(\vec{r},t) + \eta(\vec{r},t) \tag{2.12}$$

while the LC model is described by the Mullins-Herring (MH) equation [Mullins, 1957; Herring, 1950] with $K = -v_4\nabla^2 h$:

$$\frac{\partial h(\vec{r},t)}{\partial t} = -v_4\nabla^4 h(\vec{r},t) + \eta(\vec{r},t) \tag{2.13}$$

when v_2 and v_4 are constants.

The DT model, on the other hand, is believed to be described by a nonlinear growth equation which indicates that the model does not have up-down symmetry. The DT model is more realistic for MBE growth study. The DT model has been studied extensively in the literature [Punyindu and Das Sarma, 1998; Brendel et al. 1998; Das Sarma et al. 2002; Punyindu and Das Sarma, 2002; Krug, 1994; Dasgupta et al. 1997] because it has features that cannot be explained by simple scaling arguments based on a continuum description [Krug, 1994; Dasgupta et al. 1997]. The (1+1)-dimensional DT model is believed to be described by the nonlinear MBE growth equation with infinite terms [Krug, 1994; Das Sarma et al. 1996; Dasgupta et al. 1996; Dasgupta et al. 1997; Krug, 1997]:

$$\frac{\partial h(\vec{r},t)}{\partial t} = -v_4 \nabla^4 h(\vec{r},t) + \lambda_{22} \nabla^2 \left(\nabla h\right)^2 + \sum_{n=4,6,8,\ldots} \lambda_{2n} \nabla^2 \left(\nabla h\right)^n + \eta(\vec{r},t) \quad (2.14)$$

where λ_{22} and λ_{2n} are constants. It has been shown [Das Sarma et al. 2002] that the higher order terms with $n \geq 4$ have very weak influence in the (1+1)-dimensional DT model. As a result, the model can be approximately described by the nonlinear fourth order equation. For the (2+1)-dimensional DT model, it is described by the following continuum equation [Das Sarma et al. 2002]:

$$\frac{\partial h(\vec{r},t)}{\partial t} = v_2 \nabla^2 h(\vec{r},t) - v_4 \nabla^4 h(\vec{r},t) + \sum_{n=1,2,3,\ldots} \lambda_{2(2n)} \nabla^2 \left(\nabla h\right)^{2n} + \eta(\vec{r},t). \quad (2.15)$$

It can be seen that, asymptotic behaviors of the same growth model may differ when the systems have different substrate dimensions.

2.4 Universality Class

Discrete growth models can be classified by the set of critical exponents (α, β, z) used to defined the universality class. The universality class describes asymptotic properties of the kinetic roughness of a growth process. Two models that have the same set of (α, β, z) are said to be in the same universality class and have the same asymptotic behaviors.

The Family model has been extensively studied [Edwards and Wilkinson, 1982; Family, 1986; Barabasi and Stanley, 1995; Castez et al. 2004; Röthlein et al. 2006] and found to

asymptotically belong to the EW universality class in which the associated critical exponents obtained from Eq. (2.12) are [Edwards and Wilkinson, 1982] $\alpha = \frac{2-d}{2}, \beta = \frac{2-d}{4}$ and $z = 2$. The LC model has also been thoroughly studied [Kim and Das Sarma, 1994; Krug, 1994; Barabasi and Stanley, 1995; Krug et al. 1997]. The critical exponents for the LC model that belongs to MH universality class are [Barabasi and Stanley, 1995] $\alpha = \frac{4-d}{2}, \beta = \frac{4-d}{8}$ and $z = 4$. In these equations, d is the dimension of the substrate.

The (1+1)-dimensional DT model belongs to the MBE universality class and the associated critical exponents are [Barabasi and Stanley, 1995; Das Sarma and Tamborenea, 1991] $\alpha = \frac{4-d}{3}, \beta = \frac{4-d}{8+d}$ and $z = \frac{8+d}{3}$. However, the (2+1)-dimensional DT model is determined [Das Sarma et al. 2002] by the noise reduction technique [Punyindu and Das Sarma, 1998] to belong to the generic EW universality class where the critical exponents are $\alpha = \frac{2-d}{2}, \beta = \frac{2-d}{4}$ and $z = 2$.

In addition, it was well-established that all models studied here when the film is grown on a flat substrate obey the Family-Vicsek scaling relation [Family and Vicsek, 1985] i.e. $\beta = \alpha / z$. The scaling relation implies that only two independent exponents are required.

In this dissertation, sets of (α, β, z) for each model are obtained from our simulations. Figures 2.5-2.10 show the scaling collapse of W / L^{α} versus t / L^{z} and W / t^{β} versus t / L^{z} from different system sizes L for all models in both one and two dimensional substrates. The critical exponents are the values that lead to the best data collapse. For the (1+1)-dimensional Family model shown in Figure 2.5, we obtain the same values of the critical exponents as those from the EW equation: $(0.5,\ 0.25,\ 2)$. For the LC model, we obtain $(1.5,\ 0.375,\ 4)$ and $(1,\ 0.25,\ 4)$ for one and two dimensional substrates respectively. These are consistent with theoretical values (see Figures 2.7-2.8).

However, in simulations, transient conditions, finite size effects and crossover effects can cause differences in values of the critical exponents. For instant, growth from initially flat substrate leads to small nonzero values of α and β for (2+1)-dimensional Family model which, according to the EW equation, the interface width should saturate immediately. The values of critical exponents found from the collapse of the scaling curve in Figure 2.6 are $(0.08,\ 0.04,\ 2)$ instead of the theoretical values of $(0,\ 0,\ 2)$. Moreover, our results show that the DT model has strong dependence on the system size. For the (1+1) and (2+1)-dimensional DT models, the

critical exponents for limited substrate size in this work are (see Figures 2.9-2.10) $(1.30,\ 0.375,\ 3.25)$ and $(0.5,\ 0.19,\ 2.6)$ respectively. These are different from those obtained from the continuum equations. Besides, there are crossover effects of the growth exponent from $\beta = 0.25$ to $\beta = 0.19$ for (2+1)-dimensional DT model. As a result, the early-time data for different values of β do not exhibit a scaling collapse. Even if the universality class of the nonlinear DT model is known, the model is still not completely understood due to the existence of the higher order terms and the very long transient regime in two dimensional systems.

Another interesting point for models belonging to the EW universality class in two dimensional substrates is that the critical exponents are $\alpha = 0$, $\beta = 0$ and $z = 2$. This means that the scaling function of the interface width is logarithmic [Barabasi and Stanley, 1995]. It can be seen from results of the (2+1)-dimensional Family model shown in Figure 2.11(a). When we plot W as a function of t in a semi-log scale, W scales logarithmically with t in the early time range and can be fit with

$$W(t,L) = \beta' \log(t-1) + \text{const} \tag{2.16}$$

for $t << L^z$. We then consider the saturation part of the interface width by plotting $\Delta(t,L) = \beta' \log(t-1) - W(t,L)$ as a function of t/L^z where $z = 2$. We found that Δ saturates in the early time range and it scales logarithmically with t/L^z in the late time range. The collapse of all plots shown in Figure 2.11(b) shows that Δ scales with L and t. The scaling form of $\Delta(t,L)$ is

$$\Delta(t,L) \sim f\left(\frac{t}{L^z}\right). \tag{2.17}$$

Comparing with the scaling form of the interface width $W(t,L) \sim L^{\alpha} f\left(t/L^z\right)$, the critical exponents of models belonging to the EW universality class in two dimensional substrates are $\alpha = 0$ (log), $\beta = 0$ (log) and $z = 2$ which are consistent with those obtained from the EW equation.

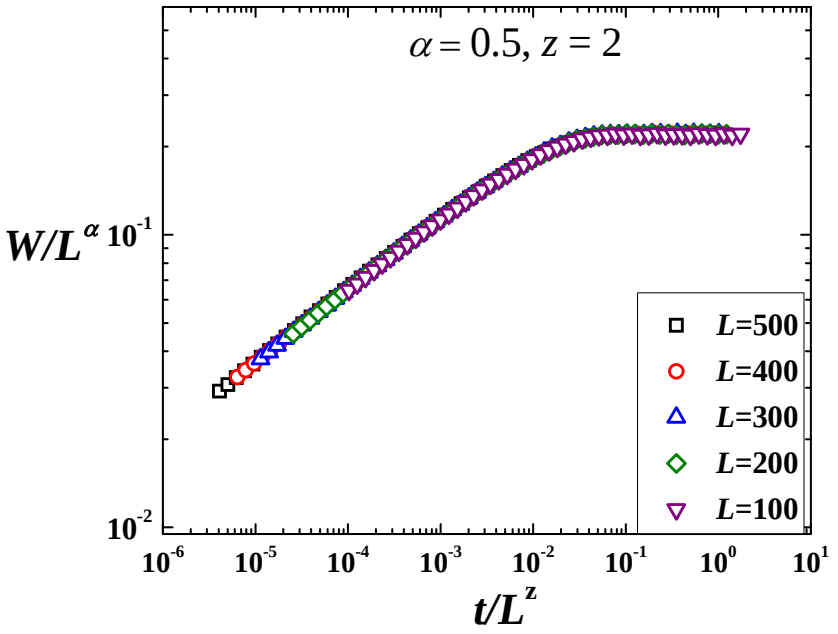

(a)

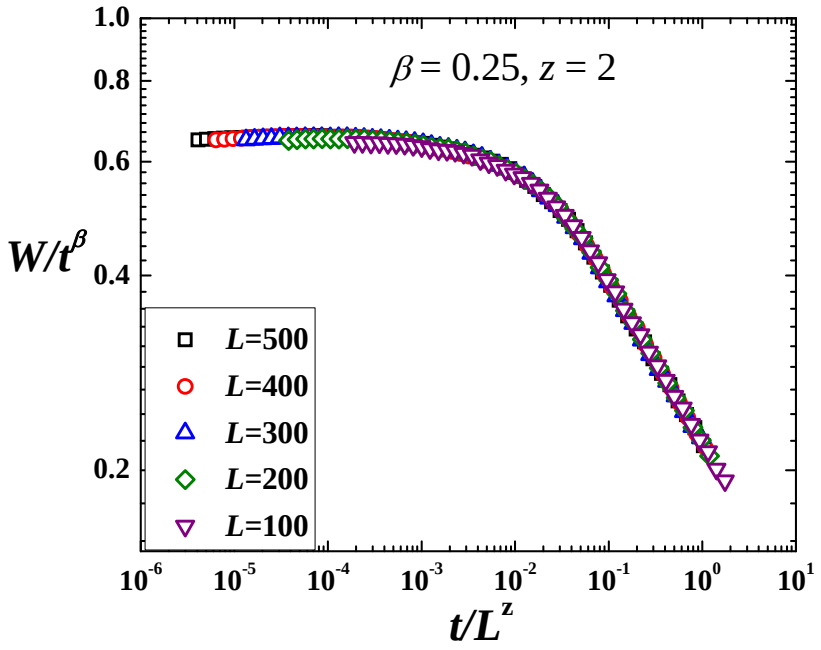

(b)

Figure 2.5 Scaling plots showing the data collapse of (1+1)-dimensional Family model for five system sizes. The best collapse is obtained when $\alpha = 0.5$, β=0.25 and $z = 2$.

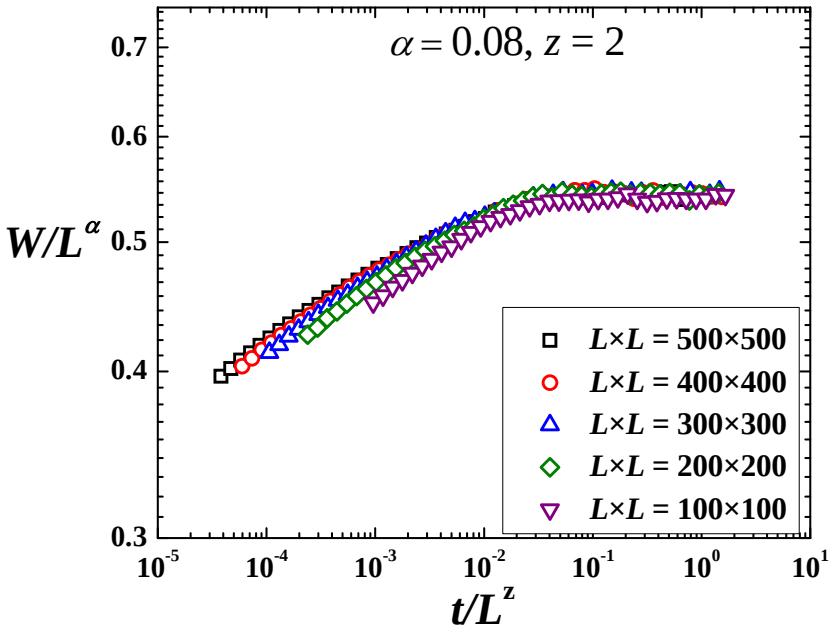

(a)

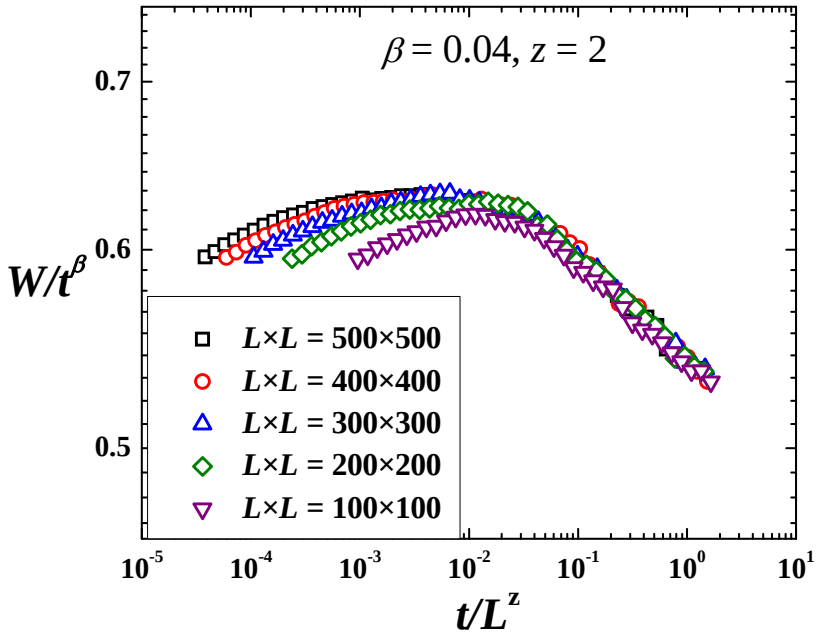

(b)

Figure 2.6 Scaling plots showing the data collapse of (2+1)-dimensional Family model for five system sizes. The best collapse is obtained when $\alpha = 0.08$, β=0.04 and $z = 2$.

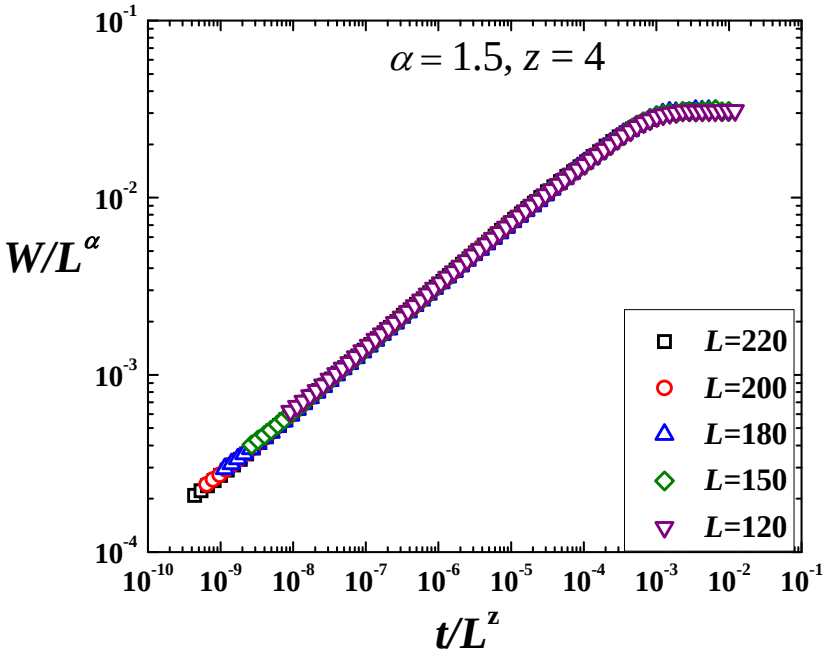

(a)

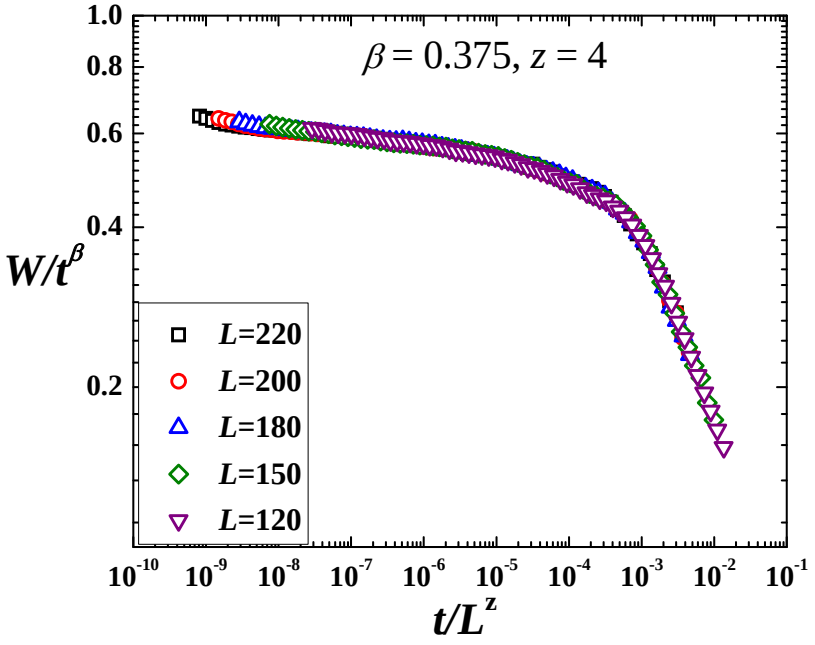

(b)

Figure 2.7 Scaling plots showing the data collapse of (1+1)-dimensional LC model for five system sizes. The best collapse is obtained when $\alpha = 1.5$, $\beta = 0.375$ and $z = 4$.

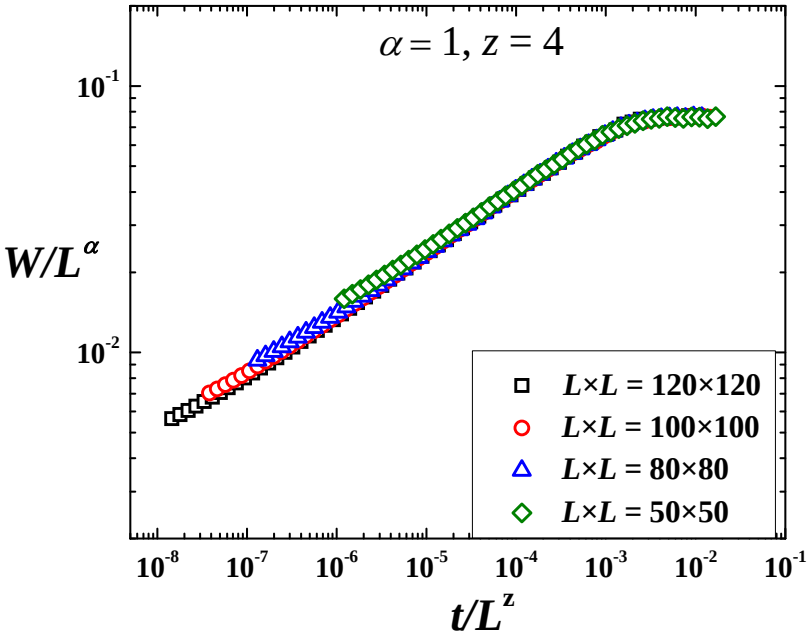

(a)

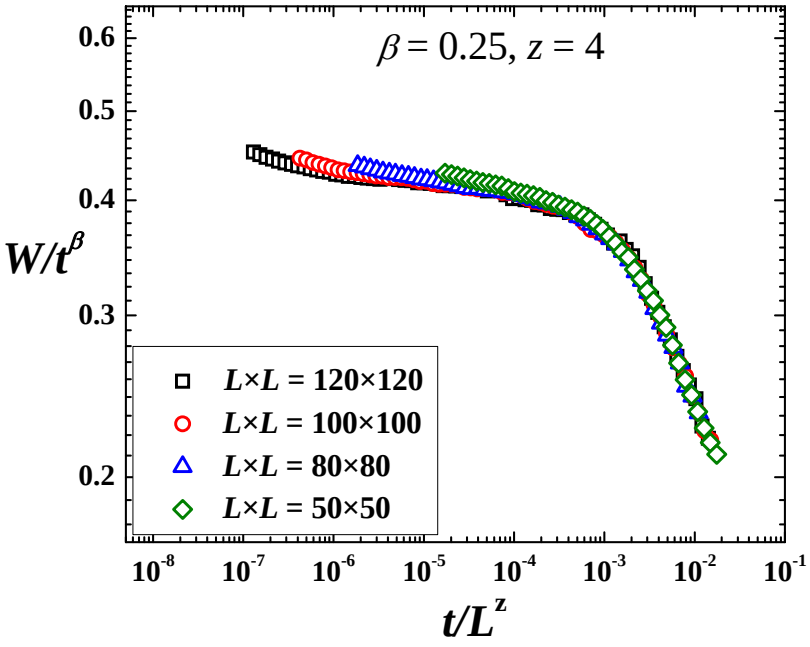

(b)

Figure 2.8 Scaling plots showing the data collapse of (2+1)-dimensional LC model for five system sizes. The best collapse is obtained when $\alpha = 1$, $\beta = 0.25$ and $z = 4$.

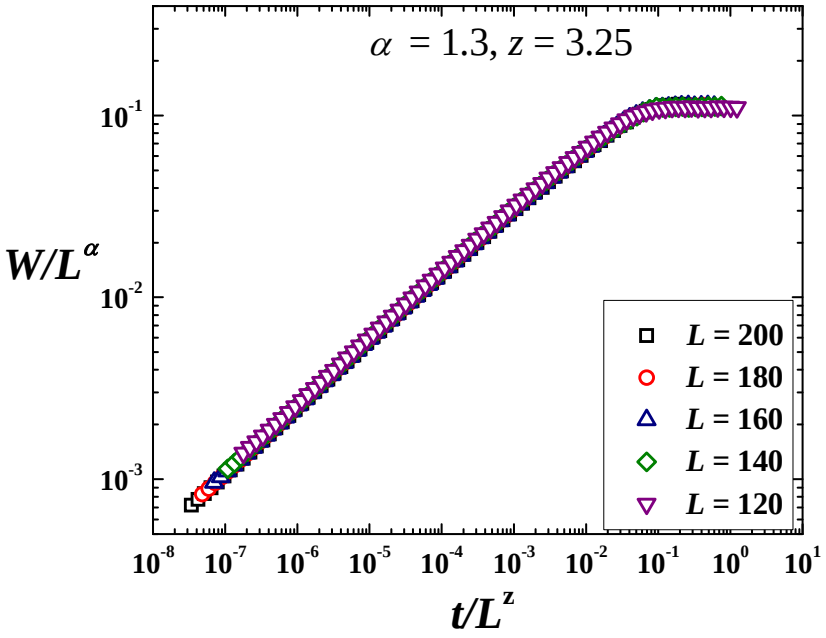

(a)

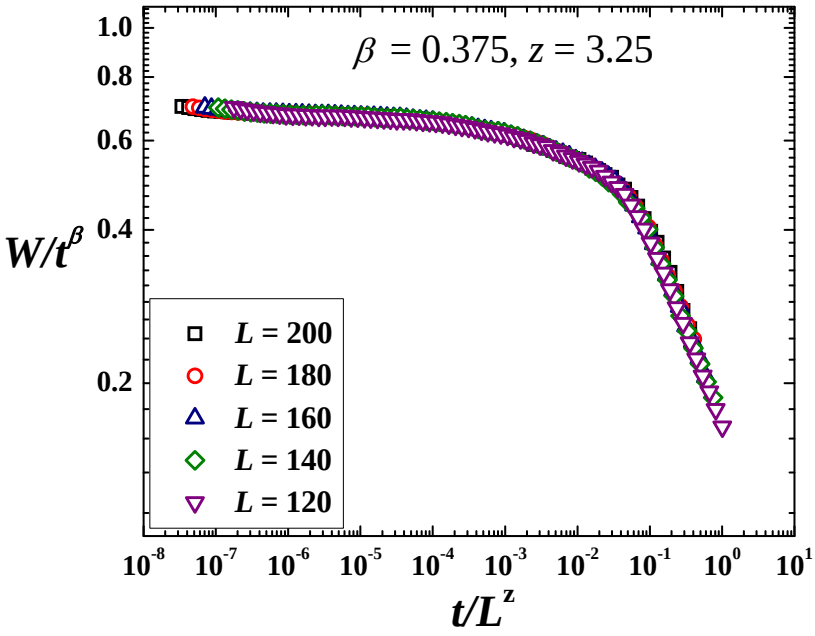

(b)

Figure 2.9 Scaling plots showing the data collapse of (1+1)-dimensional DT model for five system sizes. The best collapse is obtained when $\alpha = 1.30$, $\beta = 0.375$ and $z = 3.25$.

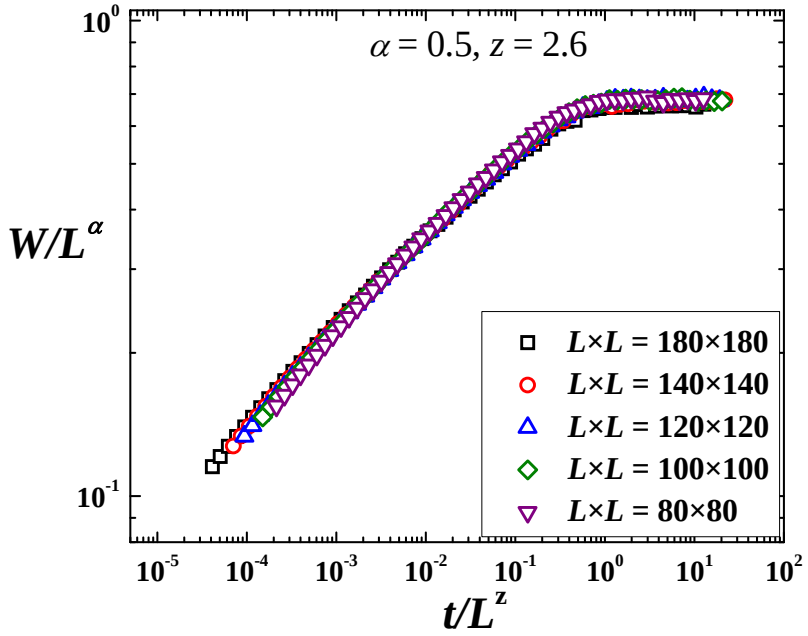

(a)

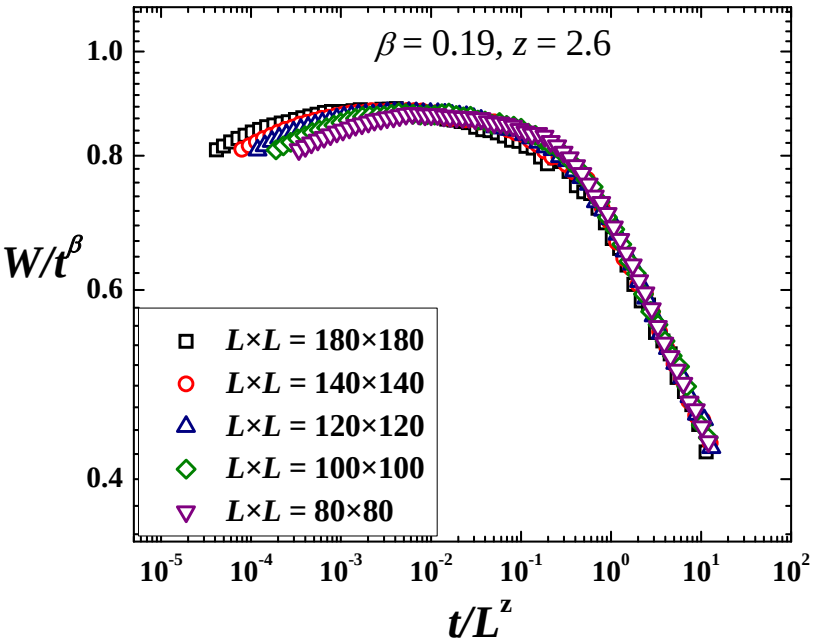

(b)

Figure 2.10 Scaling plots showing the data collapse of (2+1)-dimensional DT model for five system sizes. The best collapse is obtained when $\alpha = 0.5$, β=0.19 and $z = 2.6$.

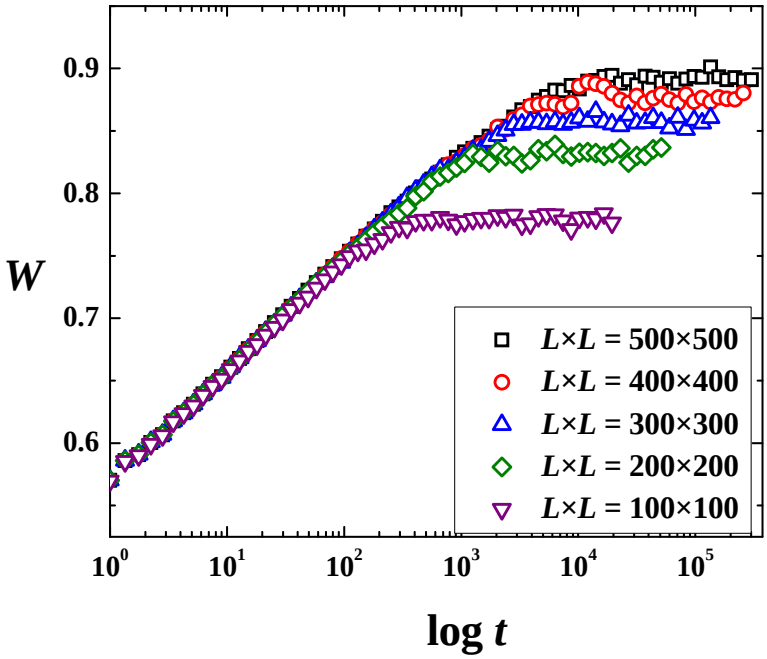

(a)

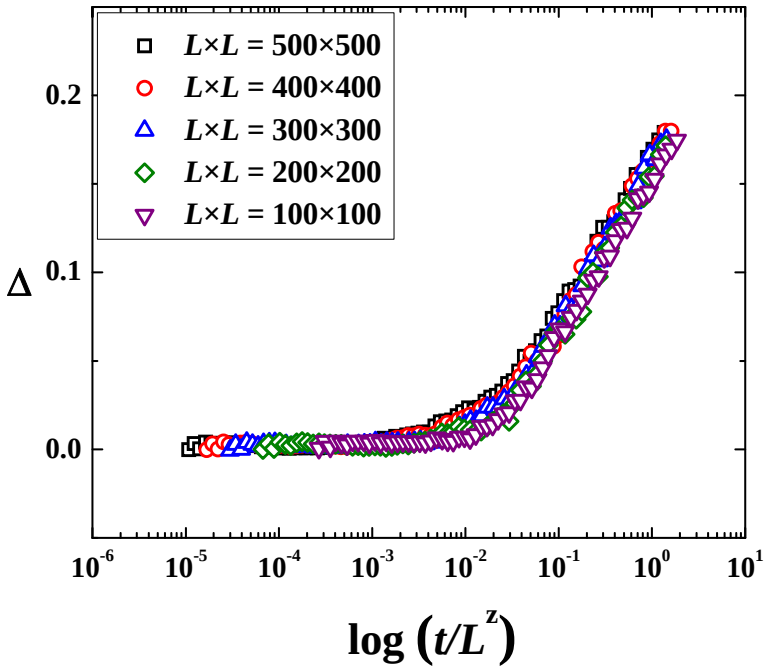

(b)

Figure 2.11 Scaling plots of the interface width in the semi-log scale of (2+1)-dimensional Family model for five system sizes. (a) The interface width in the semi-log scale. (b) The data collapse of $\Delta(t, L)$ which gives the scaling form $\Delta(t, L) \sim f\left(t / L^{z}\right)$.

Chapter III

Effects of Discrete Sampling Time and System Size on Persistence Probabilities

3.1 Persistence Probabilities of Models with and without Up-Down Symmetry

The positive and negative persistence probabilities after averaging over all values of the initial height of the Family and the DT models grown on two dimensional flat substrates are found to have a power-law decay with time. Figure 3.1 shows the transient and steady-state persistence probabilities of the two models. The system size used for the Family model is $L \times L = 500 \times 500$ sites while that used for the DT model is $L \times L = 100 \times 100$ sites. The transient persistence probabilities ($t_0 = 0$) shown in Figure 3.1(a) decrease with time as a power law at late times for both models. The persistence exponents of the Family model, calculated from the slopes of the curves, are $\theta_+^T \approx 5.31$ and $\theta_-^T \approx 5.31$. The positive and negative persistence exponents are equal to each other for this model with up-down symmetry, so are the persistence probabilities at each time instant. The large value of the transient persistence exponents of the Family model indicates that the persistence probabilities of the model decrease rapidly with time. For the transient region of the DT model, the persistence exponents are $\theta_+^T \approx 2.82$ and $\theta_-^T \approx 2.39$. It can be seen that for the model without up-down symmetry, the positive persistence exponent is not equal to the negative persistence exponent. Moreover, by comparing the value of the positive and negative persistence probabilities at the same time, it can be seen from Figure 3.1(a) that they are not equal to each other. In this region, the initial heights for all sizes are zero. The almost-flat morphology of the Family model leads to the rapid zero-crossing of the height fluctuation. As a result, the transient persistence exponents of the Family model is larger than those of the DT model i.e. the transient persistence probabilities of the Family model decrease faster than those of the DT model as can be seen in Figure 3.1(a).

The persistence probabilities in the steady-state region are shown in Figure 3.1(b). The initial time t_0 is larger than the saturation time of the system i.e. $t_0 = 10^5$ MLs for the Family model while $t_0 = 6 \times 10^6$ MLs for the DT model. For the Family model, the steady-state

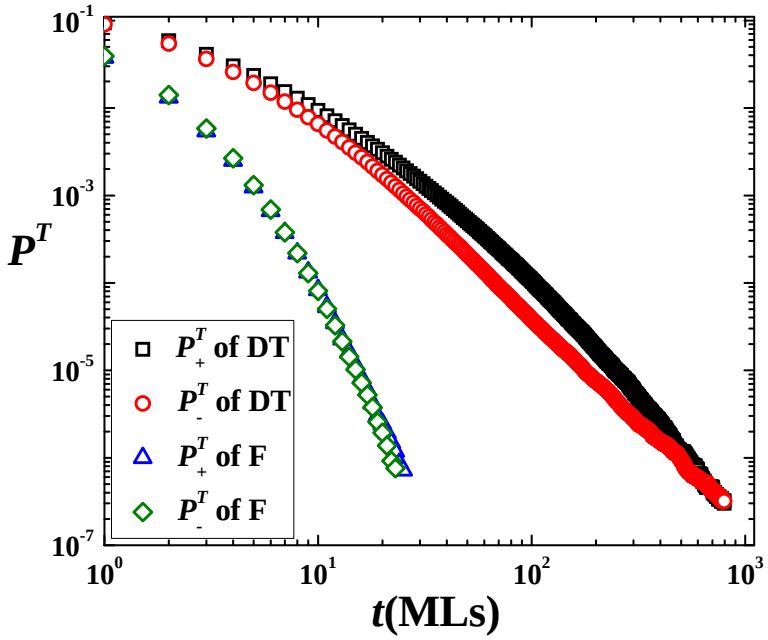

(a)

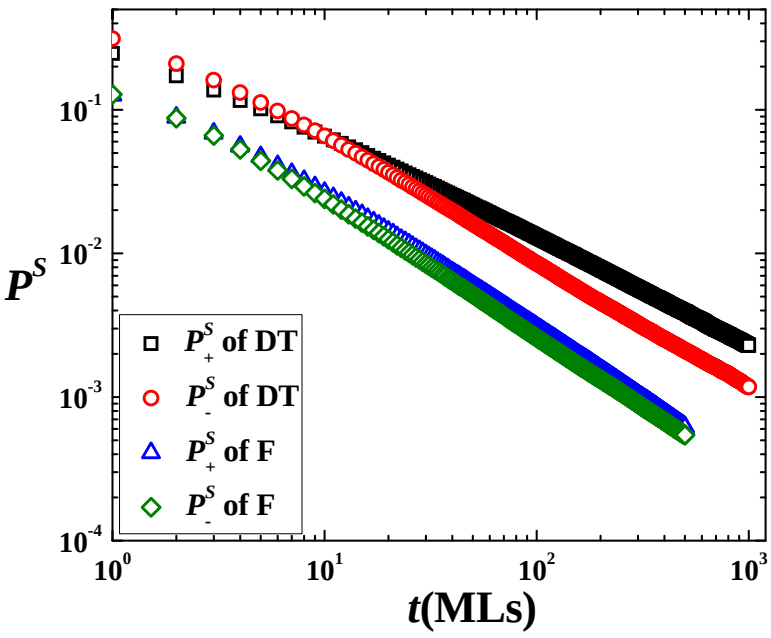

(b)

Figure 3.1 Positive and negative persistence probabilities of DT and Family models: (a) transient region, and (b) steady-state region.

persistence exponents are $\theta_+^S \approx 0.98$ and $\theta_-^S \approx 0.98$. We observe that for the Family model, $\theta_+ = \theta_-$ for both regions. We also obtain similar results for the larger curvature model, another up-down symmetric model. As a result, for models with up-down symmetry, the positive persistence exponent is equal to the negative persistence exponent in both regions. Like the persistence exponents, the positive and negative persistence probabilities are approximately equal to each other when they are compared at the same time. For the DT model, the positive and negative persistence exponents are $\theta_+^S \approx 0.77$ and $\theta_-^S \approx 0.88$. Like the transient region, the positive and negative persistence exponents are not equal to each other due to the effect of the up-down asymmetry of the model. Similar results are found for the persistence probabilities. Our results for these models are consistent with results by Constantin et al. [Constantin et al. 2004].

By comparing the value of the persistence probabilities between the two models at the time $t = t_0 + 1$, the persistence probabilities of the DT model are larger than those of the Family model. As the definition of the persistence probability, the persistence probability of a site r, $p(r)$, is zero when the height fluctuation of the site r is equal to that at the initial time t_0. The average of the persistence probability over all sites, P, will be large when the morphology of the film is very different from the initial pattern (flat substrate in this case). The morphology of the DT model is rougher than that of the Family model; as a result, $P(t_0 + 1)$ of the DT model is larger.

By comparing the persistence exponent between transient and steady-state regions in the same model, it is found that $\theta^T > \theta^S$ which means that P^T decreases with time more rapidly than P^S. In the steady-state region ($t_0 >> t_s$), the roughness is the largest: there are many sites that the initial value of the height fluctuation, $|h_0|$, is much larger than the average value (0). After one monolayer of atoms is deposited, most of these sites will have $|h(t_0 + 1)| < |h_0|$ and the difference between values of the height fluctuation and h_0 becomes larger as t increases in the early time range, so these sites take long time for their height fluctuation to return to h_0. As a result, P^S decreases slower than P^T, therefore $\theta^T > \theta^S$.

For the steady-state exponent, θ^S, it was pointed out by Krug, et al [Krug, et al. 1997] that θ^S for models with up-down symmetry is related to the growth exponent, β as

$$\theta_+^S = \theta_-^S = 1 - \beta. \tag{3.1}$$

For (2+1)-dimensional Family model, $\beta = 0$. Our results for the Family model agree with this relation which is $\theta^S \approx 0.98 \approx 1$. For models without up-down symmetry, Constantin, et al. [Constantin, et al. 2004] pointed out that the smaller persistence exponent is related to the relation of Eq. (3.1). For (2+1)-dimensional DT model with $\beta = 0.19$ (see Figure 2.10), our results are approximately consistent with Eq. (3.1) with $\theta_+^S \approx 0.77$.

The effects of the initial time on the steady-state persistence probabilities are also studied. Numerical results of the DT model for the system of size $L \times L = 200 \times 200$ sites using different values of t_0 show that the choice of t_0 is not very significant (except for a very small t_0) to the calculated steady-state persistent exponents as shown in Figure 3.2. Similar results are obtained from the Family model. This means that we can choose the value of initial time to be less than the saturation time in order to get the results more quickly.

3.2 Effects of System Size and Discrete Sampling Time on Persistence Probability

In this section, we consider results for the average steady-state persistence probabilities $P^S(t)$ which is the average of $P_+^S(t)$ and $P_-^S(t)$. We determine the dependence of $P^S(t)$ on the discrete sampling time δt and the sample system size L for the Family, the LC and the DT models grown in one and two dimensional substrates. Similar results are obtained from all models. To avoid repetition, only results from a selected model are shown for each plot.

3.2.1 Effects of Sample System Size on Persistence Probability

In the study of effects of the substrate size on the persistence probability, we observe that the persistence exponent increases as the system size is decreased. Figure 3.3 shows the plots of $P^S(t)$ of (1+1)-dimensional DT model for different system sizes with the same sampling time. It can be seen that all plots show a good power-law decay for relatively small value of t; however, the decay rate of $P^S(t)$ for small sample is greater than that for large sample. The reason is that when t approaches t_s the fluctuations at time $t_0 + t$ is completely uncorrelated with the fluctuations at time t [Constantin et al. 2004]. As a result, the decay of the persistence probability becomes faster when $t \geq t_s$ which occurs earlier for smaller size of the substrate. When considering the same range of t, the decay rate of the persistence probability as well as the

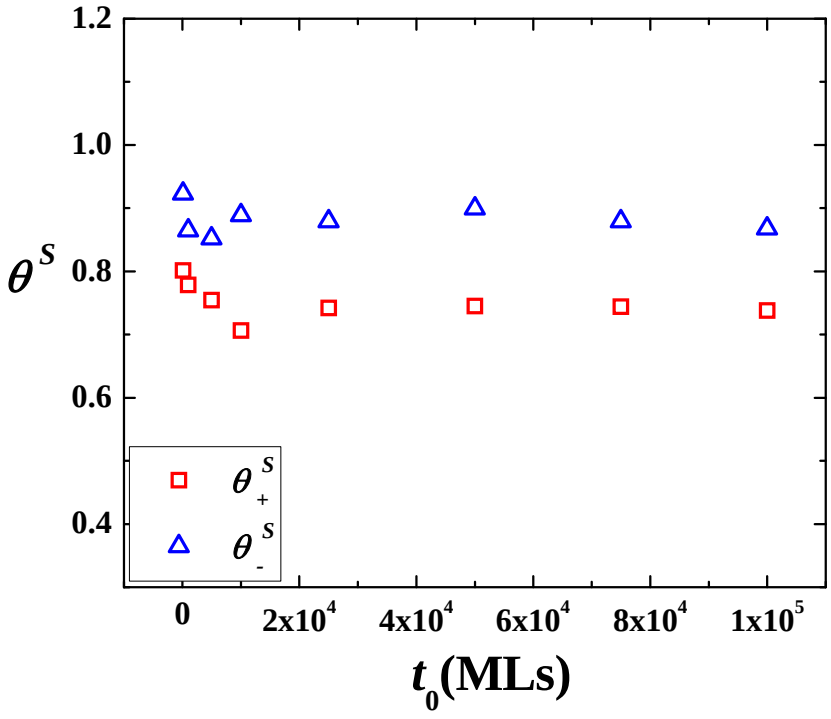

Figure 3.2 Positive and negative steady-state persistence exponents of the DT model for various initial times.

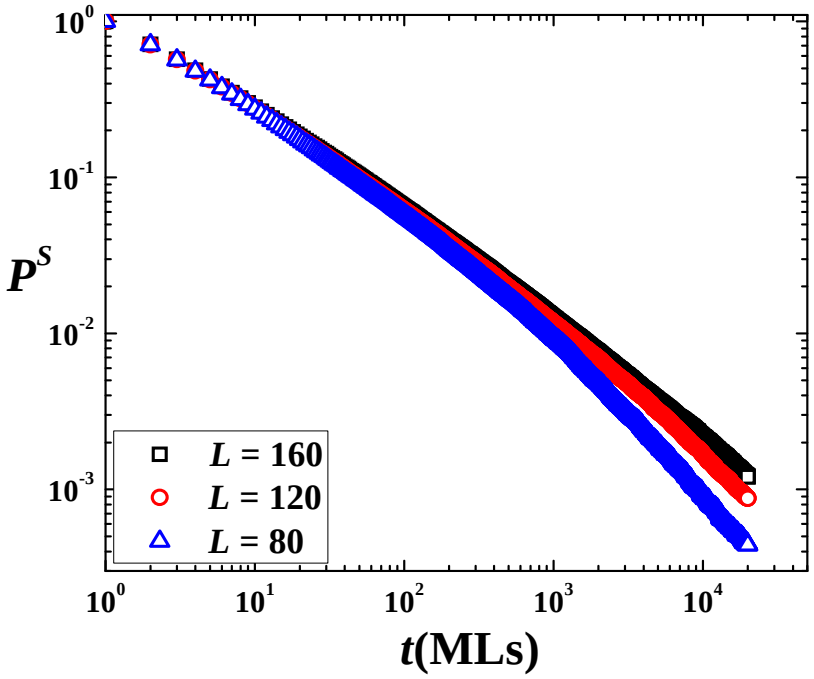

Figure 3.3 Steady-state persistence probability of (1+1)-dimensional DT model for three different substrate sizes with the same discrete sampling time $\delta t = 135$.

value of the persistence exponent increases with the decrease of L.

Moreover, the growth exponent β decreases when L is decreased because the system of smaller size reaches steady-state faster. The crossover region from power-law growth of the interface width to a constant saturated width, which occurs earlier, causes smaller value of β. The ways P^S and θ^S depend on L as mentioned above preserve the relation $\theta_+^S = \theta_-^S = 1-\beta$.

3.2.2 Effects of Discrete Sampling Time on Persistence Probability

The study of effects of the sampling time on the persistence probability shows that the sampling time strongly affects the value of persistence probabilities. Figure 3.4 show the plots $P^S(t)$ of (2+1)-dimensional Family model for different values of discrete sampling time with the same system size. All plots decay with a power-law behavior. At a particular value of t, $P^S(t)$ is found to increase as δt is increased. The reason is that when δt is large, there are sites that the height fluctuation actually returns to its initial value already but the fluctuation then becomes larger or smaller than the initial value again. If these returning events occur within a short period of time which is smaller than δt, they cannot be measured and those sites are still counted for $P^S(t)$. The number of undetectable crossing events is smaller when the time interval between two successive measurements (δt) is small. However, as we observe from Figure 3.4, the persistence exponents computed from the slopes of the graph are not affected by δt.

3.2.3 Scaling Relation for the Persistence Probability on Sampling Time and System Size.

The average steady-state persistence probability $P^S(t)$ for a system of size L with sampling time δt of (1+1)-dimensional Family model has been investigated to be a function of t/L^z and $\delta t/L^z$ [Constantin et al. 2004]. We expect a similar behavior for $P^S(t)$ measured in other models and also for (2+1)-dimensional systems. The value of δt and L are chosen in such a way that the ratio $\delta t/L^z$ is kept as a constant for each model. For up-down symmetric models, linear theory that describes large scale behavior of the model has been used successfully in the calculation of the exact value of the critical exponents. For the Family model, the dynamical exponent is found to be $z=2$ (Family, 1986), while $z=4$ for (1+1)- and (2+1)-dimensional LC model [Kim and Das Sarma, 1994; Krug, 1994]. On the other hand, the nonlinear DT model is

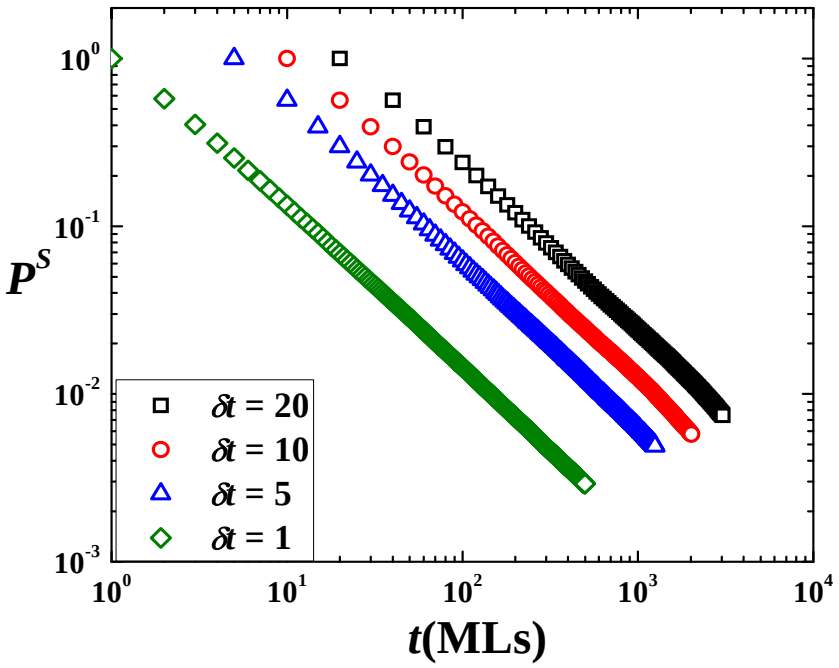

Figure 3.4 Steady-state persistence probability of (2+1)-dimensional Family model for four different values of discrete sampling time with the same substrate size $L \times L = 200 \times 200$ sites.

still not completely understood. Our results show that the DT model has strong system size dependence. For the (1+1) and (2+1)-dimensional DT models, the dynamical exponents for limited substrate size in this work are $z = 3.25$ and $z = 2.6$ respectively (see Figures 2.9 - 2.10).

In this work, the expected scaling variables are t / L^z, and $\delta t / L^z$. We measure $P^S(t)$ for three different values of L and δt while the value of $\delta t / L^z$ are fixed. As shown in Figure 3.5(a), different L and δt yield very different P^S versus t plots in the (1+1)-dimensional LC model. Despite the difference in the values, P^S from all systems show very good power-law behavior for relatively small value of time, $t < t_s$ with the same slope. When P^S is plotted against the scaled $t / \delta t$ axis, data from all three systems with the same value of $\delta t / L^z$ collapse into the same curve as shown in Figure 3.5(b). The same collapse is obtained for (2+1)-dimensional LC, the Family and the DT models. Figure 3.6 shows scaling collapse of (1+1)-dimensional DT model with $z = 3.25$. These results lead to the scaling relation for the dependence of the steady-state persistence probability on the system size and sampling time. The expected scaling relation of $P^S(t, L, \delta t)$ is the same scaling form as Constantin et al. [Constantin et al. 2004], that is

$$P^S(t, L, \delta t) = f\left(\frac{t}{L^z}, \frac{\delta t}{L^z}\right) \tag{3.2}$$

when the scaling function is $f(x, y) \sim x^{-\theta^S}$ where $x << 1$ and $y << 1$ is a constant, where θ^S is the steady-state persistence exponent. The same scaling relation is obtained for all models.

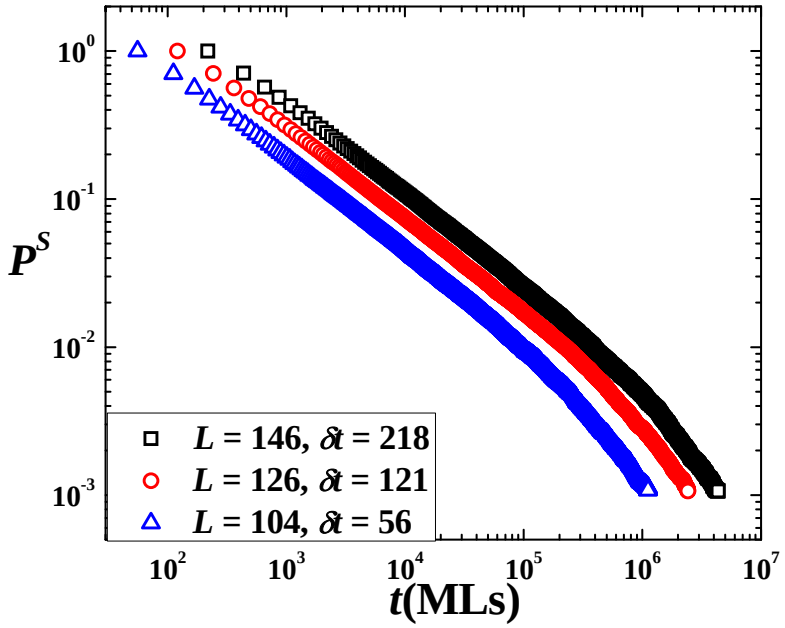

(a)

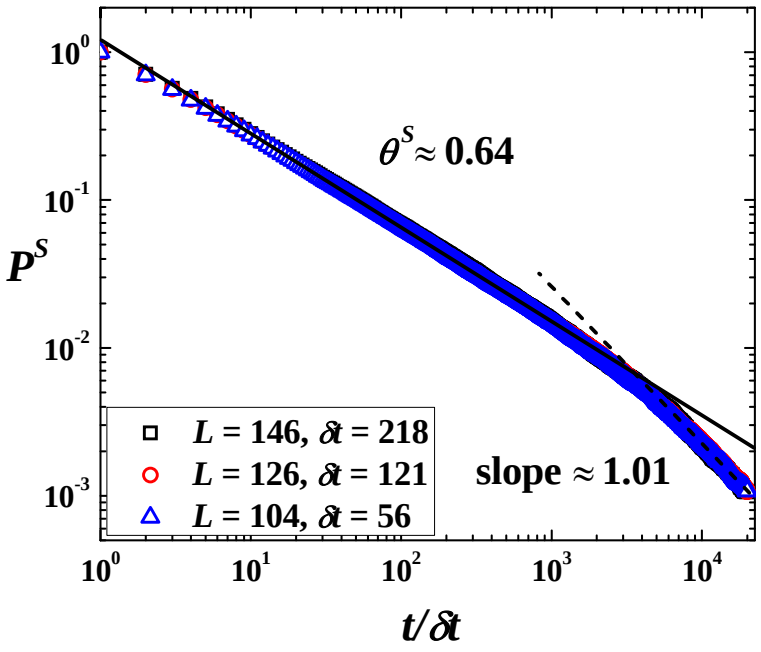

(b)

Figure 3.5 Steady-state persistence probability of the (1+1)-dimensional LC model for different substrate sizes and different discrete sampling times with the same ratio of $\delta t / L^z \approx 4.8\times10^{-7}$ (a) persistence probabilities versus time. (b) Finite size scaling of $P^S\left(t,L,\delta t\right)$.

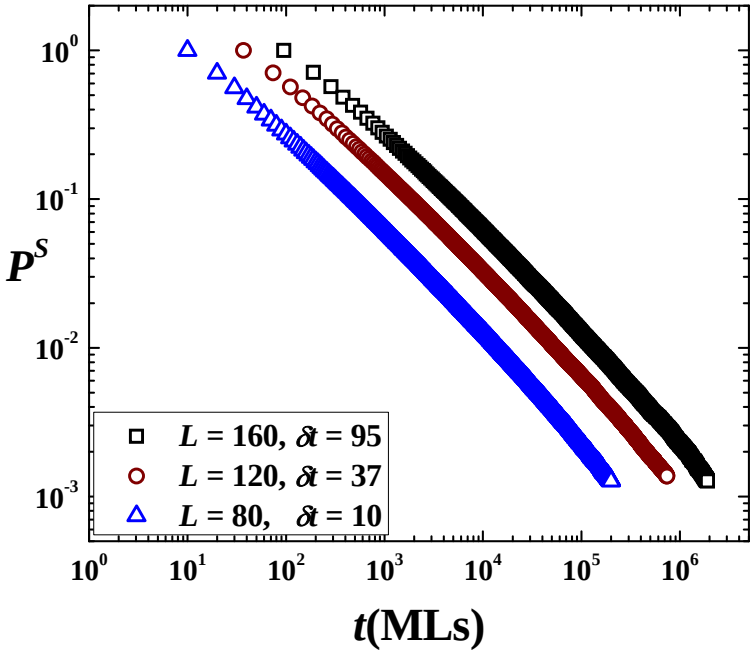

(a)

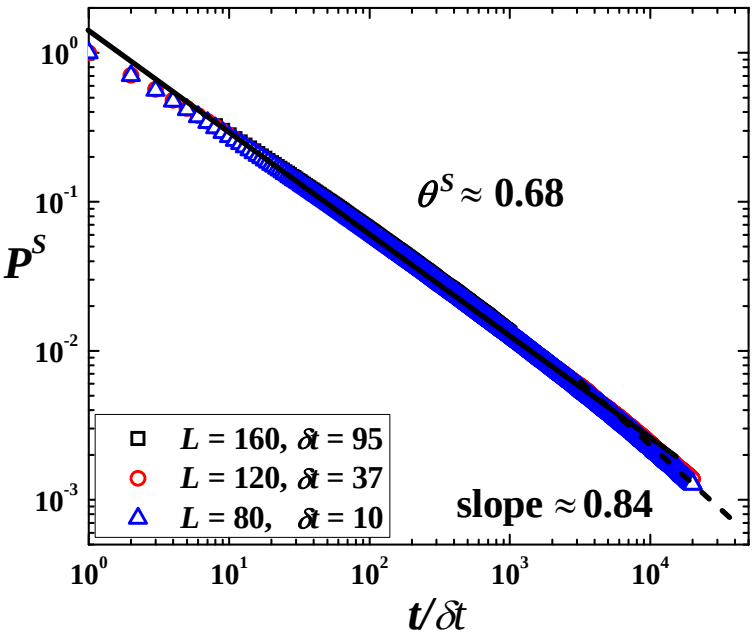

(b)

Figure 3.6 Steady-state persistence probability of the (1+1)-dimensional DT model for different substrate sizes and different discrete sampling times with the same ratio of $\delta t / L^z \approx 6.5\times10^{-6}$ (a) persistence probabilities versus time. (b) Finite size scaling of $P^S\left(t,L,\delta t\right)$.

Chapter IV

Effects of Initial Height on the Steady-State Persistence Probability

We investigate here the dependence of the steady-state persistence probabilities on the initial height, h_0. The models used are the (1+1)-dimensional Family and (1+1)/(2+1)-dimensional LC models. For the (2+1)-dimensional Family model, the film surface is very smooth and there are very small numbers of different values of h_0 available for the simulation. This makes it unsuitable for a study of the dependence of P^S on h_0. The positive and negative persistence probabilities for a fixed nonzero value of h_0 are expected to be different from each other even for models with up-down symmetry. Qualitative information for the behavior of the positive and negative persistence probabilities for a fixed nonzero value of h_0 may be obtained from the following considerations.

4.1 Distribution of the Height Fluctuations

In the up-down symmetric models considered here, the distribution of the values of the height fluctuation h is symmetric about zero. This distribution is Gaussian for the continuum growth equations appropriate for the Family and LC models. The discrete values of h obtained from simulations of these two models are also found to satisfy a Gaussian distribution with a high degree of accuracy. Figure 4.1 shows the distribution of h of the (1+1)-dimensional Family model. The persistence probabilities for a fixed value of the initial height h_0 are closely related to the statistics of the time intervals between successive instances when the height h at a site crosses the value h_0 during its evolution over a long time interval T. The positive (negative) persistence probability is obtained from the statistics of the intervals during which h remains larger (smaller) than h_0. The numbers of positive ($h > h_0$) and negative ($h < h_0$) time intervals in total time T are the same. However, for all positive values of h_0, the sum of the positive intervals, which is proportional to the probability that h is larger than h_0, is smaller than the sum of the negative intervals, which is proportional to the probability that h is smaller than h_0.

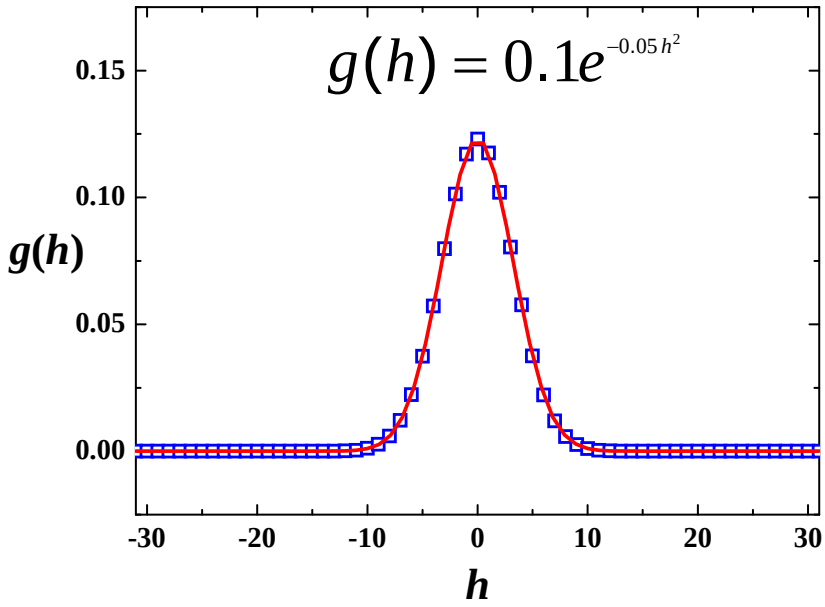

Figure 4.1 Distribution of h for the (1+1)-dimensional Family model of system size $L = 200$ sites ($t = 5\times10^5$ MLs). The solid line indicates a Gaussian fit with zero mean.

So the typical positive intervals are shorter than the negative ones for positive values of h_0 .This implies that the positive persistence probability should decrease faster in time than the negative persistence probability for positive values of the initial height h_0 . Also the symmetry of the distribution of h in up-down symmetric models considered here implies that the positive (negative) persistence probability for positive h_0 should be the same as the negative (positive) persistence probability for negative initial height, $-h_0$. Numerical results for these persistence probabilities are presented in the next section.

4.2 The Dependence of the Persistence Probability on the Initial Height

For both models, the positive and negative steady-state persistence probabilities, along with the persistence exponents are found to be approximately equal after averaging over all values of h_0 . These results from the (1+1)-dimensional LC model can be seen in Figure 4.2.

We now present the results for the positive and negative steady-state persistence probabilities for different values of h_0 . The initial time of each model is chosen to be larger than the saturation time of the model: $t_0 > t_s$. The range of the values of $h(t_0) \equiv h_0$ is determined by the value of the saturation width $W_s \sim L^{\alpha}$, which characterizes the roughness of the steady-state interface. Large values of the saturation width make it possible to use a larger number of initial heights.

Figure 4.3 shows plots of $P_+^S\left(+|h_0|,t\right)$, the positive persistence probability for positive values of h_0 , versus t for the (1+1)-dimensional Family model. It can be seen that the plots do not show any sign of a power-law decay for any value of h_0 . Similar behavior is seen for $P_-^S\left(-|h_0|,t\right)$, the negative persistence probability for negative h_0 . Both (1+1) and (2+1)-dimensional LC models also exhibit similar behavior.

We next present results for the positive persistence probability for negative initial heights, $P_+^S\left(-|h_0|,t\right)$, and the negative persistence probability for positive initial heights, $P_-^S\left(+|h_0|,t\right)$. Figure 4.4 shows plots of $P_+^S\left(-|h_0|,t\right)$ of (1+1)-dimensional Family model for different $|h_0|$, compared with that of the average over all values of h_0 i.e. $P_+^S\left(t\right)$. The dotted line represents the slope of the plot for the averaged probability which is $\theta_+^S = 1-\beta$. One can see from this figure that for values of $|h_0|$ that are substantially smaller than the saturation width

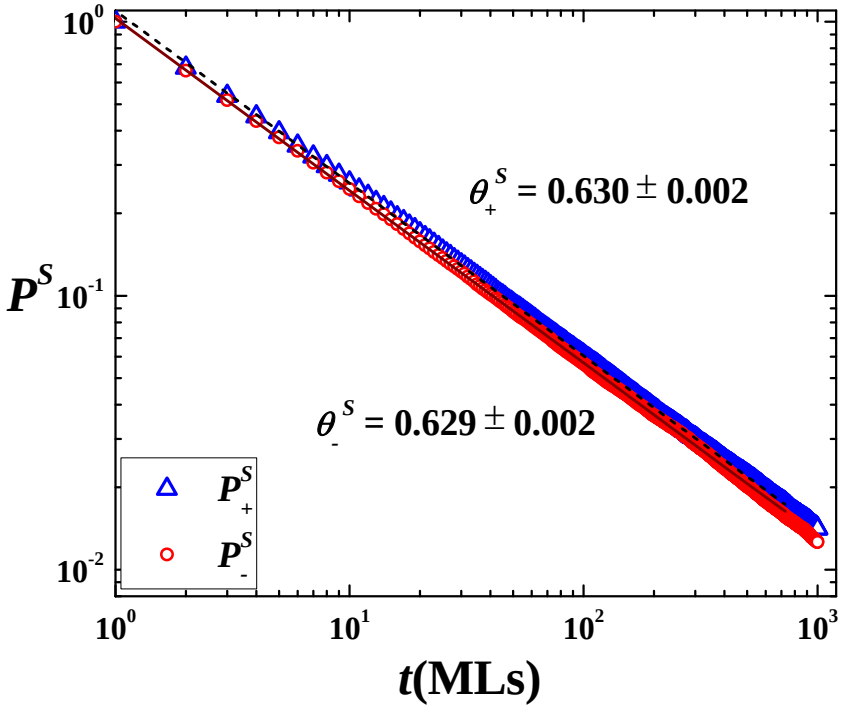

Figure 4.2 Positive and negative steady-state persistence probabilities after averaging over all values of initial height of the (1+1)-dimensional LC model of system size $L = 200$ sites ($t_0 = 8\times10^6$ MLs). The expected values of both exponents are $\theta_+^S = \theta_-^S = 1-\beta = 0.625$.

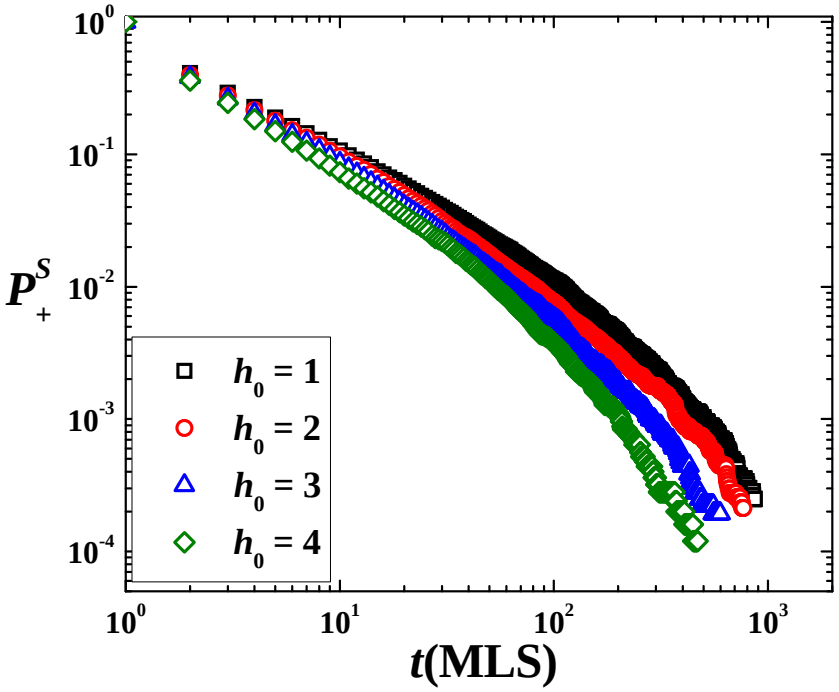

Figure 4.3 Positive steady-state persistence probabilities for different positive values of the initial height for the (1+1)-dimensional Family model of system size $L = 200$ sites ($t_0 = 10^5$ MLs).

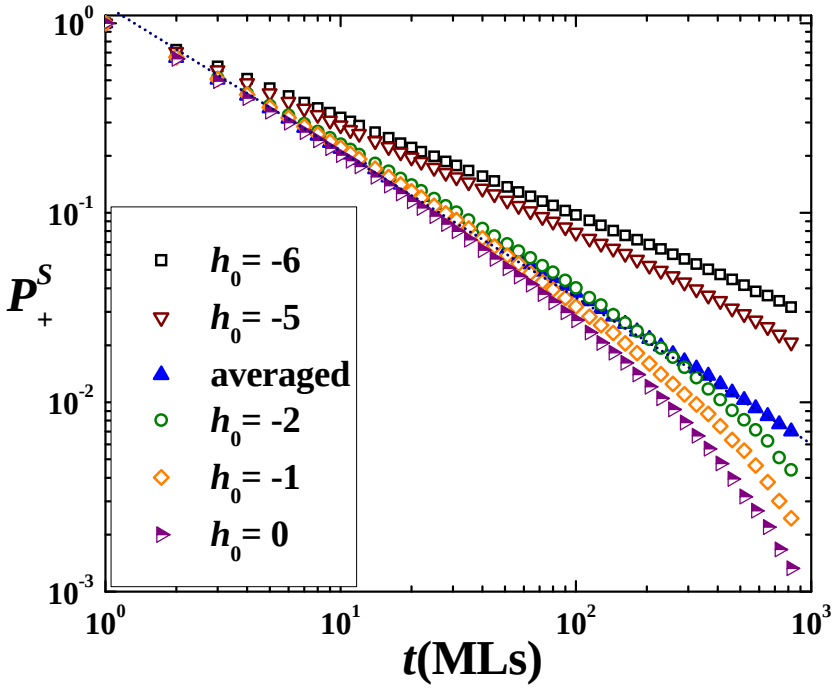

Figure 4.4 Positive steady-state persistence probabilities for different negative values of the initial height and averaged persistence probability for the (1+1)-dimensional Family model of system size $L = 200$ sites ($t_0 = 10^5$ MLs) with $W_s = 3.12$.

$W_s = 3.12$ (e.g. for $|h_0| = 1$ and $|h_0| = 2$), the $P_+^S(-|h_0|, t)$ plots do not exhibit clear power-law decay. The departure from power-law behavior occurs at late times when the plots exhibit a rapid decay. On the other hand, $P_+^S(-|h_0|, t)$ shows clear power-law decay with exponents smaller than $(1-\beta)$ for $|h_0| = 5$ and 6, which are larger than W_s. These results suggest a crossover in the time-dependence of $P_+^S(-|h_0|, t)$ as $|h_0|$ is changed across W_s. The plot for $h_0 = 0$, for which the positive and negative persistence probabilities are the same, exhibits power-law behavior with exponents close to $(1-\beta)$ at short times, but a much faster decay at longer times. This behavior suggests that the decay of the persistence probability for $h_0 = 0$ is not described by a power law.

The most important feature of the results shown in Figure 4.4 is the power-law decay of $P_+^S(-|h_0|, t)$ (and equivalently, of $P_-^S(+|h_0|, t)$) for $|h_0| \gtrsim W_s$. This behavior is clearly shown in Figure 4.5 where $P_+^S(-|h_0|, t)$ and $P_-^S(+|h_0|, t)$ for the (1+1) dimensional Family model are plotted versus time in a double-log scale for a value of $|h_0|$ that is slightly larger than W_s. Both plots collapse into the same straight line, corresponding to power-law decay over 3 decades in time, with an exponent ≈ 0.68 that is clearly different from $(1-\beta) = 0.75$. Figure 4.6 shows the $P_+^S(-|h_0|, t)$ versus t plots for the (1+1)-dimensional Family model for three different values of $|h_0|$. For any value of $|h_0| \gtrsim W_s$, the graph shows a good power-law decay. Similar results are found for the (1+1) and (2+1)-dimensional LC models (see Figures 4.7-4.8). These figures show the most important result of our study: the persistence probabilities $P_+^S(-|h_0|, t)$ and $P_-^S(+|h_0|, t)$ exhibit power-law decay in time for $|h_0| \gtrsim W_s$, and the exponent that describes this power-law decay decreases as the initial height $|h_0|$ increases. When we plot the exponents θ^S versus $|h_0|/W_s$ for each model, the obtained graph is a straight line with a negative slope as shown in the insets of Figures 4.6-4.8. From these plots, it can be concluded that the persistence exponent decreases linearly with $|h_0|/W_s$:

$$\theta_{\pm}^S = -\kappa\left(\frac{|h_0|}{W_s}\right) + \text{ constant} \tag{4.1}$$

where κ is a parameter that describes how fast the persistence exponent decreases with the initial value of the height fluctuation. The parameter κ depends on the model being considered. We found $\kappa = 0.074 \pm 0.003$ for the Family model while $\kappa = 0.046 \pm 0.002$ and

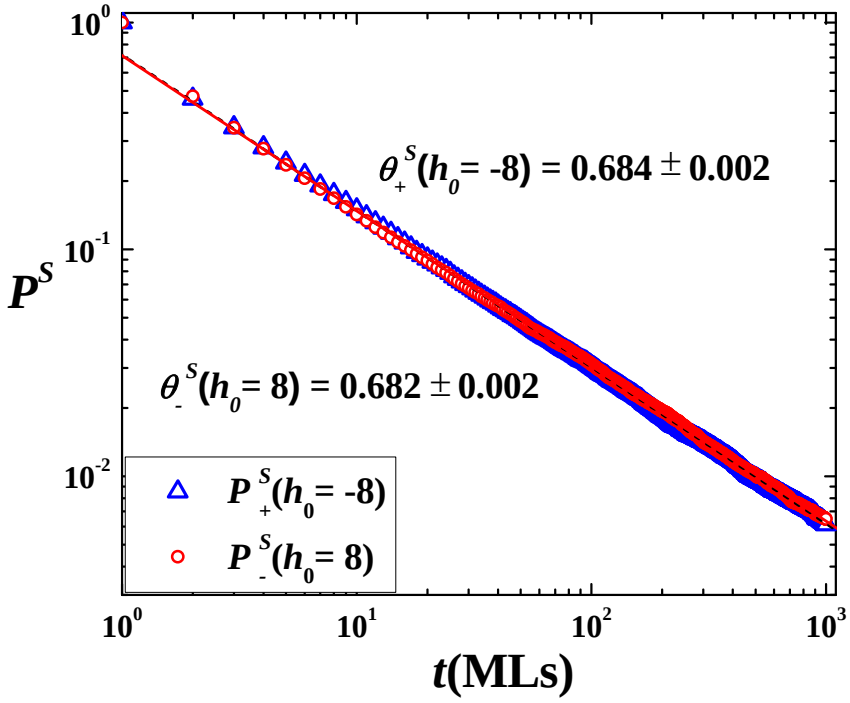

Figure 4.5 $P_+^S\left(-|h_0|,t\right)$ and $P_-^S\left(|h_0|,t\right)$ of the (1+1)-dimensional Family model of system size $L=1,000$ sites with $W_s=7$.

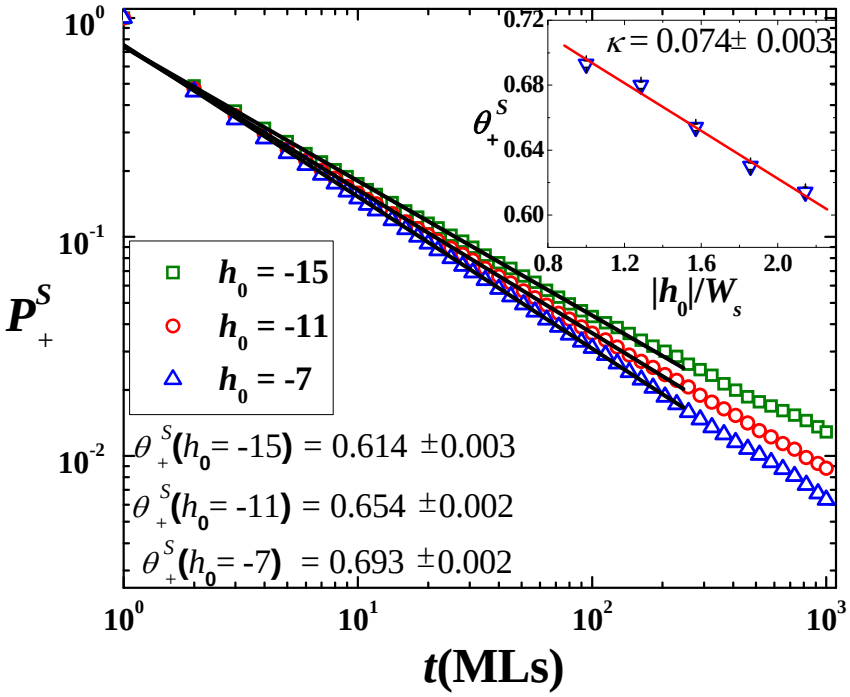

Figure 4.6 Positive steady-state persistence probabilities for different negative values of the initial height with $|h_0|/W_s \geq 1$, $W_s \approx 7.0$ for the (1+1)-dimensional Family model of system size $L = 1,000$ sites ($t_0 = 5\times10^5$ MLs). Inset: persistence exponent as a function of $|h_0|/W_s$.

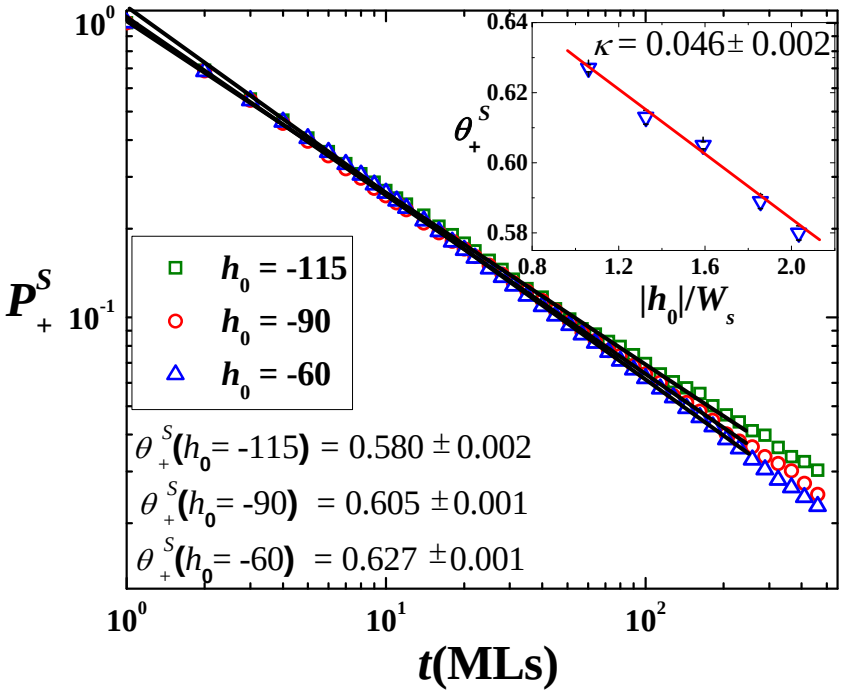

Figure 4.7 Positive steady-state persistence probabilities for different negative values of the initial height with $|h_0|/W_s \geq 1$, $W_s \approx 56.6$ for the (1+1)-dimensional LC model of system size $L = 150$ sites ($t_0 = 2\times10^6$ MLs). Inset: persistence exponent as a function of $|h_0|/W_s$.

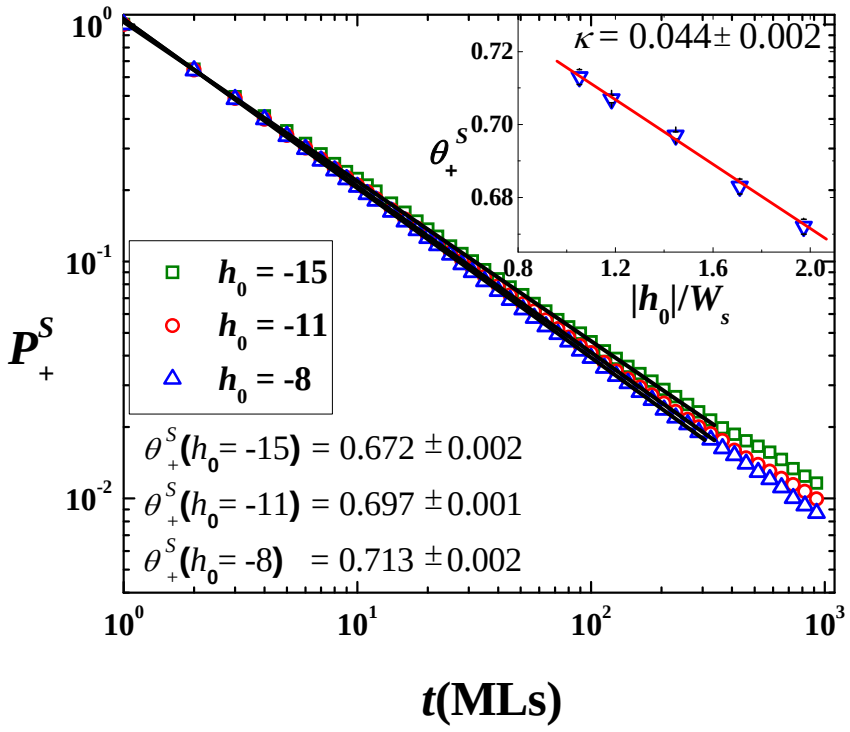

Figure 4.8 Positive steady-state persistence probabilities for different negative values of the initial height with $|h_0|/W_s \geq 1,\ W_s \approx 7.6$ for the (2+1)-dimensional LC model of system size $L \times L = 100 \times 100$ sites ($t_0 = 7 \times 10^5$ MLs). Inset: persistence exponent as a function of $|h_0|/W_s$.

$\kappa = 0.044 \pm 0.002$ for the (1+1) and (2+1)-dimensional LC models respectively. Interestingly, the values of κ for the (1+1) and (2+1)-dimensional LC models agree with each other within the error bars. Since the saturation width is proportional to L^{α}, the persistence exponent is a function of $|h_0| / L^{\alpha}$ i.e. $\theta_{\pm}^{S} \sim \left(\frac{|h_0|}{L^{\alpha}} \right)$.

These results may be qualitatively understood from arguments similar to those described at the end of Section 4.1. Let us assume, without any loss of generality, that $h_0 > 0$. As discussed in Section 4.1, the positive persistence probability for $h_0 > 0$ must decay faster in time than the negative persistence probability. The difference between the behavior of the positive and negative persistence probabilities should increase as h_0 is increased. Also, the temporal decay of the negative persistence probability should be slower for larger values of h_0 because the typical length of negative excursions increases as h_0 is increased. In particular, for $h_0 >> W_s$, the height fluctuation at a site is expected to take a very long time to return to its initial value after a departure in the negative direction. This suggests that $P_{-}^{S}\left(+|h_0|, t\right)$ decays as a power law with exponent close to zero for $h_0 >> W_s$. By continuity, a power-law decay of $P_{-}^{S}\left(+|h_0|, t\right)$ is also expected for other large values of h_0. The exponent for this power-law decay should decrease with increasing h_0 because the negative persistence probability decays more slowly for larger values of h_0. For $h_0 = 0$, on the other hand, our numerical results suggest that the decay of the persistence probability is not described by a power law. By continuity, the persistence probabilities for $h_0 \leq W_s$, for which the positive and negative persistence probabilities are not very different from each other, are not expected to exhibit power-law decay in time.

The observation that the positive persistence probabilities for $h_0 > 0$ do not exhibit power-law decay in time may be rationalized from the requirement that the averaged positive persistence probability, which is a weighted sum of the positive persistence probabilities for all values (positive, negative and zero) of h_0, must decay in time as a power law with exponent $(1-\beta)$. The argument is as follows. In the sum that determines the average positive persistence probability $P_{+}^{S}(t)$, the probabilities $P_{+}^{S}\left(+|h_0|, t\right)$ and $P_{+}^{S}\left(-|h_0|, t\right)$ appear with the same weight. We have argued above that $P_{+}^{S}\left(-|h_0|, t\right) = P_{-}^{S}\left(+|h_0|, t\right)$ should exhibit a power-law decay with exponent smaller than $(1-\beta)$ if $|h_0|$ is large. If $P_{+}^{S}\left(+|h_0|, t\right)$ also decays as a power law with a different exponent, then it would be very difficult to satisfy the requirement that

the sum of $P_+^S\left(+|h_0|,t\right)$ and $P_+^S\left(-|h_0|,t\right)$, averaged over $|h_0|$ with Gaussian weights, must yield a quantity that decays in time as a power law with exponent $(1-\beta)$. On the other hand, this requirement can be satisfied if $P_+^S\left(+|h_0|,t\right)$ does not decay as a power law. For example, if $P_+^S\left(-|h_0|,t\right) \sim t^{-\theta}$ with $\theta < (1-\beta)$, then the average of $P_+^S\left(-|h_0|,t\right)$ and $P_+^S\left(+|h_0|,t\right)$ would decay as $t^{-(1-\beta)}$ if $P_+^S\left(+|h_0|,t\right) \sim 2t^{-(1-\beta)} - t^{-\theta}$, which represents a decay that is faster than a power law. Although this form cannot be valid at very long times (it would give a negative value if t is sufficiently large), it does provide a qualitatively correct description of the actual time-dependence of $P_+^S\left(+|h_0|,t\right)$, shown in Figure 4.3, for roughly 3 decades in time. The non-power-law behavior of $P_+^S\left(h_0,t\right)$ for small values of $|h_0|$ would also help in making the averaged positive persistence probability decay as a power law with exponent $(1-\beta)$.

As noted above, the persistence probabilities $P_-^S\left(+|h_0|,t\right)$ and $P_+^S\left(-|h_0|,t\right)$ are expected to decay very slowly in time, with the decay exponent approaching zero, if $|h_0|$ is much larger than W_s. The behavior of the persistence probabilities for such large values of $|h_0|$ is difficult to study in simulations because of poor statistics. This is because the occurrence of values of $|h_0| >> W_s$ is extremely rare. Our data for such values of $|h_0|$ are consistent with the expectation of the decay exponent approaching zero. This result implies that the dependence of the decay exponent on $|h_0|$ given in Eq. (4.1) is valid only for values of $|h_0|$ that are not much larger than W_s.

4.3 Scaling Behavior of the Persistence Probability

We have studied the effects of finite system size (L) and discrete sampling time (δt) on the steady-state persistence probabilities for different initial heights. We now study the average persistence probability, $P^S\left(|h_0|\right)$ which is the average of $P_+^S\left(-|h_0|,t\right)$ and $P_-^S\left(|h_0|,t\right)$. The scaling variables are expected to be t/L^z, $\delta t/L^z$ and $h_0/W_s(L)$ where $W_s(L) \propto L^\alpha$ is the saturation width of the interface. We measure the average steady-state persistence probabilities for three sets of values of L and δt. These values are chosen so that we have the same values of $|h_0|/W_s$ and $\delta t/L^z$ in all three cases. From our results, the plots of $P^S(t)$ versus $t/\delta t$ exhibit a good scaling collapse and power-law decay with exponents that depend on $|h_0|/W_s$. The scaling plots for the Family model are shown in Figure 4.9. This power-law dependence occurs

when $|h_0|/W_s \gtrsim 1$. Similar results are obtained for the LC model (see Figures 4.10-4.11). These results imply the following scaling form for the dependence of the average steady-state persistence probability $P^S\left(t,L,\delta t,|h_0|\right)$ on the initial height $|h_0|$:

$$P^S\left(t,L,\delta t,|h_0|\right) = f\left(\frac{t}{L^z},\frac{\delta t}{L^z},\frac{|h_0|}{L^\alpha}\right) \tag{4.2}$$

where $f\left(x_1,x_2,x_3\right) \sim x_1^{-\theta^S(x_3)}$ for $x_1 << 1$, $x_2 << 1$ and $x_3 \gtrsim 1$.

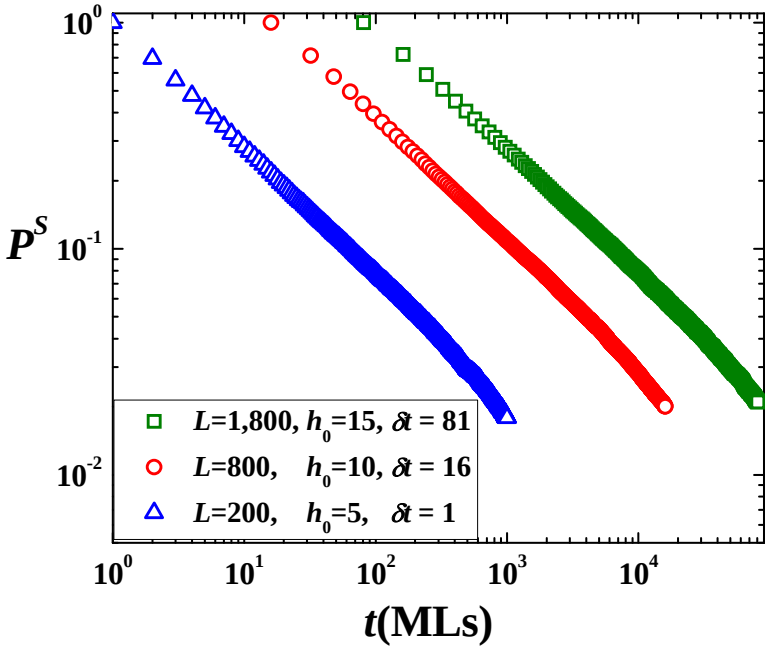

(a)

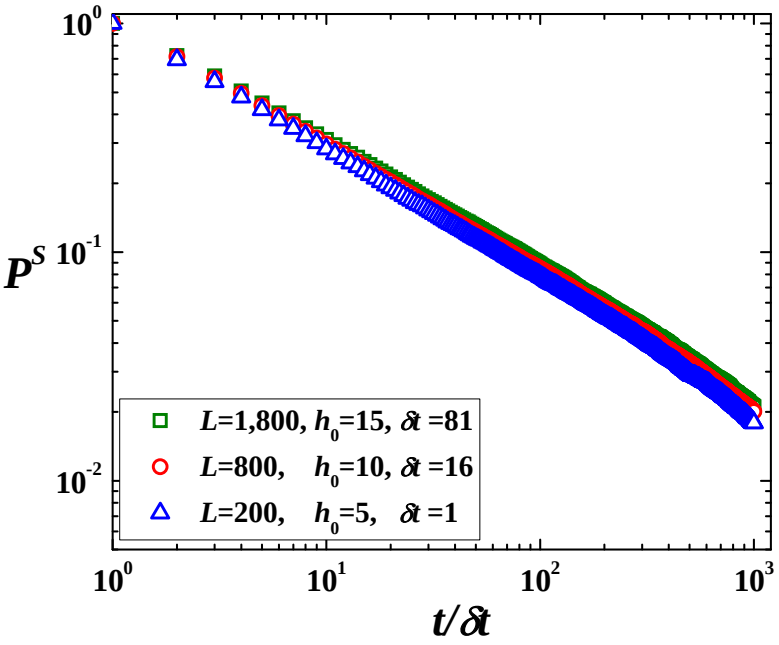

(b)

Figure 4.9 Average persistence probability of the (1+1)-dimensional Family model for different initial height, different substrate sizes and different discrete sampling times with the same ratio of $|h_0|/L^{\alpha} \approx 1.61$ and $\delta t / L^{z} \approx 2.5\times10^{-5}$. (a) Average persistence probabilities versus time. (b) Finite size scaling of $P^S\left(t,L,\delta t,|h_0|\right)$.

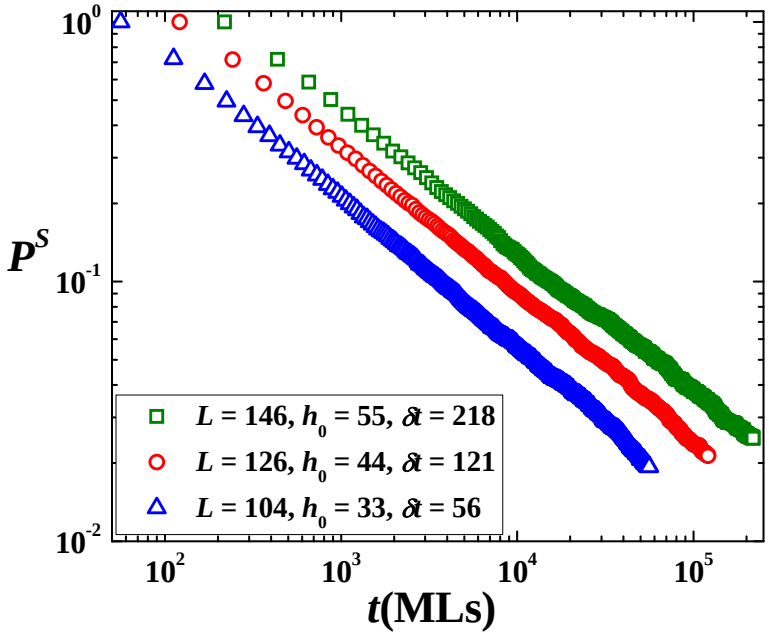

(a)

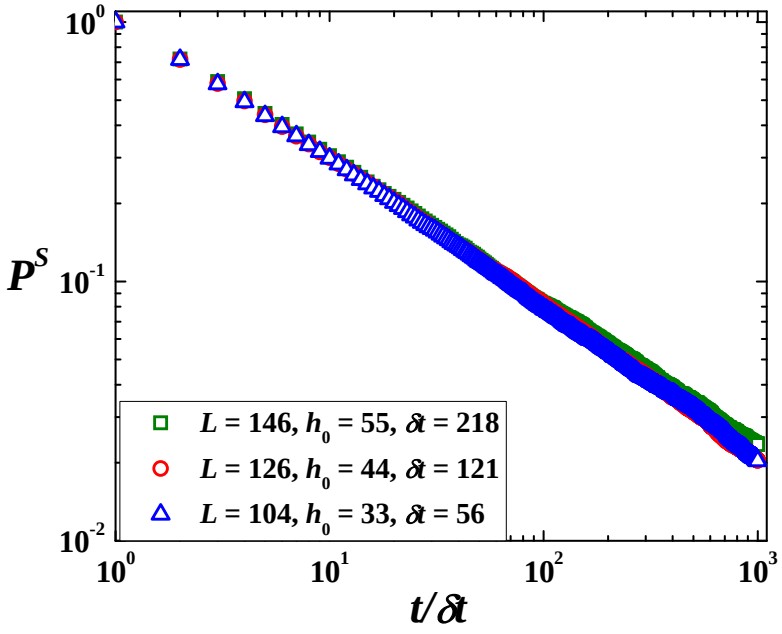

(b)

Figure 4.10 Average persistence probability of the (1+1)-dimensional LC model for different initial height, different substrate sizes and different discrete sampling times with the same ratio of $|h_0|/L^{\alpha} \approx 1$ and $\delta t / L^{z} \approx 4.8\times10^{-7}$. (a) Average persistence probabilities versus time. (b) Finite size scaling of $P^S\left(t,L,\delta t,|h_0|\right)$.

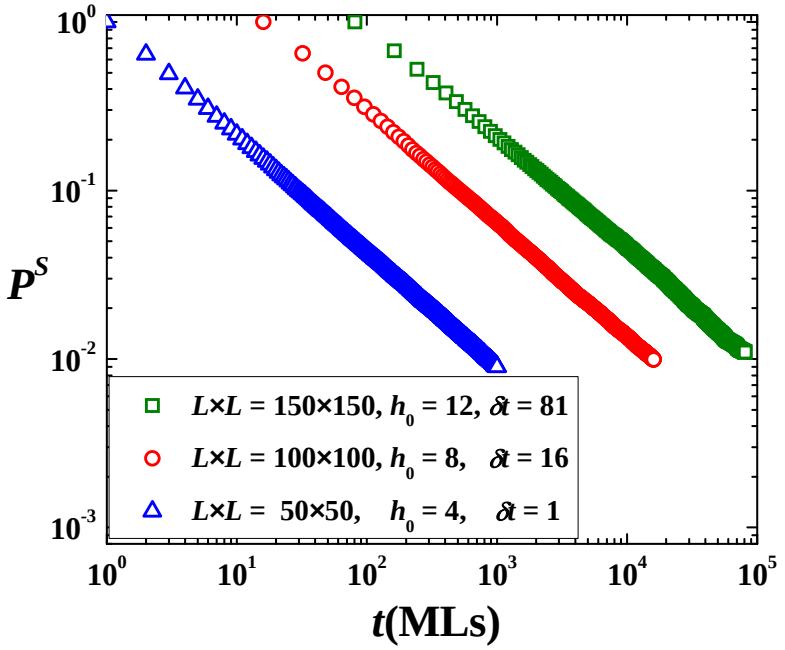

(a)

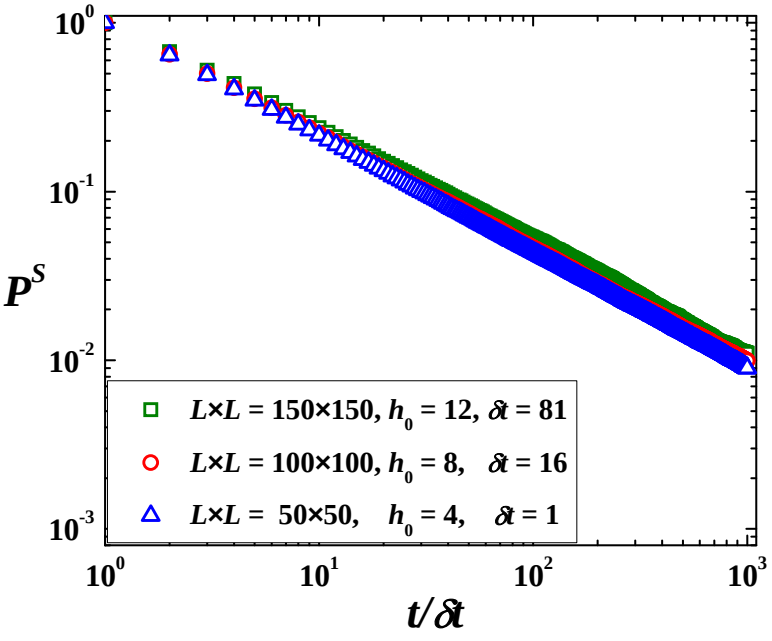

(b)

Figure 4.11 Average persistence probability of the (2+1)-dimensional LC model for different initial height, different substrate sizes and different discrete sampling times with the same ratio of $|h_0|/L^{\alpha} \approx 1.05$ and $\delta t/L^{z} \approx 1.6\times10^{-7}$. (a) Average persistence probabilities versus time. (b) Finite size scaling of $P^S\left(t,L,\delta t,|h_0|\right)$.

Chapter V

Effects of Patterned Substrate on Thin Films Simulated by Family Model

In this chapter, effects of the substrate pattern on statistical properties of the growing film grown by the (2+1)-dimensional Family model are studied. The patterns of interest here are the triangular and vicinal substrates with varying size L and tilt angle φ as shown in Figure 5.1. The substrate size $L \times L$ is varied from $L = 100$ to 600 sites and substrate angle φ ranges from 0° to 27°. Periodic boundary condition is performed along the triangular substrate whereas free boundary condition is used for the vicinal substrate.

5.1 Effects of Patterned Substrate on Interface Width and Critical Exponents

For models in which the roughness of the film surface is very small such as the Family model, the initial pattern strongly effects morphology and other kinetic properties of the film. From the definition of the interface width, W measures the deviation of the film surface from the initial substrate. When the film is grown on a flat substrate, W is the standard deviation of the height. For the Family model, the diffusion rules lead to very smooth surface so W is very small when the film is grown on a flat substrate (see Figure 5.1). However, W becomes larger when the film is grown on a patterned surface. This is because the growing surface becomes smoother than the initial pattern resulting in larger deviation of the grown surface from the initial height. Figure 5.2 (a) shows the interface width as a function of time for the flat and triangular substrates with various substrate angle φ of the system size $L = 600$ sites. The plots of the triangular substrates show relatively small values of W at early times because the morphologies at that time still carry the shape of the initial pattern. At larger time, the surface becomes smoother leading to the increase in W. Finally, W becomes constant when the system reaches the steady-state. The larger the tilt angle φ, the rougher the initial substrate, and the larger the saturation width W_s.

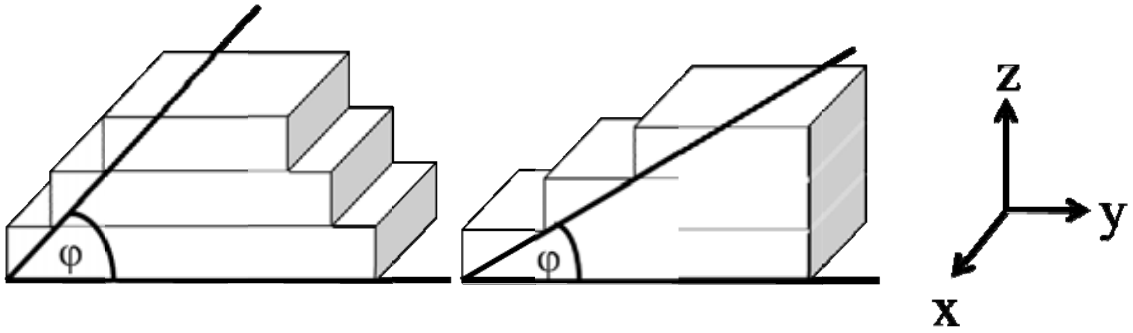

Figure 5.1 The triangular (left) and vicinal (right) substrates with the tilt substrate angle φ .

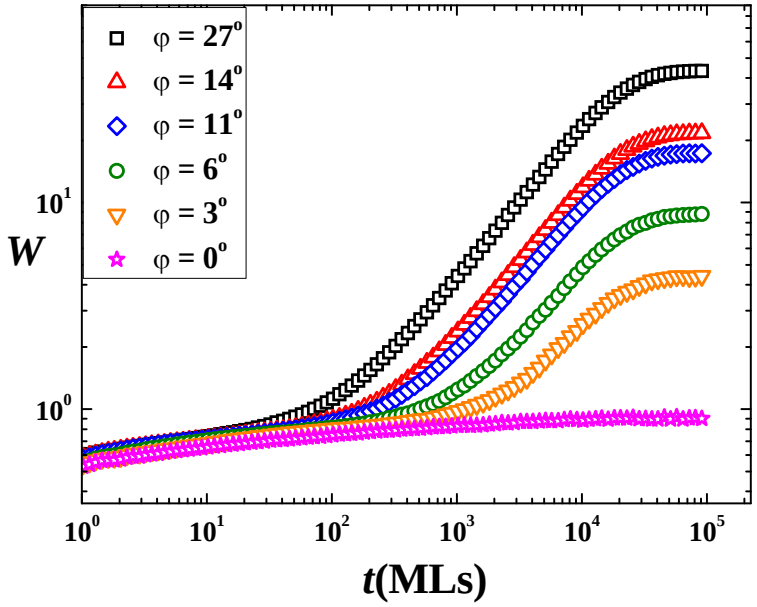

(a)

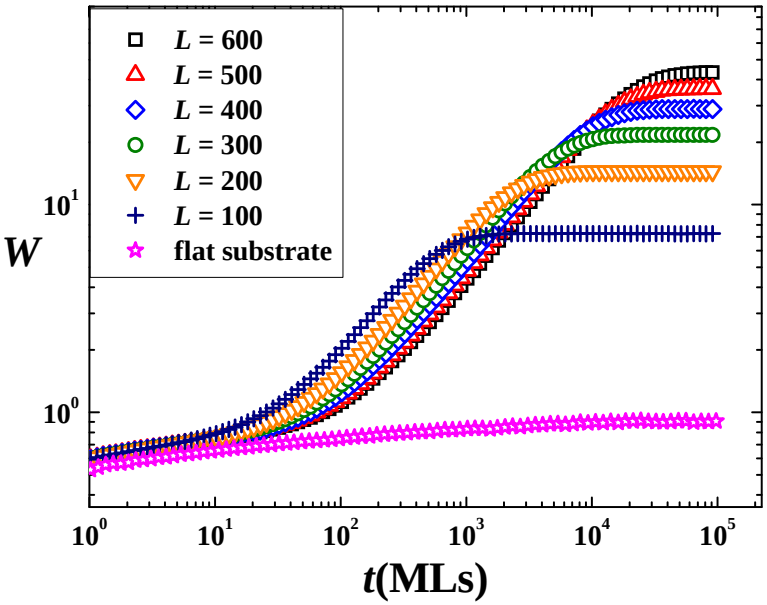

(b)

Figure 5.2 Interface width of the Family model grown on the triangular substrate with (a) $L = 600$ sites and various tilted angle φ, (b) with $\varphi = 27^{\circ}$ and various substrate size L.

Figure 5.2 (b) shows the interface width as a function of time for the flat and triangular substrates for various substrate size L of the system with tilt angle $\varphi = 27^{\circ}$. The initial roughness increases with L resulting in the larger value of W_s for large L. For the vicinal substrate, we obtain the same results as those of the triangular substrate.

The effects of the patterned substrate on the interface width lead to the change in the critical exponents that may alter the scaling relation of the model. To investigate this, the critical exponents α, β, and z are studied. In chapter 2, the scaling plots of W/L^{α} vs t/L^{z} (a) and W/t^{β} vs t/L^{z} are used to determine the values of the critical exponents. In this chapter, we study patterned substrates in which the initial roughness is different for different L. We, therefore, calculate the exponents directly from the particular interface width curve. The growth exponent is determined by the slope in the early time of the W vs L plot in the logarithmic scale. Using a fixed value of $\varphi = 27^{\circ}$, the growth exponent β in both the vicinal and triangular substrates is found to vary with the roughness of the substrate as shown in Table 5.1. The roughness exponent α and dynamical exponent z are calculated from slope of double log plots of W_s vs L and t_s vs L as can be seen in Figure 5.3. Like β, α changes with the initial roughness. The results in Table 5.1 and Figure 5.3(a) indicate that β and α of the patterned substrate are larger than those of the flat substrate ($\beta = 0$, $\alpha = 0$) due to the initial roughness.

Table 5.1 The growth exponents of the Family model on patterned substrates with $\varphi = 27^{\circ}$.

The substrate size $(L \times L)$	β_{vicinal}	$\beta_{\text{triangular}}$
100×100	0.68	0.66
200×200	0.71	0.69
300×300	0.72	0.71
400×400	0.73	0.72
500×500	0.74	0.73
600×600	0.74	0.73

Moreover, when the Family model is grown on a sufficiently rough patterned substrate, e.g. the substrate with $\varphi = 27^{\circ}$, the growth exponent computing from the Family-Vicsek scaling

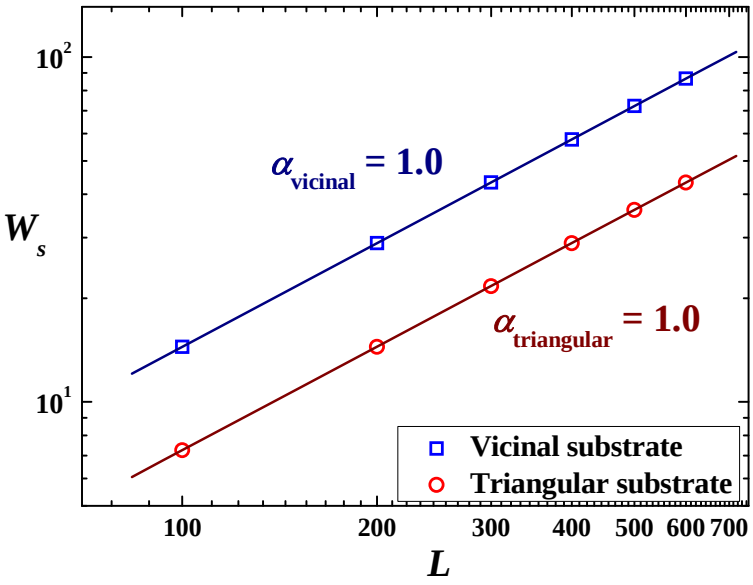

(a)

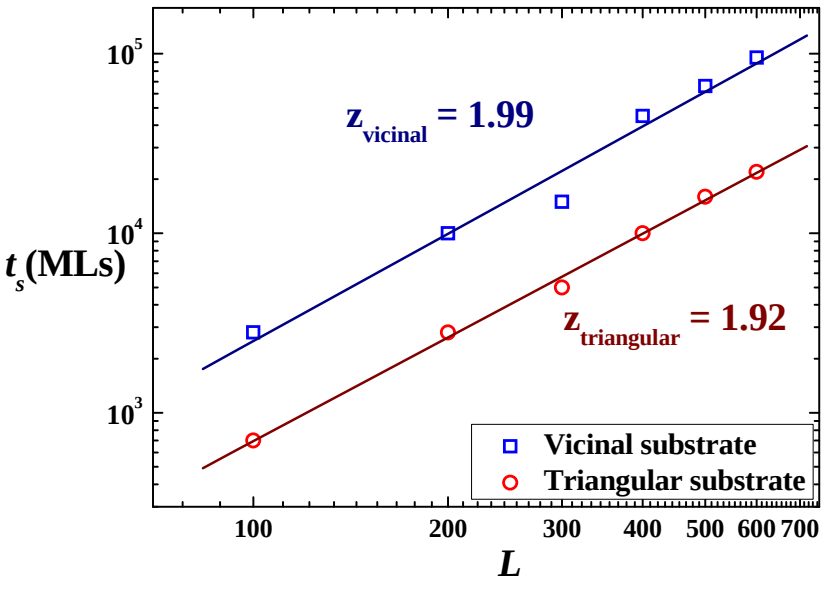

(b)

Figure 5.3 (a) The saturation width and (b) the saturation time for systems with triangular and vicinal substrates.

relation using α and z in Figure 5.3 is $\beta \approx 0.5$ which does not equal the value obtained from the interface width versus time plot directly (see Table 5.1). As a result, three independent exponents rather than two are required, and their relation is not consistent with the Family-Vicsek scaling relation.

5.2 Effects of Patterned Substrate on Persistence Probability

From our results, the transient persistence probability does not show power-law decay with time if the film is grown on a sufficiently rough substrate. Our results show that the pattern has a very weak effect on whether the positive and negative persistence probabilities will be equal at a particular time, but it strongly effects the value of $P^T(t)$. When φ is increased, width of the flat terraces on the substrate decrease and it is easier for a deposited atom to move to one of the step edges. The number of sites that deposited atoms are left in the middle of a terrace - sites that the height fluctuation returns to the initial value - becomes smaller leading to larger value in P^T. Figure 5.4 shows the transient persistence probability of films grown by the Family model on flat and triangular substrates. The plots show that the bigger the angle, the larger the persistence probabilities (more persist sites) at a particular time t. The same results are seen in systems with vicinal substrates.

Another effect the pattern has on P^T can be seen at large t when $P^T(t)$ does not decay to zero but converts to a nonzero constant for cases with large φ. This is because the tilted initial surface creates a specific direction in the substrate and majority of deposited atoms end up in the "lower" sites due to the Family diffusion rule. As more and more layers are deposited, along the tilt direction of the triangular substrate, the height fluctuations near the edges of both sides of the film increase on the average, while those near the middle of the film decrease on the average. As a result, P_+^T for sites near the substrate edges remains non-zero for a long time while P_-^T remains non-zero for sites in the middle. For the vicinal substrate, P_+^T remains non-zero for the initially lower sides whereas P_-^T remains non-zero for the initially higher sides.

The persistence exponents are also affected by the substrates. From Figure 5.4, it can be seen that $\theta_{pattern}^T < \theta_{flat}^T$. The reason is that, in a rough surface, range of the initial height is very large and it takes more time for the persistence probability to become zero for sites with large $|h_0|$.

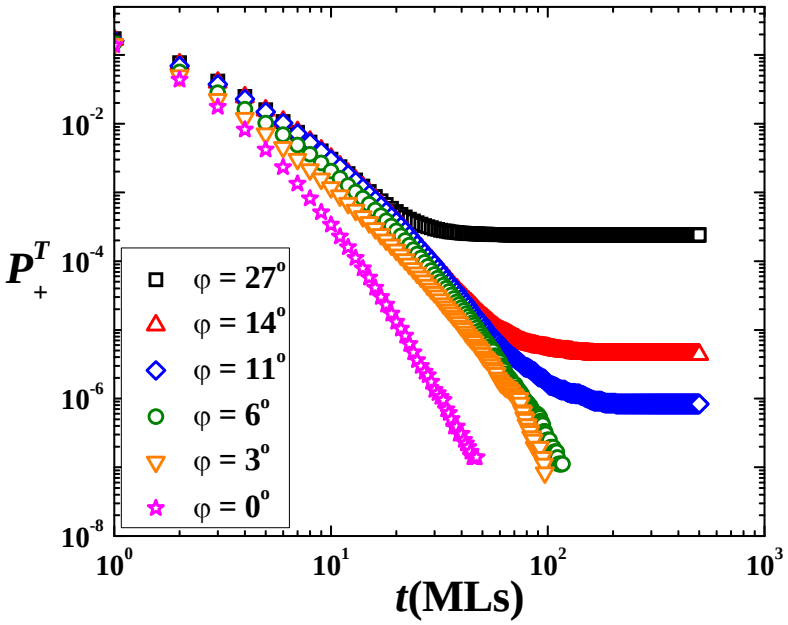

(a)

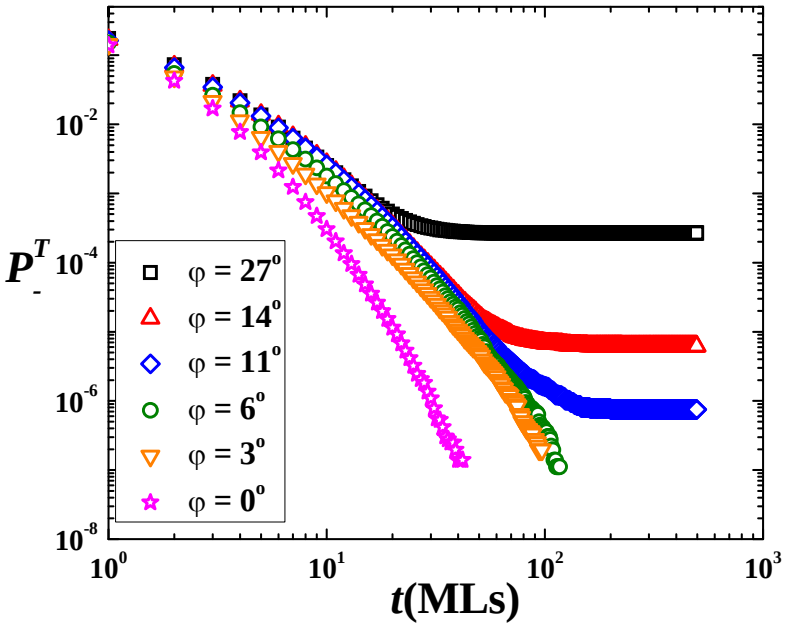

(b)

Figure 5.4 (a) Positive and (b) negative transient persistence probabilities of the Family model grown on the flat and triangular substrates for various φ .

As can be expected, the patterned substrate does not have any effect on the steady-state persistence probability and steady-state persistence exponent because any evidence of the initial pattern no longer exist by the time the film reaches the steady-state.

5.3 Effects of Patterned Substrate on Correlation Functions

The height-height correlation function is calculated in two directions i.e. the flat direction G_x and the tilted direction G_y. For the Family model, we can clearly see different behavior between the correlation functions calculated in different direction in the early times. Figure 5.5 shows the plots of G_x and G_y of the Family model grown on flat and triangular substrates with $L = 600$ sites and varying φ. As shown in Figure 5.5(a), G_x of the triangular substrates with all values of φ shows the same behavior as that of a flat substrate, and all plots collapse into the same curve. However, G_y of the triangular substrates, in Figure 5.5(b), continue to show power-law behavior up to the largest Δr used. Moreover, the value of G_y increases as φ is increased due to the large value of height difference caused by the very rough substrate. Interestingly, slopes of these plots, which are local roughness exponents at a certain φ, range from 0.94 when $\varphi = 27^\circ$ to 0.82 when $\varphi = 3^\circ$. The value obtained here for $\varphi = 27^\circ$ ($\alpha = 0.94$) differ from the global roughness exponent of $\alpha = 1.0$ shown in Figure 5.3 revealing anomalous scaling in the systems. The same results are obtained for the vicinal substrate.

Finally, the multifractality of the Family model grown on two dimensional patterned substrates is investigated via the study of the generalized correlation G_q. Figure 5.6 shows the plots of G_q in the tilted direction of the Family model grown on flat and vicinal substrates with $L = 500$ sites and $\varphi = 27^\circ$ using $q = 1 - 4$. For a flat substrate (see Figure 5.6(a)), the value of α_q is the same for all q. However, G_q for patterned substrate in Figure 5.6(b) show strong dependence of α_q on q revealing profound multifractality in the Family model grown on patterned substrates. For the triangular substrate, our results exhibit similar multifractal behavior.

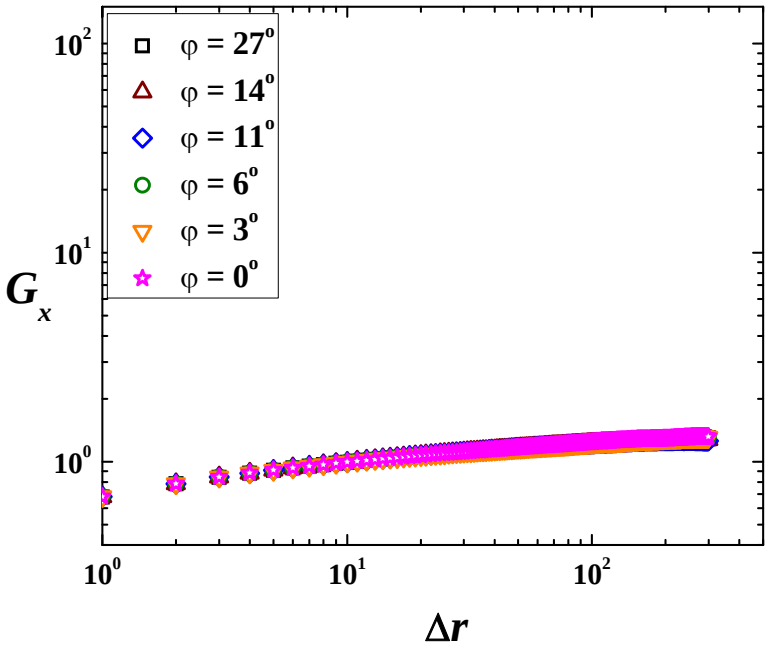

(a)

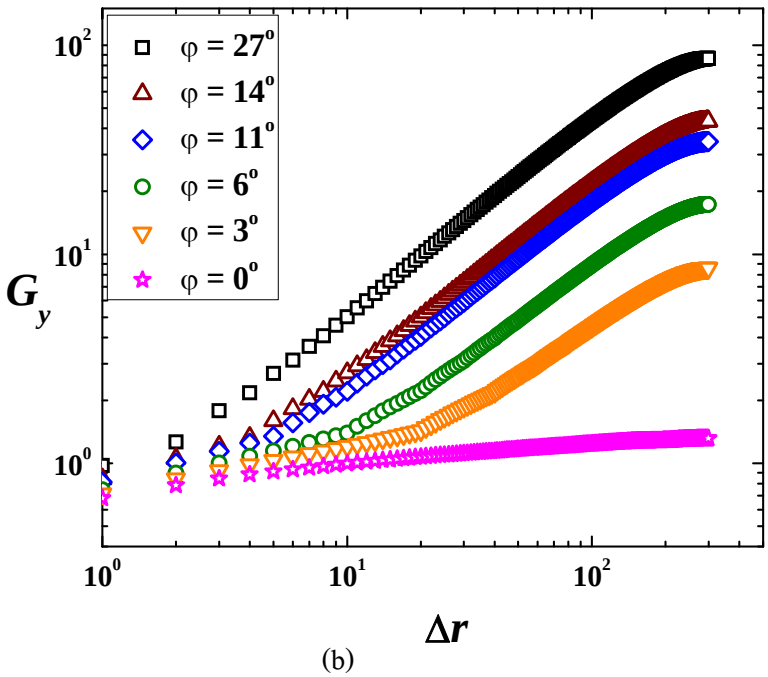

(b)

Figure 5.5 Height-height correlation function in the (a) flat and (b) tilted directions of the Family model grown on the flat and triangular substrates with $L = 600$ sites for various φ at growth time $t = 10^5$ MLs.

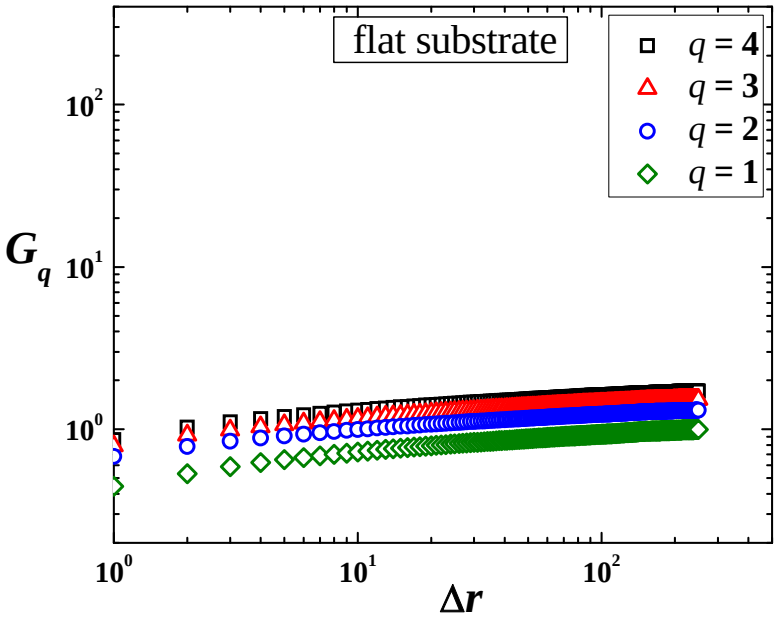

(a)

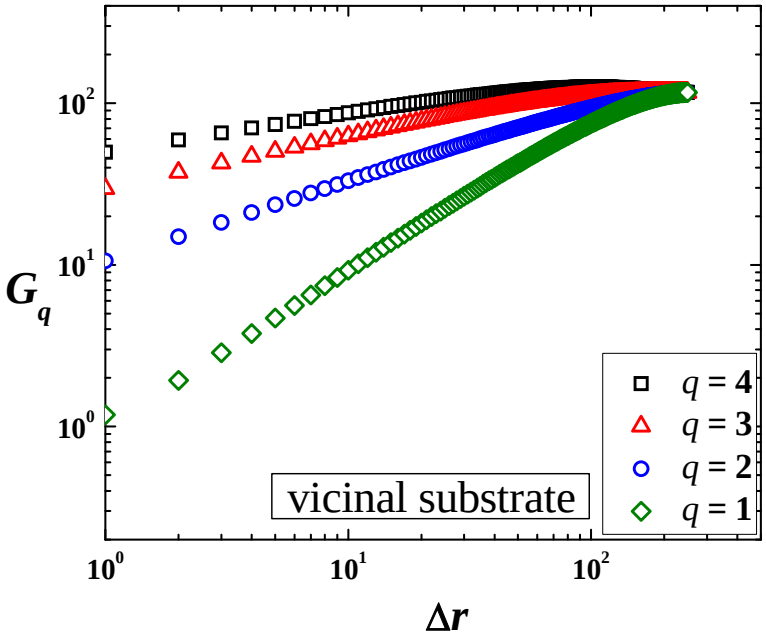

(b)

Figure 5.6 Height-height correlation function in the tilted direction ($\varphi = 27^{\circ}$) of the Family model grown on (a) flat and (b) vicinal substrates with $L = 500$ sites at growth time $t = 10^4$ MLs.

Chapter VI

Healing Time for the Growth of Thin Films on Patterned Substrates

The main goal of this chapter is to study effects of patterned substrate and investigate how long the initial pattern influences the growing film. The linear Family model and the more complicated nonlinear DT model grown on two dimensional substrates are used in this chapter. The first pattern considered here is a tent-shaped triangular substrate of varying slope and size. The initial substrate is tilted by angle φ in the y-direction as shown in Figure 6.1(a). By definition, the size of the triangular pattern depends on the size of the substrate which means that the initial roughness increases as the substrate size is increased. The other pattern of interest is one consisting of pillars or grooves of varying size but constant areal density (see Figure 6.1(b)). Unlike the triangular substrate, the size of the pillars and grooves do not vary with the substrate size. We consider both the situations of periodic and random distributions of the pillars and grooves on the substrate. Pillars (grooves) with random height (depth) are also studied. Periodic boundary condition is used in all systems. In addition to simulations, we carry out analytical calculations for the Family model for both types of initial pattern, using the continuum EW equation.

The nearest-neighbor height difference correlation function σ defined in chapter 2 is used to identify the healing time t_h. The healing time is defined as the time at which σ of a film grown on a patterned substrate becomes equal to that of a film grown on a flat substrate.

6.1 Triangular Pattern

As more and more layers are deposited, influence of the initial pattern decreases. This can be seen from the morphology of the film surface at different times. When $t << t_h$, the surface (Figure 6.2(a)) clearly shows the shape of the initial pattern. As the growth time increases, the morphology (Figure 6.2(b)) becomes smoother due to surface diffusion; however, characteristics

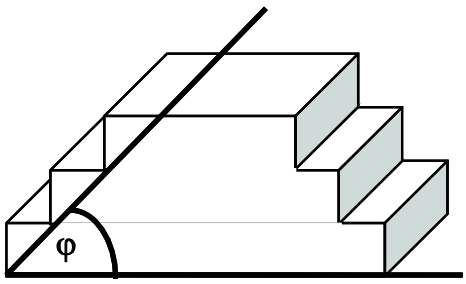

(a)

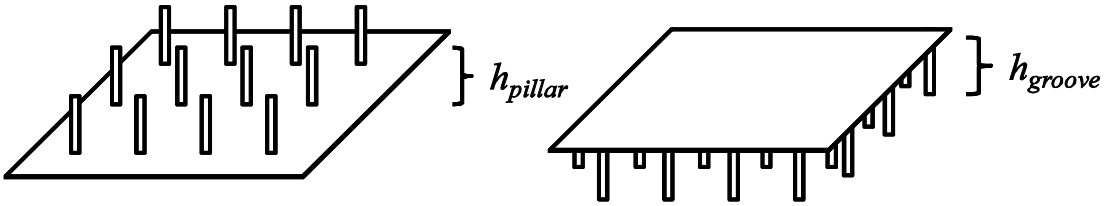

(b)

Figure 6.1 (a) The tent-shaped triangular substrate with substrate angle φ , (b) the substrates with pillar (left) and groove (right).

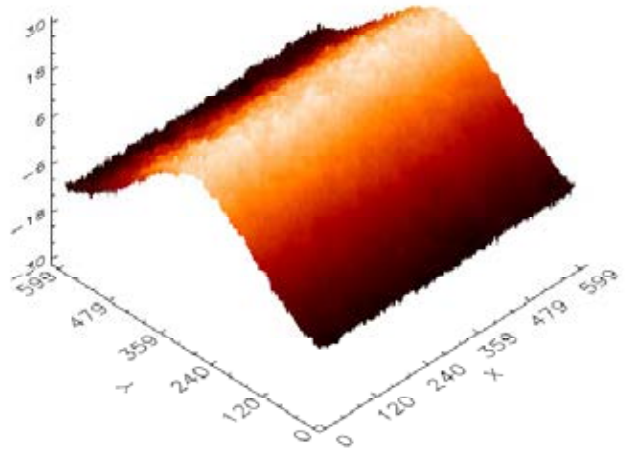

(a)

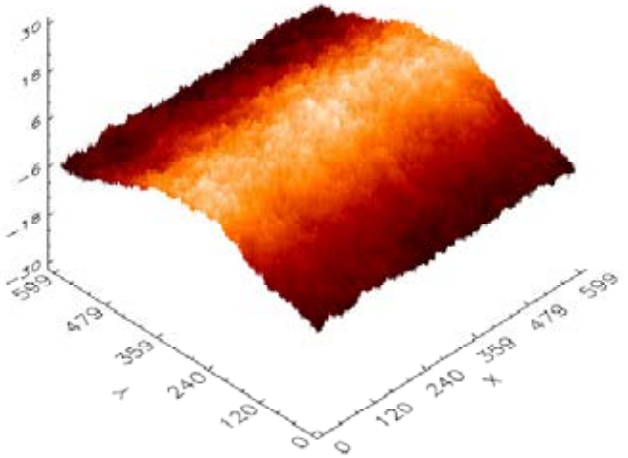

(b)

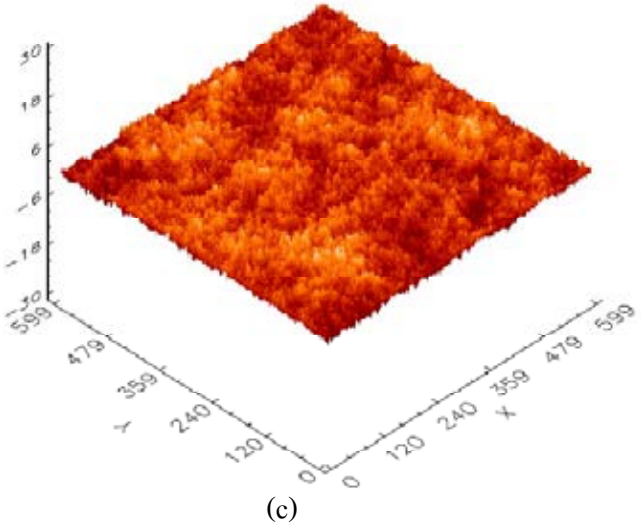

(c)

Figure 6.2 Morphologies of the Family model on a triangular substrate with $L = 600$ sites at (a) $t = 1,000 < t_h$, (b) $t = 10,000 < t_h$, and (c) $t = 100,000 > t_h$.

of the initial pattern are still visible. When $t \geq t_h$, the morphology of the film (Figure 6.2(c)) is indistinguishable from that of a film grown on a flat substrate, indicating that the initial patterns no longer have any effect on the grown film after the growth time exceeds the healing time.

The healing times of the Family and DT models grown on triangular substrates have been obtained from our simulations. Control variables are the angle of the substrate and the substrate size. First, the substrate size is fixed at $L \times L$ with $L = 600$ sites for the Family model and $L = 100$ sites for the DT model while the tilt angle is varied from $\varphi = 0^\circ$ (flat substrate) to $\varphi = 27^\circ$. The values of φ considered here correspond to the following values of the slope of the initial pattern: $0, 1/20, 1/10, 1/5, 1/4$ and $1/2$ (for a discrete model, the slope must be of the form m/n where m and n are integers). The nearest-neighbor height difference correlation functions in the tilt direction ($\sigma(t) \equiv \sigma_y(t)$) are calculated. The plots of $\sigma(t)$ for the Family model grown on substrates with different values of φ (Figure 6.3(a)) show relatively large values of σ at early times. This is due to the initial width of the patterned substrate. When more layers are deposited, atomic diffusion leads to a decrease in the interface roughness. This effectively reduces the value of σ at late times. Finally, at t_h, the value of σ becomes equal to that of a film grown on an initially flat substrate. Note that the plots for small value of φ show oscillations in the early time range due to layer-by-layer growth on substrates with small tilt. An increase in φ causes the value of σ to increase in the early time range. This is because σ measures the height difference between nearest neighbors which increases when the slope of the substrate is increased. Substrates with larger initial values of σ need more time for the initial characteristics of the interface to be healed. So, as expected, the value of t_h increases with φ. Similar results are obtained from the DT model. It should be mentioned that the values of t_h cannot be determined very accurately from the simulations because this requires finding the time at which two fluctuating quantities (σ for flat and patterned initial states) become equal.

In order to find the dependence of t_h on substrate size, the tilt angle is then fixed at 27° while the substrate size is varied from $L = 100$ to 600 sites for the Family model and from $L = 60$ to 160 sites for the DT model. For the triangular substrate with any substrate size (see Figure 6.3(b) for the results for the Family model), the initially roughness of the surface causes large values of σ in the early time range. As t increases, the interface becomes smoother because atoms diffuse in order to minimize their heights. As a result, the value of σ is reduced

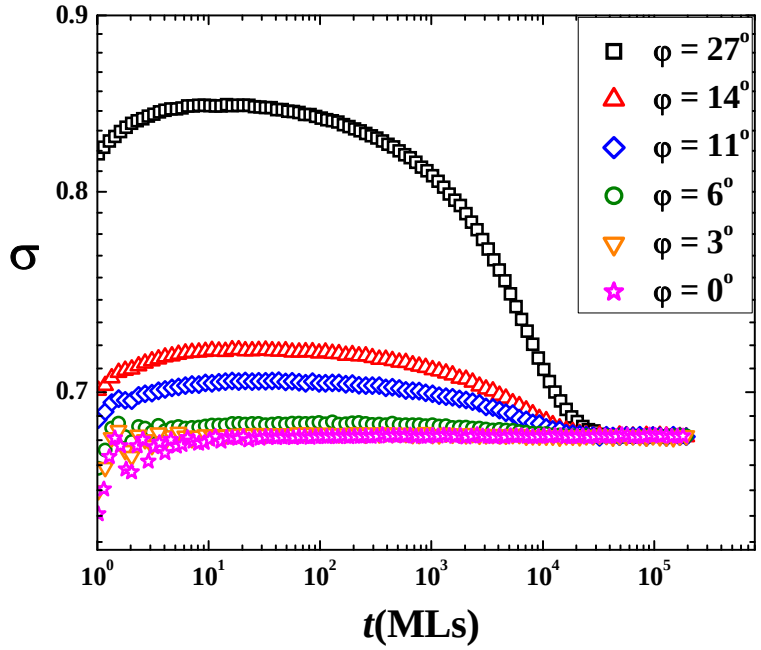

(a)

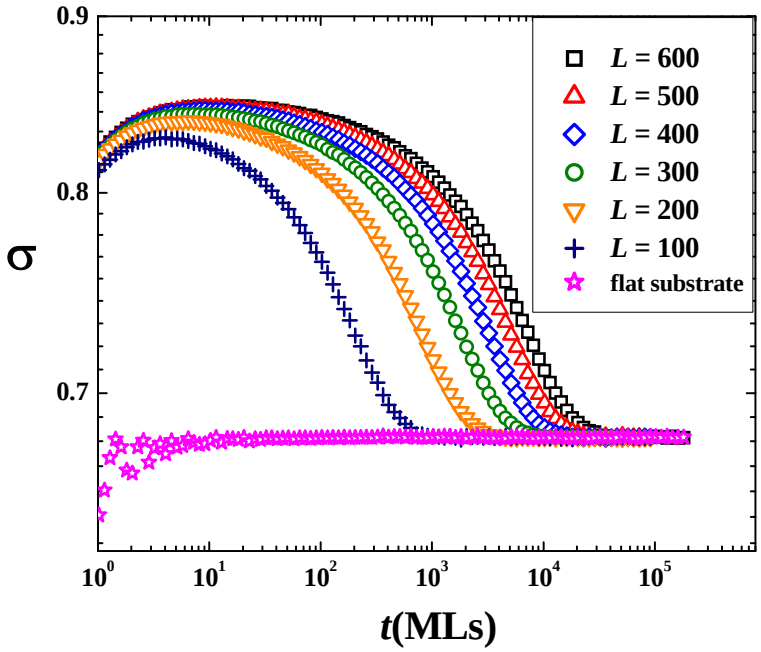

(b)

Figure 6.3 Nearest-neighbor height difference correlation function σ of the Family model grown on a triangular substrate (a) with $L = 600$ sites and various tilted angle φ, and (b) with $\varphi = 27^{\circ}$ and various substrate sizes L.

and it becomes equal to that for a flat substrate at $t = t_h$. When L is increased, the value of σ in the early time range increases. This is because for the same tilt angle, the substrate roughness increases with the value of L. The larger initial roughness takes more time to recover, so t_h increases with L. It should be noted that all plots reach a constant value of σ when $t \geq t_h$. We can, therefore, conclude that the healing time in this case is close to the saturation time (the time beyond which the interface width becomes essentially constant) for the patterned initial states.

From our results for the Family model, we find that the ratio t_h / L^z ($z = 2$) is constant for each φ. For $\varphi = 27^\circ$, $t_h / L^z \approx 0.1$, which is nearly the same as the value of t_s / L^z of this model when t_s is the saturation time [Constantin et al. 2004]. The scaling relation between the healing time and the substrate size is then investigated by rescaling the time axis in the σ vs. t plot by a factor of L^z. We find that the data for triangular substrates show a good scaling collapse for relatively large values of t. The early-time data do not exhibit a scaling collapse because the behavior at early times is determined primarily by the initial pattern. The points corresponding to the healing time fall on approximately the same spot as can be seen in Figure 6.4. From the data collapse for various substrate sizes, the scaling description for the healing time is determined to be $t_h \sim L^z$. Since the saturation time t_s also scales with the substrate size as $t_s \sim L^z$, a linear relation between t_h and t_s is implied.

For the DT model, we find that the results exhibit strong system-size dependence for the relatively small values of L used in our simulations (our simulations for the DT model are restricted to smaller systems because the healing time in the DT model is much larger than that in the Family model with the same value of L). Effective critical exponents for the limited range of substrate sizes considered in this work, obtained from finite-size scaling collapse of W / L^α versus t / L^z and W / t^β versus t / L^z plots for different L are $\alpha = 0.5$, $\beta = 0.19$ and $z = 2.6$ (see Figure 2.10). In addition, the saturation value of σ depends weakly on L for the values of L used in our simulations. As a result, a scaling collapse of the data, similar to that for the Family model (Figure 6.4) is not possible for the DT model. However, it is possible to check whether the power-law scaling relation between t_h and L remains valid. A plot of t_h as a function of L (see Figure 6.5) shows that $t_h \sim L^z$ with $z \approx 2.6$. Thus, it can be concluded that for the triangular substrate, the healing time scales with L^z for both the models studied here. It is clear from a comparison of the results shown in Figures 6.3 and 6.5 that the healing time of the

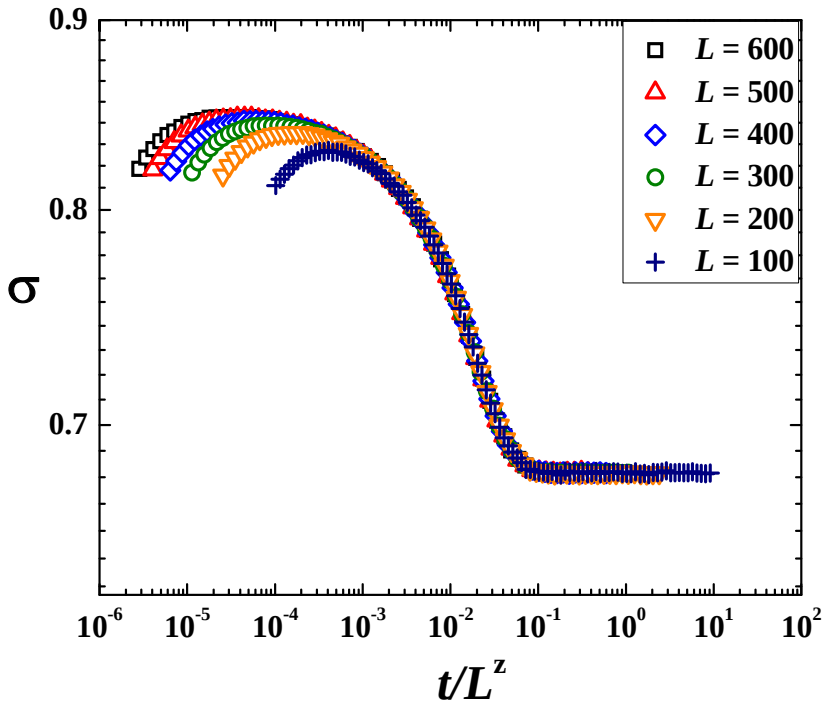

Figure 6.4 Data collapse for σ of the Family model on a triangular substrate with substrate angle $\varphi = 27^{\circ}$ for various substrate sizes.

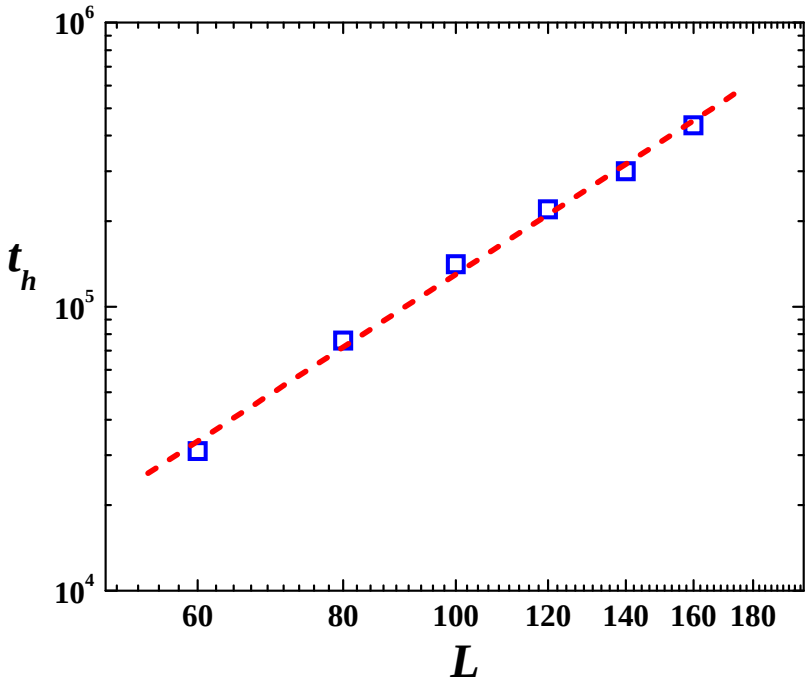

Figure 6.5 Power-law dependence of the healing time on the substrate size of the DT model with $z = 2.6 \pm 0.1$.

DT model is much larger than that of the Family model simulated with the same conditions. This is a consequence of the characteristically rough morphology of the DT model.

To study effects of patterned substrate theoretically, the nearest-neighbor height difference correlation function of the Family model grown on the triangular substrate is calculated analytically from a continuum description. The continuum equation describing the large scale behavior of the Family model is the EW equation [Edwards and Wilkinson, 1982]:

$$\frac{\partial H(\vec{r},t)}{\partial t} = \nu \nabla^2 H(\vec{r},t) + \eta(\vec{r},t), \tag{6.1}$$

where ν is a constant representing surface tension and $\eta(\vec{r},t)$ is the noise arising from random fluctuations in the deposition process. To solve the linear EW equation, the discrete Fourier decomposition [Krug, 1997] is used and the height profile H is written as

$$H(x,y,t) = \sum_{n_x=-\frac{L}{2}}^{\frac{L}{2}} \sum_{n_y=-\frac{L}{2}}^{\frac{L}{2}} \tilde{H}(n_x,n_y,t)\, \mathrm{e}^{2\pi i(n_x x + n_y y)/L} \tag{6.2}$$

with the inverse transform denoted by $\tilde{H}(n_x,n_y,t)$. The general solution of the EW equation in Fourier space is written as

$$\tilde{H}(n_x,n_y,t) = \mathrm{e}^{\frac{-4\pi^2\nu(n_x^2+n_y^2)t}{L^2}} \left[\tilde{H}(n_x,n_y,0) + \int_0^t \mathrm{e}^{\frac{4\pi^2\nu(n_x^2+n_y^2)u}{L^2}} \tilde{\eta}(n_x,n_y,u)du \right], \tag{6.3}$$

where $\tilde{H}(n_x,n_y,0)$ is the Fourier transform of the height profile at the initial time, $H(\vec{r},0)$. The noise in this model is uncorrelated and has zero mean:

$$\begin{aligned} \left\langle \eta(x,y,t)\eta(x',y',t') \right\rangle &= D\delta(x-x')\delta(y-y')\delta(t-t') \\ \left\langle \tilde{\eta}(n_x,n_y,t)\tilde{\eta}(n_x',n_y',t') \right\rangle &= \frac{D}{L^2}\delta(n_x+n_x')\delta(n_y+n_y')\delta(t-t'), \end{aligned} \tag{6.4}$$

where D is a coefficient indicating the strength of the noise. The height difference correlation function (G) is defined as

$$G(\Delta\vec{r},t) \equiv \left\langle \left| H(\vec{r}+\Delta\vec{r},t) - H(\vec{r},t) \right|^2 \right\rangle^{1/2}. \tag{6.5}$$

Replacing Eqs. (6.2) and (6.3) in Eq. (6.5), the height difference correlation function is found to be the sum of a "smooth" term, $G^{smooth}(\Delta y,t)$, and a "rough" term, $G^{rough}(\Delta y,t)$ [Nguyen et al. 2009]:

$$\left(G(\Delta y,t)\right)^2 \equiv \left(G^{smooth}(\Delta y,t)\right)^2 + \left(G^{rough}(\Delta y,t)\right)^2. \tag{6.6}$$

These two terms have the following expressions in our case:

$$\left(G^{smooth}(\Delta y,t)\right)^2 = \frac{2}{L^2}\sum_{n_x=-\frac{L}{2}}^{\frac{L}{2}}\sum_{n_y=-\frac{L}{2}}^{\frac{L}{2}}\left|\tilde{H}(n_x,n_y,0)\right|^2 \mathrm{e}^{-8\pi^2\nu t(n_x^2+n_y^2)/L^2}\left(1-\cos(2\pi n_y\Delta y/L)\right) \tag{6.7}$$

$$\left(G^{rough}(\Delta y,t)\right)^2 = \frac{D}{4\pi^2\nu}\sum_{n_x=-\frac{L}{2},n_x\neq 0}^{\frac{L}{2}}\sum_{n_y=-\frac{L}{2},n_y\neq 0}^{\frac{L}{2}}\frac{1}{(n_x^2+n_y^2)}\left(1-\mathrm{e}^{-8\pi^2\nu t(n_x^2+n_y^2)/L^2}\right)\left(1-\cos(2\pi n_y\Delta y/L)\right). \tag{6.8}$$

The smooth term depends on the initial height profile or the shape of the substrate with the exponential decay function representing the effect of the surface tension ν. This term decays with time which means that the initially rough patterned surface is smoothened by the surface tension. On the other hand, effects of the noise D are represented in the rough term. This term indicates that, growing from a flat surface, the interface becomes rough due to the fluctuations from the noise. The theoretical form of the nearest-neighbor height difference correlation function in the tilt direction $\left(\sigma(t)\equiv\sigma_y(t)=G(\Delta y=1,t)\right)$ as a function of time for the triangular substrate is then determined as

$$\sigma(h_0)\equiv\sqrt{\left(G^{smooth}(\Delta y=1,t)\right)^2+\left(G^{rough}(\Delta y=1,t)\right)^2} \tag{6.9}$$

while σ for the flat substrate is given by

$$\sigma(H_0 = 0) \equiv G^{rough}(\Delta y = 1, t). \tag{6.10}$$

Comparing the results of our simulation with those of the analytical calculation, the plots for the numerical and analytic results for σ for the same initial roughness are found to collapse into the same curve for $D \approx 1.7,\ \nu \approx 0.63$ for all substrate sizes of interest. Figure 6.6 shows such a plot for $L = 200$ sites with two different values of φ. The healing time t_h corresponds to the value of t at which the smooth term in Eq. (6.7) becomes smaller than the resolution in the measurement of the nearest-neighbor height difference correlation function σ. It is clear from the structure of Eq. (6.7) that this time should be proportional to L^2. The form of Eq. (6.7) also implies that the healing time t_h for a fixed value of L should increase linearly with the logarithm of the slope of the initial pattern. Our numerical results are consistent with this prediction.

We have checked that for the Family model, the healing time of an inverse triangular (V-shaped) substrate is identical to that of a triangular substrate with the same slope.

6.2 Pillar/Groove Pattern

In this section, the healing time of the Family and DT models grown on substrates with pillar and groove patterns is studied. For both models, the substrate size is varied from $L = 100$ to 500 sites. For each L, the height/depth of the pillars/grooves is varied from 100 to 500 atomic units. The plots of $\sigma(t)$ from films grown on substrates with periodic arrangements of pillars (Figure 6.7(a)) and grooves (Figure 6.7(b)) are qualitatively similar to that for the films grown on triangular substrates. The $\sigma - t$ plots for any value of h_{pillar} and h_{groove} show relatively large values at early times due to the initial roughness of the patterned substrate. The value of σ decreases at late times due to the diffusion of deposited atoms. For both models, the healing time t_h increases when h_{pillar} and h_{groove} are increased as shown in the plots for the DT model in Figure 6.7. The reason is that the roughness of the initial substrate is proportional to the height (depth) of pillars (grooves). The rougher the initial pattern, the longer is the time needed for the correlation function to be healed. Our DT results show that t_h for pillars is larger than that for grooves with depth equal to the height of the pillars. This is because the DT morphology generally exhibits rounded top surfaces and deep grooves [Dasgupta et al. 1997]. The healing time for grooves is smaller than that for pillars because grooves occur naturally in the

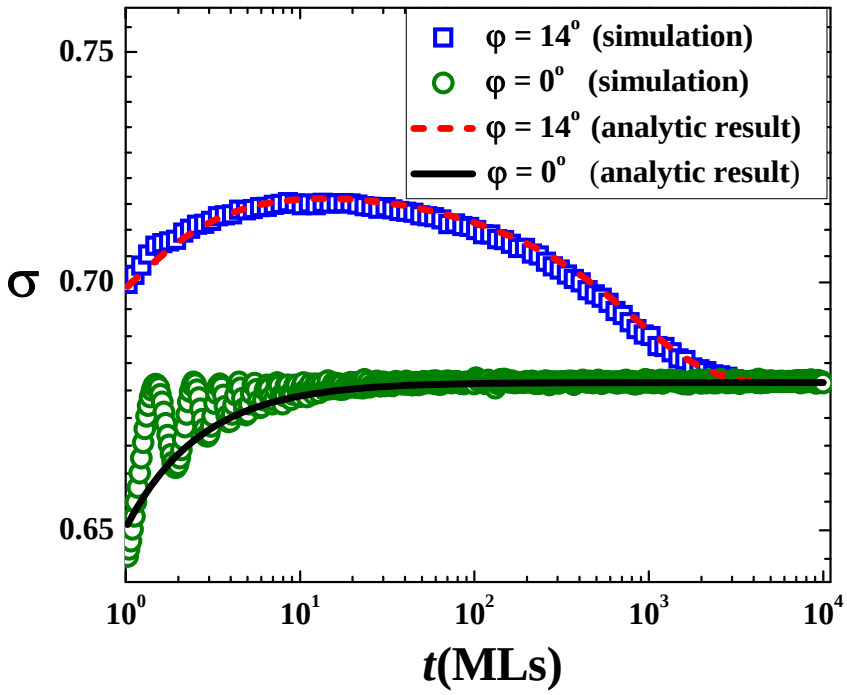

Figure 6.6 Simulation results for the Family model, compared with the analytic results for σ for flat ($\varphi = 0^{\circ}$) and triangular ($\varphi = 14^{\circ}$) substrates for $L = 200$ sites.

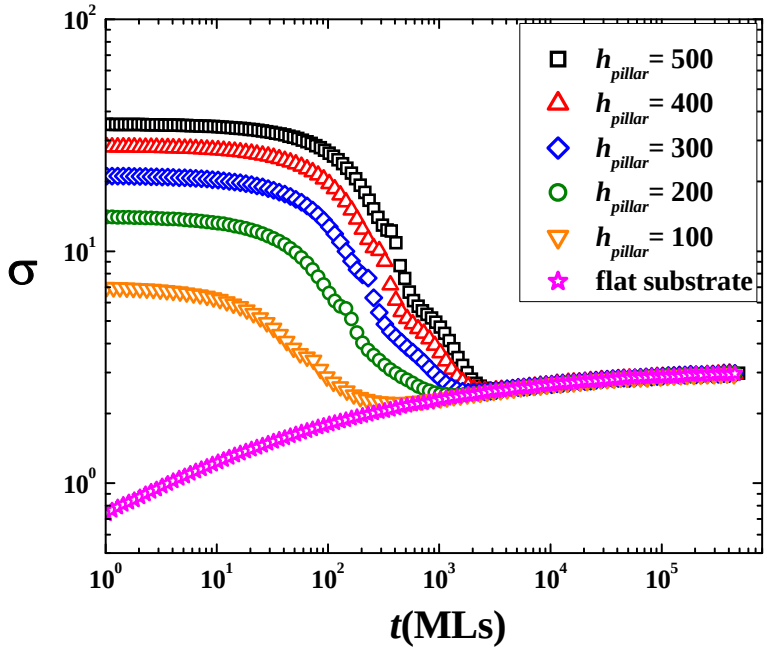

(a)

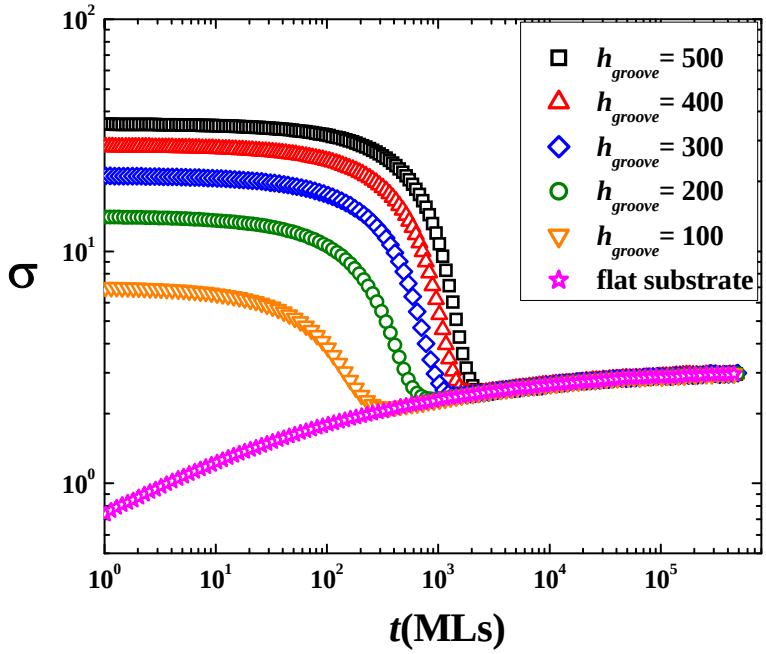

(b)

Figure 6.7 σ of the DT model grown on substrates with periodic arrangement of (a) pillars and (b) grooves of various heights. The areal density of pillars (grooves) is 0.0025. The substrate size is $L = 500$ sites.

morphology of films grown according to the diffusion rule of the DT model. This difference reflects the lack of up-down symmetry in the DT model and is related to the fact that the continuum equation that is believed to describe the coarse-grained behavior of the DT model is nonlinear.

For the Family model, whose continuum description yields the same results for substrates with pillars and grooves (because they are related to each other by the $h \to -h$ transformation), our simulations show the surprising result that the healing behavior is different for substrates with pillar and groove patterns (see Figure 6.8). We find that the healing time for grooves is smaller than that for pillars. These results establish that a continuum description (the EW equation) cannot describe growth on a substrate with pillars/grooves.

Similar to the triangular substrate cases, the healing time in the DT model is larger than that in the Family model simulated with the same conditions.

We have also studied the effects of the distribution of the pillars and grooves on the healing time. Figure 6.9 shows a comparison between the DT results for periodically (or uniformly) distributed and randomly distributed grooves with the same areal density. The healing time for the random case is observed to be larger than that for the periodic case. Similar plots are obtained for substrates with pillars. This is because a random distribution of the elements (grooves or pillars) of the pattern on the substrate can cause some regions of the substrate to have a high density of the elements. Films on densely patterned substrates require more time for the correlation function to be restored. As a result, the dense regions in the random distribution case cause t_h to be larger than that for the periodic case. Similar results are obtained for the Family model.

The small kink seen in Figure 6.7(a) is observed only for the DT model in all $\sigma - t$ plots for substrates with pillars of the same height. When the areal density of the pillars equals 0.0025, there is one pillar of height h_{pillar} in every $l \times l$ section of the square lattice where $l = 20$ sites. According to the DT diffusion rules, atoms deposited at the pillar sites move to one of the nearest-neighbor sites whereas atoms deposited at the nearest-neighbor sites of the pillar do not diffuse because they already have a lateral bond. The height at pillar sites should be close to h_{pillar} after the deposition of t monolayers, and the heights at the nearest-neighbor sites should be close to $5t/4$. The heights at other sites evolve as if the initial substrate were flat. So, the value of σ after the deposition of t monolayers should be given by

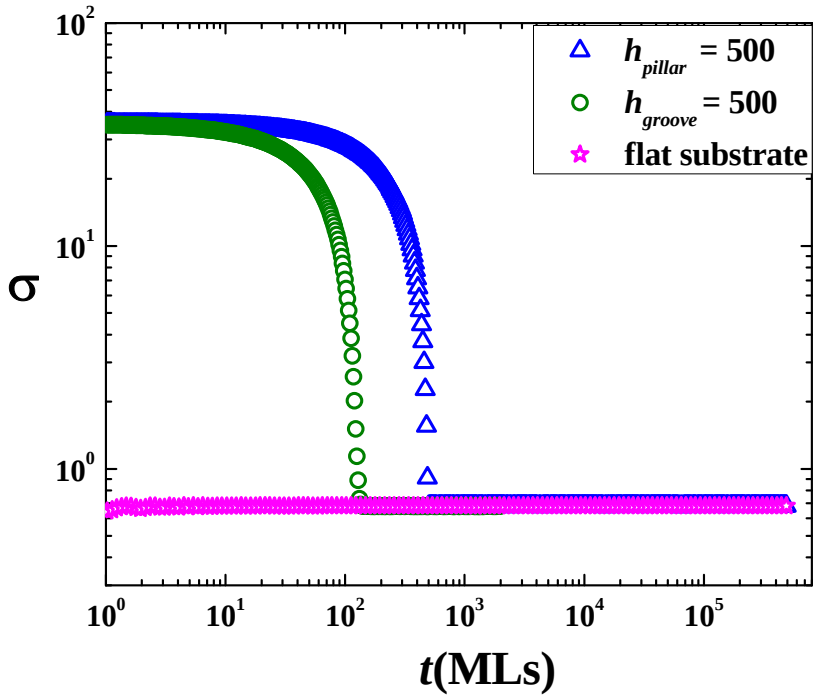

Figure 6.8 σ of the Family model grown on a substrate with a periodic arrangement of pillars and grooves with $h_{pillar} = h_{groove} = 500$, for $L = 100$ sites. The areal density of grooves is 0.0025.

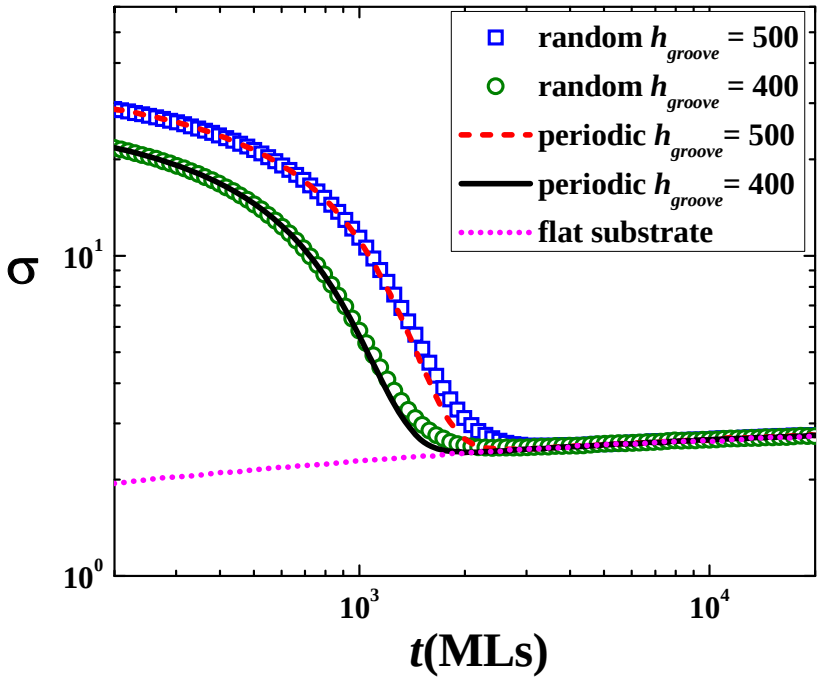

Figure 6.9 σ of the DT model grown on substrates with periodic and random arrangements of grooves of depth $h_{groove} = 400$ and 500. The areal density of grooves is 0.0025. The substrate size is $L = 500$ sites.

$$\sigma(t) \equiv \left[\frac{1}{2l^2} \left(4\left(h_{pillar} - \frac{5}{4}t \right)^2 + 12\left(\frac{t}{4} \right)^2 + \left(2l^2 - 16 \right) \sigma_f^2(t) \right) \right]^{1/2}, \qquad (6.11)$$

where $\sigma_f(t)$ is the correlation function of the film grown on a flat substrate. The formula is valid until $t \approx 4h_{pillar}/5$ when the heights of the nearest-neighbor sites become comparable to that of the pillar site and atoms deposited at the pillar site do not always move to the nearest neighbors. The kink seen in Figure 6.7(a) is at the crossover time $t \approx t_c = 4h_{pillar}/5$. As shown in Figure 6.10, the simple approximate formula of Eq. (6.11) provides an accurate description of the simulation data for times up to this crossover time. For the initial pattern with grooves, such a crossover does not exist because the evolution of isolated grooves according to the DT diffusion rules is very different for that of isolated pillars. This difference is discussed in detail in Dasgupta et al. 1997.

Since the crossover time depends on h_{pillar}, the kink should not be expected when the height of the pillars is chosen randomly. Figure 6.11 shows $\sigma - t$ plots for a substrate with pillars of uniform height and one with pillars of random height with the average equal to the height in the uniform case. For the random case, the crossover in each $l \times l$ section occurs at a different time, leading to a smooth correlation function curve. The healing time in the random case is larger because pillars with heights larger than the average value take longer to heal.

The dependence of the healing time on the size of the initial pattern and the substrate size is also investigated. We find that the healing time depends strongly on the height (depth) of the pillars (grooves). We obtain a linear dependence for both periodically distributed and randomly distributed pillars. For the DT model, the healing time, measured from the crossover time t_c, is plotted as a function of h_{pillar} in Figure 6.12. The results show a good linear relation in both cases with $t_h - t_c \sim 12.2 h_{pillar}$ when the pillars are randomly distributed and $t_h - t_c \sim 6.9 h_{pillar}$ for periodically distributed pillars. Since the crossover time t_c is itself proportional to h_{pillar}, the healing time t_h in these cases is proportional to h_{pillar}. Similar behavior is observed in systems with grooves. For the Family model, we obtain similar results except that there is no kink in the $\sigma - t$ plots (see Figure 6.13). However, with the same density of pillar, we find that the shape of the correlation function as well as the healing time do not depend on L. Figure 6.13 shows that

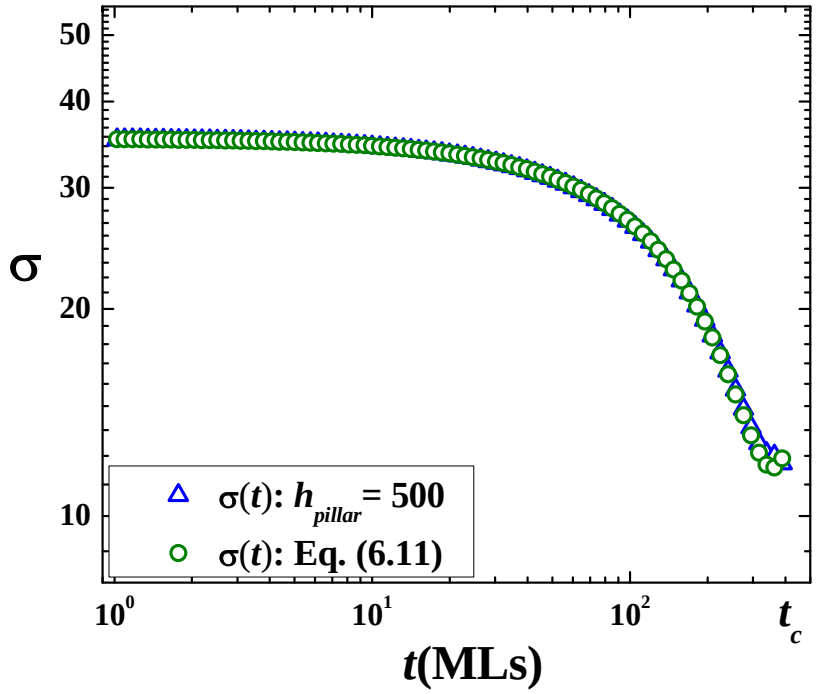

Figure 6.10 Comparison of the simulation result for σ for the DT model on a substrate with a periodic arrangement of pillars with $h_{pillar} = 500$ with the approximate result given in Eq (6.11).

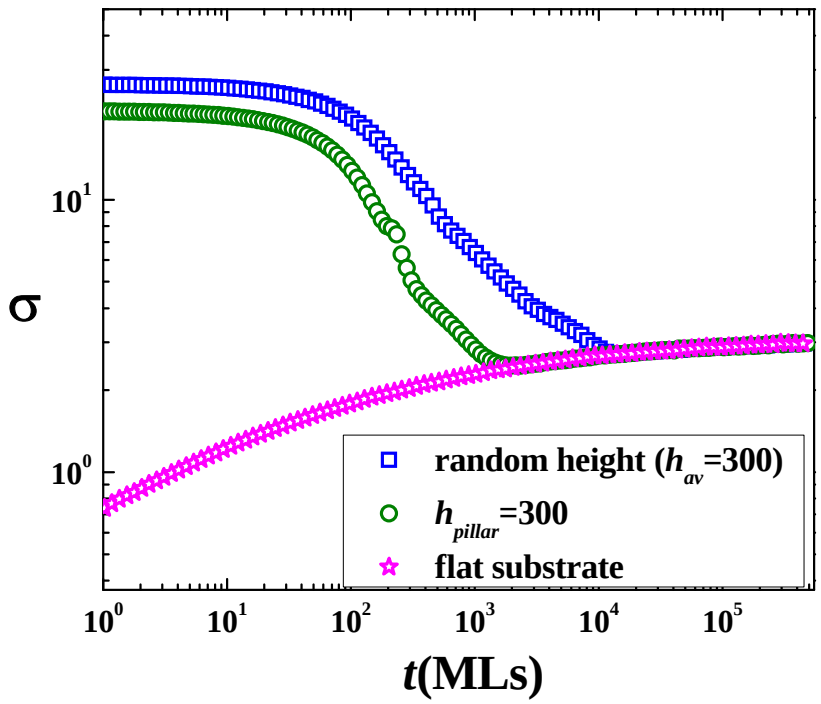

Figure 6.11 σ of the DT model grown on substrates with a periodic arrangement of pillars, when $h_{pillar} = 300$ for all the pillars and when the pillars have random heights with $h_{av} = 300$. The areal density of pillars is 0.0025 and the substrate size is $L = 200$ sites.

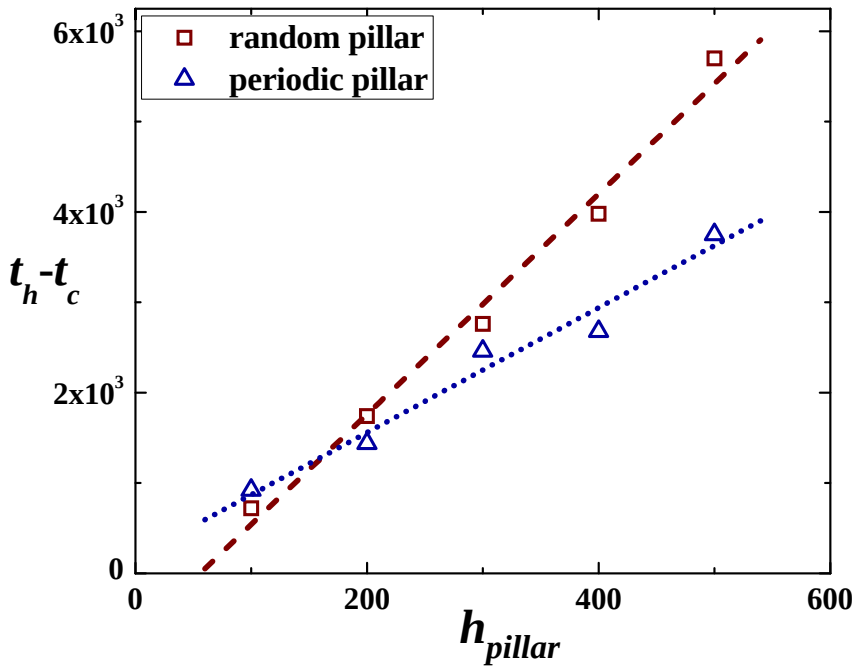

Figure 6.12 Dependence of the healing time on h_{pillar} for both randomly distributed and periodically distributed cases. The areal density of pillars is 0.0025.

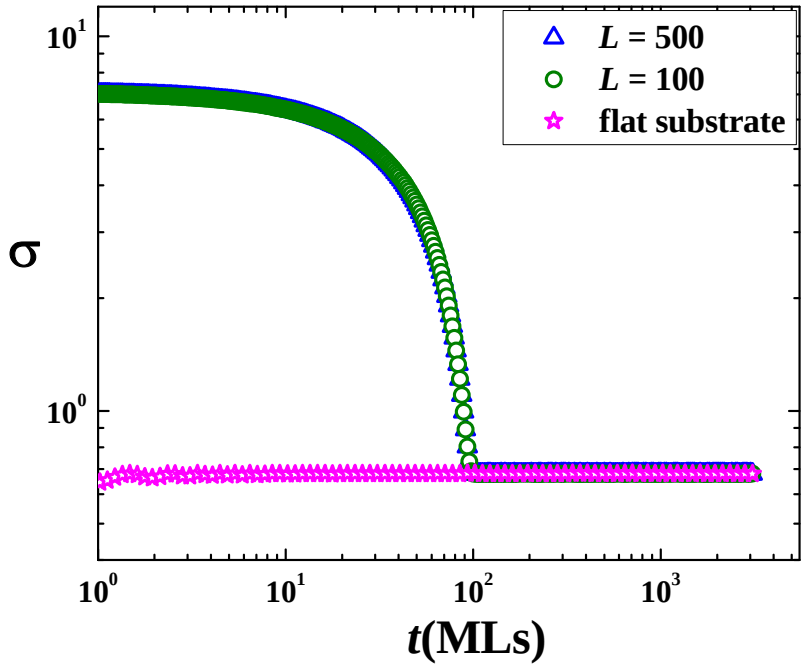

Figure 6.13 σ of the Family model grown on a substrate with a periodic arrangement of pillars, for two different substrate sizes $L = 100$ and 500 sites. The areal density of pillars is 0.0025.

the $\sigma - t$ plots for films grown on substrates with a periodic arrangement of pillars with $h_{pillar} = 100$ for two systems with $L = 100$ and 500 sites collapse into the same curve. We find similar behavior for a random distribution of pillars, as well as for both periodic and random distribution of grooves.

The theoretical calculation of the Family model grown on a pillar substrate is studied using the EW equation. The plots for analytic results are found to disagree with the simulation results for the same initial roughness as can be seen in Figure 6.14. For the analytic calculation, the correlation function decreases with time as an exponential decay while that of the simulation results decreases linearly with time. We can conclude that the healing time cannot be predicted by the continuum description when the initial pattern is atomically rough and does not extend with the size of the substrate.

The healing properties of the Family model grown on a substrate with pillars/grooves can be studied analytically in the continuum limit using the EW equation. The calculation is essentially the same as that described above in the context of growth on a triangular substrate. The only change in Eq.(6.7) is that the values of the Fourier components $\tilde{H}(n_x, n_y, 0)$ of the initial height profile are now different from those for a triangular substrate. For a periodic arrangement of pillars, the values of n_x, n_y for which $\tilde{H}(n_x, n_y, 0)$ is not zero are determined by the periodicity of the initial arrangement. In this case, the healing behavior in the continuum description is expected to be essentially independent of the system size. For a random arrangement of pillars, other Fourier components of the initial height profile should be nonzero and the healing behavior should exhibit some dependence on the system size. A comparison of the analytic result with that obtained from simulations for the same initial roughness (see Figure 6.14) shows that the two sets of results are very different from each other. In the analytic calculation, the correlation function decreases with time as an exponential decay and it reaches the value obtained for a flat substrate at a time that is much shorter than the healing time obtained in the simulation. The simulation result for σ decreases linearly with time for small values of t. The time-dependence of σ found in the simulation may be understood from the diffusion rule of the Family model, using arguments similar to those use earlier for the DT model. In the initial stage of the healing process, an atom deposited at a pillar sites moves to one of the nearest-neighbor sites because these sites have lower heights. An atom deposited at one of the nearest-neighbor sites can diffuse to one of its neighboring sites if that site has a lower height. So, unlike

the behavior in the DT model, atoms deposited at the nearest-neighbor sites of a pillar site diffuse in a way that is similar to the diffusion of atoms on a flat substrate. Arguments similar to those used earlier for the DT model then lead to the following approximate expression for the time dependence of σ for $t < h_{pillar}$.

$$\sigma(t) \equiv \left[\frac{1}{2l^2} \left(4\left(h_{pillar} - t \right)^2 + \left(2l^2 - 4 \right) \sigma_f^2 (t) \right) \right]^{1/2}. \tag{6.12}$$

As shown in Figure 6.14, this approximate expression provides a good description of the simulation data. This argument also implies that the healing time should be nearly equal to h_{pillar} in this case. The simulation results are consistent with this prediction. In the case of a groove, an atom deposited at the site of the groove stays there and atoms deposited at the four nearest-neighbor sites move to the site of the groove because it has a lower height. Thus, the depth of the groove initially decreases by 4 units on the average after the deposition of each monolayer. This leads to the following approximate expression for σ for $t < h_{groove} / 4$.

$$\sigma(t) \equiv \left[\frac{1}{2l^2} \left(4\left(h_{groove} - 4t \right)^2 + \left(2l^2 - 4 \right) \sigma_f^2 (t) \right) \right]^{1/2}. \tag{6.13}$$

As shown in Figure 6.14, the simulation data for the healing of grooves are well-described by this expression which implies that $t_h \approx h_{groove} / 4$.

These results show explicitly that the healing behavior of the Family model on substrates with pillars or grooves cannot be understood from a coarse-grained continuum description. An analytic treatment similar to that described above for the Family model cannot be worked out for the DT model because the growth equation believed to be appropriate for the DT model is nonlinear. For this reason, an explicit comparison between analytic and simulation results is not possible for the DT model. However, we believe that the conclusion that a continuum description does not provide a correct account of the healing process for substrates with pillars or grooves applies to the DT model also. As noted earlier, the healing time of the DT model on a substrate with pillars or grooves is proportional to the height (depth) of the pillars (grooves), similar to the behavior found for the Family model. We also found also that some of the features observed in the simulation results for the DT model, such as the kink in the $\sigma - t$ plots for substrates with

pillars, arise from atomistic details of the diffusion rules which would be lost in a continuum description. These results indicate that simple scaling theories based on a coarse-grained continuum description of the healing process do not provide a correct account of the behavior of the DT model grown on substrates with pillars or grooves.

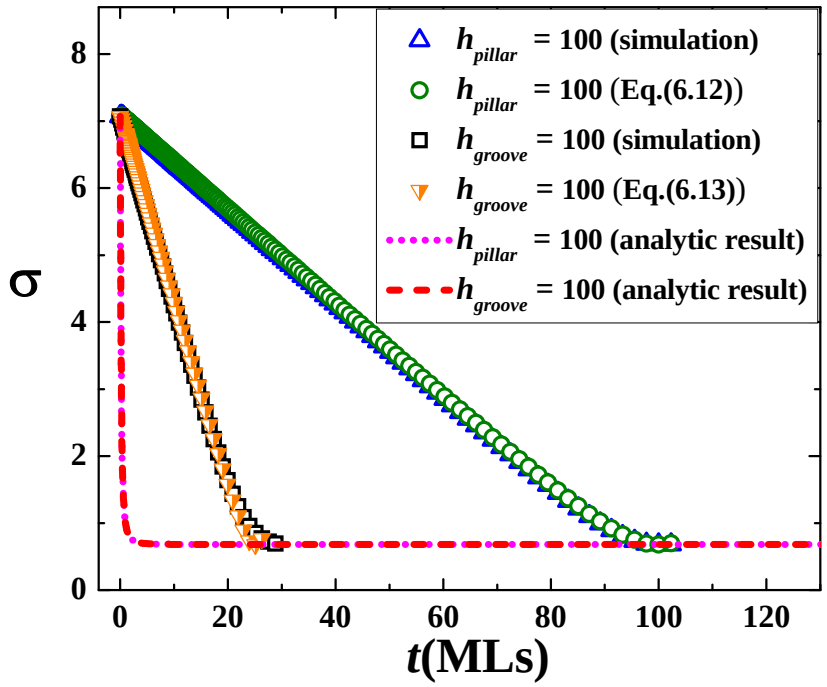

Figure 6.14 Comparison of the simulation result for σ for the Family model on a substrate with a periodic arrangement of pillars and grooves with $h_{pillar} = h_{groove} = 100$, $L = 100$ sites with the approximate result given in Eqs. (6.12) and (6.13), and the analytic result obtained from a continuum description. The areal density of pillars equals 0.0025.

Chapter VII
Conclusion

In our detailed study of the persistence probabilities, we found that different values of the sampling time and the system size lead to different results of the persistence probabilities. When the system size is decreased, the persistence exponent increases. Increasing value of the sampling time leads to the increase of persistence probabilities. However, the value of the sampling time does not affect the persistence exponents. By keeping the ratio $\delta t / L^z$ constant, the scaling form for the Family, the LC and the DT Models can be written in terms of t / L^z and $\delta t / L^z$. That is $P^S(t, L, \delta t) = f\left(t/L^z, \delta t/L^z\right)$, where the scaling function decays as a power law with t/L^z with an exponent corresponding to models. This relation is valid for $t / L^z << 1$ and $\delta t / L^z << 1$.

Our numerical study of the dependence of the steady-state temporal persistence probabilities for three discrete growth models with up-down symmetry on the choice of the initial height h_0 leads to the important conclusion that the positive persistence probability for negative initial heights, $P_+^S\left(-|h_0|, t\right)$ and equivalently, the negative probability for positive initial heights, $P_-^S\left(+|h_0|, t\right)$ decay in time as a power law under the condition $|h_0|/W_s \gtrsim 1$. The other two persistence probabilities do not show any indication of power-law decay. The persistence exponent that describes the power-law decay of $P_+^S\left(-|h_0|, t\right)$ and $P_-^S\left(+|h_0|, t\right)$ decreases with $|h_0|/W_s$ and the observed behavior is consistent with a linear dependence on $|h_0|/W_s$. Our study, thus, provides strong numerical evidence for the existence of a new set of persistence exponents for the simple growth models considered here. We also show that the persistence probability for a fixed initial height h_0 is a function of the scaling variables t / L^z, $\delta t / L^z$ and $|h_0| / L^\alpha$.

Although our numerical study provides strong evidence for the power-law decay of $P_+^S\left(-|h_0|, t\right)$ and $P_-^S\left(+|h_0|, t\right)$ for $|h_0|/W_s \gtrsim 1$, true power-law behavior and the existence of the associated persistence exponents can be established only from exact analytic work. We have presented interesting arguments that provide a qualitative understanding of our numerical results, but these arguments are by no means exact. Analytic studies of persistence probabilities are usually carried out for continuum systems. Continuum growth equations that are appropriate for describing the long-time, large-scale behavior of the discrete growth models considered here are well known. However, analytic studies of the persistence probabilities for these growth equations

are difficult because the exponent β for all these systems is less than 1. The persistence probabilities considered in our work are closely related to the statistics of the interval between successive zero-crossings of the stochastic variable $h(t) - h_0$. For growth equations with $\beta < 1$, the density of zero crossings of this stochastic variable is infinite – once this variable crosses zero, it immediately crosses zero again many times within a short time interval. For this reason, the persistence probabilities for these growth equations are not mathematically well-defined in the truly continuum limit. This does not pose a problem for defining and studying persistence probabilities in simulations and experiments because there is always a finite sampling time between two successive measurements of the variable under consideration. However, this mathematical problem makes exact analytic studies of persistence probabilities in these systems quite difficult. Development of methods for performing such studies would be most welcome.

The models considered here exhibit up-down symmetry, which implies that the persistent exponents associated with $P_+^S\left(-|h_0|,t\right)$ and $P_-^S\left(+|h_0|,t\right)$ are the same. This would not be true for growth models that do not exhibit up-down symmetry such as the DT model. Our results suggest the existence of two sets of new persistence exponents, associated with $P_+^S\left(-|h_0|,t\right)$ and $P_-^S\left(+|h_0|,t\right)$ for such models. It would be interesting to check this from simulations of growth models without up-down symmetry.

In the early times when effects of the initial pattern is still strong, plots of the interface width, the transient persistence probability for large substrate slope, and the correlation function in the tilted direction show different scaling behavior from that of growth on a flat substrate. The substrate pattern also results in the breakdown of the Family-Vicsek scaling relation of the critical exponents. Our investigations in the height-height correlation functions of different moments also show that films grown with Family model on patterned substrates exhibit both anomalous scaling and multiscaling behavior in contrast to the standard scaling in systems with flat substrates.

Several properties of growing films are affected by patterns on the substrate. The healing time, defined as the time when the influence of the pattern disappears, depends on the characteristics of the initial pattern, the size of the substrate, and the nature of the dynamics that governs the growth of the film. We have studied these dependences for two atomistic models of film growth. The influence of the initial pattern appears prominently when the roughness of the initial substrate increases. In our case, this corresponds to increasing the angle φ for the

triangular substrate and increasing the height (depth) of pillars (grooves) for the pillar (groove) pattern. Our results show that for relatively smooth initial patterns such as the triangular substrate, the healing time scales with substrate size as L^z. The healing time is thus proportional to the saturation time for growth on a flat substrate. From a comparison of the numerically obtained nearest-neighbor height difference correlation function of the Family model grown on a triangular substrate with the analytic results obtained for the EW equation, the values of the noise strength D and the surface tension ν in the EW equation are found to be $D \approx 1.7,\ \nu \approx 0.63$. For atomically rough initial patterns such as those in substrates with single-site pillars or grooves, the healing time increases linearly with the size (height or depth) of the initial pillars or grooves. Random distribution in the height and/or the position of the pillars or grooves on the substrate increases the healing time. Some of the features of the healing process in this case are found to be inconsistent with the predictions of continuum theory and consequences of the atomistic details of the diffusion rules. Therefore, in contrast to the triangular substrate, simple scaling relations derived from a coarse-grained continuum description do not provide a correct description of the healing process on atomically rough substrates with tall pillars and deep grooves. In retrospect, this conclusion is not very surprising. Substrates with single-site pillars (grooves) with large heights (depths) contain sites at which the nearest-neighbor height difference is much larger than unity. A continuum description based on the assumption that the height variable varies smoothly across the substrate is less likely to work in this situation. Our results bring out explicitly the shortcomings of a continuum description of the healing process on substrates with tall pillars and deep grooves and show that the healing behavior in these situations must be understood from the atomistic details of the diffusion rules. These observations illustrate the complexity of the process of healing of the initial pattern in film growth on patterned substrates. We anticipate that our study will motivate further investigations of this process using more realistic models of film growth.

References

Asgari, M., and Moosavi, A. (2012). Coarsening Dynamics of Dewetting Nanodroplets on Chemically Patterned Substrates. Phys. Rev. E 86 : 016303.

Barabasi, A. L., and Stanley, H. E. (1995). Fractal Concepts in Surface Growth. New York: Cambridge University Press.

Bergamaschini, R., Tersoff, J., Tu, Y., Zhang, J. J., Bauer, G., and Montalenti, F. (2012). Anomalous Smoothing Preceding Island Formation During Growth on Patterned Substrates. Phys. Rev. Lett. 109 : 156101.

Bhoomanee, C., Hongsith, N., Wongrat, E., Choopun, S., and Wongratanaphisan, D. (2011). Effect of Solution on Growth of Zinc Oxide Tetrapod by Thermal Oxidation Technique. Chiang Mai J. Sci. 38(2) : 187-192.

Bray, A. J., Majumdar, S. N., and Schehr, G. (2013). Persistence and First-Passage Properties in Non-equilibrium Systems. Adv. Phys. 62 : 225.

Brendel, L., Kallabis, H., and Wolf, D. E. (1998). Layer-by-Layer Growth in Noise-Reduced Growth Models. Phys. Rev. E 58 : 664.

Castez, M. F., Salvarezza, R. C., and Solari, H. G. (2004). Probing Universality Classes in Solid-on-Solid Deposition. Phys. Rev. E 70 : 011605.

Chatraphorn, P., and Chomngam, C. (2012). Modeling of Thin Film Growth on a Tilted Miscut Substrate: Statistical Properties and the Optimum Growth Conditions. Int. J. Mod. Phys. B 26 : 1250087.

Conrad, B. R., Cullen, W. G., Dougherty, D. B., Lyubinetsky, I., and Williams, E. D. (2007). Spatial First-passage Statistics of Al/Si(111)-($\sqrt{3}\times\sqrt{3}$) Step Fluctuations. Phys. Rev. E 75 : 021603.

Constantin, M., Das Sarma, S., Dasgupta, C., Bondarchuk, O., Dougherty, D.B., and Williams, E. D. (2003). Infinite Family of Persistence Exponents for Interface Fluctuations. Phys. Rev. Lett. 91 : 086103.

Constantin, M., Dasgupta, C., Punyindu Chatraphorn, P., Majumdar, S. N., and Das Sarma, S. (2004). Persistence in Nonequilibrium Surface Growth. Phys. Rev. E 69 : 061608.

Constantin, M., Dasgupta, C., Das Sarma, S., Dougherty, D. B., and Williams, E. D. (2007). Persistence and Survival in Equilibrium Step Fluctuations. J. Stat. Mech. : P07011.

Dasgupta, C., Das Sarma, S., and Kim, J. M. (1996). Controlled instability and multiscaling in models of epitaxial growth. Phys. Rev. E 54 : R4552.

Dasgupta, C., Kim, J. M., Dutta, M., and Das Sarma, S. (1997). Instability, Intermittency, and Multiscaling in Discrete Growth Models of Kinetic Roughening. Phys. Rev. E 55 : 2235.

Das Sarma, S., Lanczycki, C. J., Kotlyar, R., and Ghaisas, S. V. (1996). Scale Invariance and Dynamical Correlations in Growth Models of Molecular Beam Epitaxy. Phys. Rev. E 53 : 359–388.

Das Sarma, S., and Punyindu, P. (1999). A Discrete Model for Nonequilibrium Growth Under Surface Diffusion Bias. Surf. Sci. Lett. 424 : L339.

Das Sarma, S., and Tamborenea, P. (1991). A New Universality Class for Kinetic Growth: One-Dimensional Molecular-Beam Epitaxy, Phys. Rev. Lett. 66, 325; (1993). Surface-Diffusion-Driven Kinetic Growth on One-Dimensional Substrates. Phys. Rev. E 48 : 2575.

Das Sarma, S., Punyindu Chatraphorn, P., and Toroczkai, Z. (2002). Universality Class of Discrete Solid-on-Solid Limited Mobility Nonequilibrium Growth Models for Kinetic Surface Roughening. Phys. Rev. E 65 : 036144.

Dimastrodonato, V., Pelucchi, E., and Vvedensky, D. D. (2012). Self-Limiting Evolution of Seeded Quantum Wires and Dots on Patterned Substrates. Phys. Rev. Lett. 108 : 256102.

Dougherty, D. B., Lyubinetsky, I. L., Williams, E. D., Constantin, M., Dasgupta, C., and Das Sarma, S. (2002). Experimental Persistence Probability for Fluctuating Steps. Phys. Rev. Lett. 89 : 136102.

Dougherty, D. B., Bondarchuk, O., Degawa, M., and Williams, E. D. (2003). Persistence Exponents for Step Edge Diffusion. Surf. Sci. 527 : L213.

Dougherty, D. B., Lyubinetsky, I., Einstein, T. L., and Williams, E. D. (2004). Distinguishing step relaxation mechanisms via pair correlation functions. Phys. Rev. B 70 : 235422.

Edwards, S. F., and Wilkinson, D. R. (1982). The Surface Statistics of a Granular Aggregate. Proc. R. Soc. A 381 : 17.

Ehrhardt, G. C. M. A., Bray, A. J., and Majumdar, S. N. (2002). Persistence of a Continuous Stochastic Process with Discrete-Time Sampling: Non-Markov Processes. Phys. Rev. E 65 : 041102.

Evans, J.W., Thiel, P.A., and Bartelt, M.C. (2006). Morphological Evolution During Epitaxial Thin Film Growth: Formation of 2D Islands and 3D Mounds. Surf. Sci. Rep. 61 : 1–128.

Family, F. (1986). Scaling of Rough Surfaces: Effects of Surface Diffusion. J. Phys. A 19 : L441.

Family, F., and Vicsek, T. (1985). Scaling of the Active Zone in the Eden Process on Percolation Networks and the Ballistic Deposition Model. J. Phys. A 18 : L75-L81.

Giesen, M. (1997). Step-step interaction energy on vicinal copper surfaces. Surf. Sci. 370 : 55-63

Giesen, M. (2001). Step and Island Dynamics at Solid/Vacuum and Solid/Liquid Interfaces. Prog. Surf. Sci. 61 : 1.

Hedayatifar, L., Masoudi, A. A., and Vasheghani Farahani, S. (2012). Scaling properties of surface growth on rough substrates generated by standard models. Physica A 391 : 4159–4164.

Hegeman, P. E., Zandvliet, H. J. W., Kip, G. A. M., Kersten, B. A. G., and Poelsema, B. (1995). Experimental Investigation of Criteria for Thermal Roughening. Surf. Sci. 331-333 : 1110.

Hongsith, N., Choopun, S., Tanunchai, S., Chairuangsri, T., Mangkorntong, P., and Mangkorntong, N. (2005). Synthesis of ZnO Nanobelts by RF Sputtering. Chiang Mai J. Sci. 32(3) : 417-420.

Hontinfinde, F., Ferrando, R., and Levi, A. C. (1998). A numerical study of the epitaxial growth of silver on silver (1 1 0). Physica A 248 : 288–304.

Jnawali, G., Wagner, Th., Hattab, H., MÖller, R., and Horn-von Hoegen, M. (2009). Nucleation and Initial Growth in the Semimetallic Homoepitaxial System of Bi on Bi(111). Phys. Rev. B 79 : 193306.

Kallabis, H., and Krug, J. (1999). Persistence of Kardar-Parisi-Zhang Interfaces. Europhys. Lett. 45 : 20.

Kanjanaput, W., Limkumnerd, S., and Chatraphorn, P. (2010). Growth Instability due to Lattice-Induced Topological Currents in Limited-Mobility Epitaxial Growth Models. Phys. Rev. E 82 : 041607.

Kim, J. M., and Das Sarma, S. (1994). Discrete Models for Conserved Growth Equations. Phys. Rev. Lett. 72 : 2903.

Krug, J. (1994). Turbulent Interfaces. Phys. Rev. Lett. 72 : 2907.

Krug, J. (1997). Origins of Scale Invariance in Growth Processes. Adv. Phys. 46 : 139.

Krug, J. (1999). Pattern-forming instabilities in homoepitaxial crystal growth. Physica A 263 : 170–179.

Krug, J. (2004). Power laws in surface physics: the deep, the shallow and the useful. Physica A 340 : 647 – 655.

Krug, J., Kallabis, H., Majumdar, S. N., Cornell, S. J., Bray, A. J., and Sire, C. (1997). Persistence Exponents for Fluctuating Interfaces. Phys. Rev. E 56 : 2702.

Levandovsky, A., Golubović, L., and Moldovan, D. (2006). Interfacial States and Far-from-Equilibrium Transitions in the Epitaxial Growth and Erosion on (110) Crystal Surfaces. Phys. Rev. E 74 : 061601.

Lin, C.-F., Hammouda, A. B. H., Kan, H.-C., Bartelt, N. C., and Phaneuf, R. J. (2012). Directing Self-Assembly of Nanostructures Kinetically: Patterning and the Ehrlich-Schwoebel Barrier. Phys. Rev. B 85 : 085421.

Lyubinetsky, I. L., Dougherty, D. B., Einstein, T. L., and Williams, E. D. (2002). Dynamics of step fluctuations on a chemically heterogeneous surface of Al/Si(111)-($\sqrt{3}\times\sqrt{3}$). Phys. Rev. B 66 : 085327.

Majumdar, S. N. (1999). Persistence in Nonequilibrium Systems. Curr. Sci. 77 : 370.

Majumdar, S. N., Sire, C., Bray, A. J., and Cornell, S. J. (1996). Nontrivial Exponent for Simple Diffusion. Phys. Rev. Lett. 77 : 2867.

Majumdar, S. N., Bray, A. J., and Ehrhardt, G. C. M. A. (2001). Persistence of a Continuous Stochastic Process with Discrete-Time Sampling. Phys. Rev. E 64 : 015101.

Man, X., Andelman, D., and Orland, H. (2012). Block Copolymer Films with Free Interfaces: Ordering by Nanopatterned Substrates. Phys. Rev. E 86 : 010801.

Marques, J. F., Lima, A. B., Araújo, N. A. M., and Cadilhe, A. (2012). Effect of Particle Polydispersity on the Irreversible Adsorption of Fine Particles on Patterned Substrates. Phys. Rev. E 85 : 061122.

Michely, T., and Krug, J. (2004). Island, Mounds and atoms : Patterns and Processes in Crystal Growth Far from Equilibrium. Springer.

Mondal, C., and Sengupta, S. (2012). Single-File Diffusion and Kinetics of Template-Assisted Assembly of Colloids. Phys. Rev. E 85 : 020402.

Mugarza, A., and Ortega, J. E. (2003). Electronic states at vicinal surfaces. J. Phys.: Condens. Matter 15 : S3281.

Mullins, W. W. (1957). Theory of Thermal Grooving. J. Appl. Phys. 28 : 333; (1950). C. Herring, Effect of Change of Scale on Sintering Phenomena. ibid. 21 : 301.

Nguyen, T. T. T., Bonamy, D., Phan Van, L., Cousty, J., and Barbier, L. (2009). Scaling and Universality in the Kinetic Smoothening of Interfaces: Application to the Analysis of the Relaxation of Rough Vicinal Steps of an Oxide Surface. Europhys. Lett. 89 : 60005.

Nurminen, L., Kuronen, A., and Kaski, K. (2000). Kinetic Monte Carlo Simulation of Nucleation on Patterned Substrates. Phys. Rev. B 63 : 035407.

Pelliccione, M., and Lu, T.-M. (2008). Evolution of Thin Film Morphology: Modeling and Simulations. Springer Series in Materials Science 108.

Persichetti, L., Sgarlata, A., Fanfoni, M., Bernardi, M., and Balzarotti, A. (2009). Step-step interaction on vicinal Si(001) surfaces studied by scanning tunneling microscopy. Phys. Rev. B 80 : 075315.

Pimpinelli, A., and Villain, J. (1998). Physics of Crystal Growth. Cambridge University Press.

Punyindu, P. (2000). Understanding Kinetic Surface Roughening Using Local, Discrete, Nonequilibrium Growth Models. Doctoral dissertation, Faculty of the Graduate School of the University of Maryland.

Punyindu, P., and Das Sarma, S. (1998). Noise Reduction and Universality in Limited-Mobility Models of Nonequilibrium Growth. Phys. Rev. E 57: R4863–R4866.

Punyindu Chatraphorn, P., and Das Sarma, S. (2002). Layer by Layer Epitaxy in Limited Mobility Nonequilibrium Models of Surface Growth. Phys. Rev. E 66 : 041601.

Redinger, A., Ricken, O., Kuhn, P., Rätz, A., Voigt, A., Krug, J., and Michely, T. (2008). Spiral Growth and Step Edge Barriers. Phys. Rev. Lett. 100 : 035506.

RÖthlein, A., Baumann, F., and Pleimling, M. (2006). Symmetry-Based Determination of Space-Time Functions in Nonequilibrium Growth Processes. Phys. Rev. E 74 : 061604.

Rousset, S., Pourmir, F., Berroir, J. M., Klein, J., Lecoeur, J., Hecquet, P., and Salanon, B. (1999). Self-organization on Au(111) vicinal surfaces and the role of surface stress. Surf. Sci. 422 : 33–41.

Sakdanuphab, R., Chityuttakan, C., Pankiew, A., Somwang, N., Yoodee, K., and Chatraphorn, S. (2011). Growth Characteristics of Cu(In,Ga)Se2 Thin Films Using 3-Stage Deposition Process with a NaF Precursor. J. Cryst. Growth 319 : 44–48.

Sire, C. (2007). Probability Distribution of the Maximum of a Smooth Temporal Signal. Phys. Rev. Lett. 98 : 020601.

Sire, C. (2008). Crossing Intervals of Non-Markovian Gaussian Processes. Phys. Rev. E 78 : 011121.

Sire, C., Majumdar, S. N., and Rudinger, A. (2000). Analytical Results for Random Walk Persistence. Phys. Rev. E 61 : 1258.

Tamborenea, P. I., and Das Sarma, S. (1993). Surface-Diffusion-Driven Kinetic Growth on One-Dimensional Substrates. Phys. Rev. E 48 : 2575.

Tang, G., Xun, Z., Wen, R., Han, K., Xia, H., Hao, D., Zhou, W., Yang, X., and Chen, Y. (2010). Discrete growth models on deterministic fractal substrate. Physica A 389 : 4552–4557.

Thongkham, W., Sakdanuphab, R., Chityuttakan, C., and Chatraphorn, S. (2010). Effect of Diffusion Barrier and Substrate Temperature on the Physical Properties of Flexible Cu(In,Ga)Se2 Thin Film Solar Cells. Journal of Metals, Materials and Minerals 20(3) : 61-65.

Toroczkai, Z., Newman, T. J., and Das Sarma, S. (1999). Sign-Time Distributions for Interface Growth. Phys. Rev. E 60 : R1115.

Wongsaprom, K., and Maensiri, S. (2013). Synthesis and Room Temperature Magnetic Behavior of Nickel Oxide Nanocrystallites. Chiang Mai J. Sci. 40(1) : 99-108.

VITAE

Miss Rangsima Chanphana received her Bachelor's degree (with first class honours) in physics from Chulalongkorn University in 2002 and her Master's Degree in physics from Chulalongkorn University in 2006. She has worked as a lecturer in Department of Physics, Faculty of Science, Chulalongkorn University since 2006. She studied for her Degree of Doctor at Chulalongkorn University in 2008.

Journal Publication:

2013 Chanphana, R., Chatraphorn, P., and Dasgupta, C. (3 December 2013). Effects of initial height on the steady-state persistence probability of linear growth models. Phys. Rev. E 88 : 062402.

Conference Presentations:

2012 Chanphana, R., Chatraphorn, P., and Dasgupta, C. (8-10 December 2012). Effects of Initial Height on Persistence Probability of Up-Down Symmetric Models. The 8th Mathematics and Physical Science Graduate Congress. Chulalongkorn University, Thailand.

Chanphana, R., Chatraphorn, P., and Dasgupta, C. (9-12 May 2012). Effects of Patterned Substrate on the Das Sarma-Tamborenea Model. Siam Physics Congress 2012. Phranakhon Si Ayutthaya, Thailand.

2011 Chanphana, R., Chatraphorn, P., and Dasgupta, C. (23-26 March 2011). Effects of Discrete Sampling Time and Sample System Size on Persistence Probability of Discrete Growth Models. Siam Physics Congress 2011. Chonburi, Thailand.

2010 Chanphana, R., Chatraphorn, P., and Dasgupta, C. (13-15 December 2010). Healing Time of Thin Films Simulated by Family Model Grown on Patterned Substrates. The 6th Mathematics and Physical Science Graduate Congress. University of Malaya, Malaysia.

Chanphana, R., Chatraphorn, P., and Dasgupta, C. (25-27 March 2010). Persistence Probabilities in Thin Film Growth Models with and without Up-Down Symmetry. Siam Physics Congress 2010. Kanchanaburi, Thailand.